

SANDIA REPORT

SAND2006-7589

Unlimited Release

Printed December 2006

Three Dimensional Simulation for Bayou Choctaw Strategic Petroleum Reserve (SPR)

Byoung-Yoon Park, Brian L. Ehgartner, and Moo Y. Lee

Prepared by
Sandia National Laboratories
Albuquerque, New Mexico 87185 and Livermore, California 94550

Sandia is a multiprogram laboratory operated by Sandia Corporation,
a Lockheed Martin Company, for the United States Department of Energy's
National Nuclear Security Administration under Contract DE-AC04-94AL85000.

Approved for public release; further dissemination unlimited.



Issued by Sandia National Laboratories, operated for the United States Department of Energy by Sandia Corporation.

NOTICE: This report was prepared as an account of work sponsored by an agency of the United States Government. Neither the United States Government, nor any agency thereof, nor any of their employees, nor any of their contractors, subcontractors, or their employees, make any warranty, express or implied, or assume any legal liability or responsibility for the accuracy, completeness, or usefulness of any information, apparatus, product, or process disclosed, or represent that its use would not infringe privately owned rights. Reference herein to any specific commercial product, process, or service by trade name, trademark, manufacturer, or otherwise, does not necessarily constitute or imply its endorsement, recommendation, or favoring by the United States Government, any agency thereof, or any of their contractors or subcontractors. The views and opinions expressed herein do not necessarily state or reflect those of the United States Government, any agency thereof, or any of their contractors.

Printed in the United States of America. This report has been reproduced directly from the best available copy.

Available to DOE and DOE contractors from
U.S. Department of Energy
Office of Scientific and Technical Information
P.O. Box 62
Oak Ridge, TN 37831

Telephone: (865) 576-8401
Facsimile: (865) 576-5728
E-Mail: reports@adonis.osti.gov
Online ordering: <http://www.osti.gov/bridge>

Available to the public from
U.S. Department of Commerce
National Technical Information Service
5285 Port Royal Rd.
Springfield, VA 22161

Telephone: (800) 553-6847
Facsimile: (703) 605-6900
E-Mail: orders@ntis.fedworld.gov
Online order: <http://www.ntis.gov/help/ordermethods.asp?loc=7-4-0#online>



Three Dimensional Simulation for Bayou Choctaw Strategic Petroleum Reserve (SPR)

Byoung-Yoon Park¹, Brian L. Ehgartner², and Moo Y. Lee¹

¹-Performance Assessment & Decision Analysis Department
Sandia National Laboratories
4100 National Parks Highway,
Carlsbad, NM 87185-MS1395

²-Geotechnology and Engineering Department
Sandia National Laboratories
P.O. Box 5800
Albuquerque, NM 87185-MS0706

Abstract

Three dimensional finite element analyses were performed to evaluate the structural integrity of the caverns located at the Bayou Choctaw (BC) site which is considered a candidate for expansion. Fifteen active and nine abandoned caverns exist at BC, with a total cavern volume of some 164 MMB. A 3D model allowing control of each cavern individually was constructed because the location and depth of caverns and the date of excavation are irregular. The total cavern volume has practical interest, as this void space affects total creep closure in the BC salt mass. Operations including both cavern workover, where wellhead pressures are temporarily reduced to atmospheric, and cavern enlargement due to leaching during oil drawdowns that use water to displace the oil from the caverns, were modeled to account for as many as the five future oil drawdowns in the six SPR caverns. The impacts on cavern stability, underground creep closure, surface subsidence, infrastructure, and well integrity were quantified.

ACKNOWLEDGMENTS

This research is funded by the SPR program administered by the U.S. Department of Energy. The authors would like to acknowledge the valuable contributions to this work by Courtney G. Herrick (SNL, Dept. 6822), Joshua S. Stein (SNL, Dept. 6852), David S. Kessel (SNL, Dept. 6821), Steven R. Sobolik (SNL, Dept. 6117) and Anna Snider Lord (SNL, Dept. 6113). Matthew L. Staten (SNL, Dept. 1421) helped us understand how to use Cubit code to generate 3D FEM mesh.

CONTENTS

ACKNOWLEDGMENTS	4
CONTENTS.....	5
FIGURES.....	6
TABLES	9
NOMENCLATURE	10
1. INTRODUCTION	11
1.1. Objective.....	11
1.2. Background.....	11
1.3. Report Organization.....	12
2. SITE DESCRIPTION	13
3. ANALYSIS MODEL.....	19
3.1. Geomechanical Model	19
3.1.1. <i>Salt dome geometry</i>	19
3.1.2. <i>Salt constitutive model</i>	21
3.1.3. <i>Material properties of lithologies around the salt dome</i>	22
3.2. Cavern Model.....	24
3.2.1. <i>Cavern geometry and layout</i>	24
3.2.2. <i>Model history</i>	29
3.3. Thermal conditions	32
4. MESH GENERATION.....	33
5. BACK-FITTING ANALYSIS.....	39
5.1. Field Data.....	39
5.2. Selection of Parameters to Calibrate.....	40
5.3. Results of Back-fitting Analysis	40
6. FAILURE CRITERIA	45
6.1. Structural Stability of Salt Dome.....	45
6.2. Allowable Strains for Well and Surface Structures	47
7. COMPUTER CODES AND FILE NAMING CONVENTION	49
7.1. Computer Codes.....	49
7.2. File Naming Convention.....	49
8. ANALYSES RESULTS	51
8.1. Cavern Deformation.....	51
8.2. Storage Loss.....	53

8.3.	Subsidence	55
8.4.	Cavern Wells.....	58
8.5.	Cavern Stability	60
8.5.1.	<i>Minimum compressive stress</i>	60
8.5.2.	<i>Minimum safety factor against dilatant damage</i>	62
8.6.	Stability of Caverns 7 and 4.....	64
9.	ALTERNATIVE ANALYSIS (SCENARIO 2)	69
9.1.	Objectives	69
9.2.	Model History	69
9.3.	Analysis Prediction	70
9.3.1.	<i>Storage loss</i>	70
9.3.2.	<i>Subsidence</i>	71
9.3.3.	<i>Cavern wells</i>	73
9.4.	Alternative Workover History Effect on Cavern Stability	74
9.4.1.	<i>Minimum compressive stress</i>	74
9.4.2.	<i>Minimum safety factor against dilatant damage</i>	77
10.	CONCLUDING REMARKS.....	79
11.	REFERENCES	81
	DISTRIBUTION.....	83

FIGURES

Figure 1:	Location of SPR Sites.....	11
Figure 2:	Bayou Choctaw site plan view	15
Figure 3:	Cross-section through Cavern 7 and Cavern 19.....	16
Figure 4:	Three dimensional representation of the Bayou Choctaw salt dome.	17
Figure 5:	Geometry of the Bayou Choctaw salt dome as viewed from directly overhead.	17
Figure 6:	Oblique view of the thickness of the caprock on top of the Bayou Choctaw salt dome.....	18
Figure 7:	Stratigraphy near the Bayou Choctaw salt dome and the thickness of each layer used for modeling.....	19
Figure 8:	Major diameter and minor diameter of salt dome for modeling.	20
Figure 9:	Schematic diagram of the SPR caverns.....	27
Figure 10:	Visualizations of the six SPR caverns (in red) in the dome.	28
Figure 11:	UTP caverns shown diagrammatically, not in actual configuration.	28
Figure 12:	Well head histories of each SPR cavern.....	31
Figure 13:	Schematic diagram of a typical SPR cavern with the inlet and outlet tubes and valves.	31
Figure 14:	Overview of the finite element mesh of the stratigraphy and cavern field at Bayou Choctaw.	34
Figure 15:	Mesh for salt dome and caprock.....	35
Figure 16:	Cavern layout in the salt dome mesh as compared with the actual salt dome. The six SPR caverns are shown in red.....	36

Figure 17: Various views of the cavern geometry within the Bayou Choctaw salt dome. For comparison purposes to show how large caverns are, a silhouette of the Sears Tower is shown inside Cavern 18.	37
Figure 18: Finite mesh discretization and boundary conditions at Bayou Choctaw.....	38
Figure 19: Normalized volume decrease of each SPR cavern in the BC salt dome.	39
Figure 20: Normalized average decrease in storage volume for the six SPR caverns in the BC salt dome.....	39
Figure 21: Predicted volumetric closure normalized by cavern volume for Cavern 101 with the field data as shown Figure 18.	41
Figure 22: Superposed volumetric closure rate for comparing with the field data.....	42
Figure 23: Uncorrected and corrected normalized average decreases in storage volume for the six SPR caverns with the field data as shown Figure 19 for SMF of 0.12.....	42
Figure 24: Dilatancy criteria for Bayou Choctaw salt with field data.	46
Figure 25: Displacement vectors around Caverns 15 and 17 at 21 years	51
Figure 26: Displacement vectors around Caverns 18 and 20 at 21 years	51
Figure 27: Displacement vectors around Caverns 19 and 101 at 21 years	52
Figure 28: Vertical displacement contours around Cavern 15 and 17 at 21 years	52
Figure 29: Vertical displacement contours around Cavern 18 and 20 at 21 years	53
Figure 30: Vertical displacement contours around Cavern 19 and 101 at 21 years	53
Figure 31: Predicted overall volumetric closure normalized to overall storage volume for the six SPR caverns immediately following each leach.	54
Figure 32: Normalized volumetric closure of each cavern with time. The volumes were normalized by the volume of the cavern immediately following each leach.	54
Figure 33: Volumetric changes of each cavern due to leaching and salt creep closure over time	55
Figure 34: Predicted volume change for each non-SPR cavern over time	55
Figure 35: Predicted subsidence on the surface near the center of each cavern.	56
Figure 36: Vertical displacement contours prior to 1st leach (upper left) and immediately before 6th leach (lower left) for the section through Cavern 15 and Cavern 17.....	57
Figure 37: Vertical displacement contours prior to 1st leach (upper left) and immediately before 6th leach (lower left) for the section through Cavern 20 and Cavern 18.....	57
Figure 38: Vertical displacement contours prior to 1st leach (upper left) and immediately before 6th leach (lower left) for the section through Cavern 101 and Cavern 19.....	58
Figure 39: Predicted radial surface strains prior to leaching (left) and after the 5 th leaching (right)	58
Figure 40: Vertical strains near Caverns 15 and 17 prior to 1 st leach (left) and after the 5 th leach (right).	59
Figure 41: Vertical strains near Caverns 18 and 20 prior to 1 st leach (left) and after the 5th leach (right)	59
Figure 42: Vertical strains near Caverns 19 and 101 prior to 1 st leach (left) and after the 5th leach (right)	60
Figure 43: Minimum compressive stress as a function of time	61
Figure 44: Minimum compressive stress contours around Caverns 18 and 20 during workover of Cavern 18.....	61
Figure 45: Minimum compressive stress contours around Caverns 18 at 37.33 years during workover. The left diagram is of the vertical cross-section through the center of the cavern	

and the right diagram is of the horizontal cross-section. The red lines show where the mesh was cut.	62
Figure 46: Minimum safety factor against dilatant damage	63
Figure 47: Safety factor contours against dilatant damage during workover of Caverns 15 and 17 after 5 th leach, vertical cross-section through the centers of caverns (Left) and horizontal cross-section at the elevation where minimum safety factor occurs (Right). The blue lines show where the mesh was cut.	63
Figure 48: Safety factor contours against dilatant damage during first workover of Cavern 20 after initial leach, vertical cross-section through the centers of Caverns 18 and 20 (Left) and horizontal cross-section at the elevation where minimum safety factor occurs (Right). The blue lines show where the mesh was cut.	64
Figure 49: Safety factor contours against dilatant damage during workover of Cavern 20 after 5 th leach, vertical cross-section through the centers of Caverns 18 and 20 (Left) and horizontal cross-section at the elevation of mid-height of Cavern 20 (Right). The blue lines show where the mesh was cut.	64
Figure 50: Contour plots of minimum compressive stress on the top of the salt dome at 12 years since initial leach. The line shows where the mesh was cut for Figure 51.....	65
Figure 51: Contour plots of minimum compressive stress of the caprock at 12 years since initial leach. The line shows where the mesh was cut for Figure 51.....	66
Figure 52: Contour plots of minimum compressive stress on the section through Caverns 7 and 4 at 12 years since initial leach.	66
Figure 53: Contour plots of the minimum compressive stress on the caprock at 1, 13, 21, and 46 years.	67
Figure 54: Well head histories of each SPR cavern for Scenario 2.....	69
Figure 55: Predicted total volumetric closure normalized to overall storage volume for the six SPR caverns immediately following each leach for Scenario 2 and original workover history.	70
Figure 56: Volumetric closure of each SPR cavern, normalized by cavern volume, immediately following each leach for Scenario 2.....	71
Figure 57: Volume change of each cavern due to salt creep closure and leach over time for Scenario 2.....	71
Figure 58: Predicted subsidence near the center of each cavern on the surface for Scenario 2 ...	72
Figure 59: Predicted radial surface strains prior to leach (left) and after 5 th leach (right) for Scenario 2.....	73
Figure 60: Vertical ground strains near Caverns 15 and 17 for Scenario 2 prior to the 1 st leach at 21 years (left) and after the 5 th leach (right).	73
Figure 61: Vertical ground strains near Caverns 18 and 20 for Scenario 2 prior to the 1 st leach at 21 years (left) and after the 5 th leach (right).	74
Figure 62: Vertical ground strains near Caverns 19 and 101 for Scenario 2 prior to the 1 st leach at 21 years (left) and after the 5 th leach (right)	74
Figure 63: Minimum compressive stress histories for Scenario 2.....	75
Figure 64: Minimum compressive stress contours around Caverns 15 and 17 during workover of both caverns. The left diagram is of the vertical cross-section through the centers of the caverns and the right diagram is of the horizontal cross-section. The red lines show where the mesh was cut.	76

Figure 65: Minimum compressive stress contours around Caverns 18 and 20 during workover of both caverns.	76
Figure 66: Minimum safety factor against dilatant damage as a function of time for Scenario 2.	77
Figure 67: Safety factor contours against dilatant damage during workover of Caverns 15 and 17 after 4 th leach for Scenario 2, vertical cross-section through the centers of caverns (Left) and horizontal cross-section at the elevation of three quarter-height of Cavern 15 (Right). The blue liens show where the mesh was cut.	78

TABLES

Table 1: Geometric parameters of the salt dome at Bayou Choctaw.....	21
Table 2: Material properties of halite measured at the WIPP and WH site.....	22
Table 3: Assumed material properties of sandy overburden	23
Table 4: Material properties of caprock.....	23
Table 5: Material properties of the rocks surrounding the salt dome (sandstone).....	23
Table 6: Geometric parameters for 24 caverns considered in the simulation.....	25
Table 7: Drill date, use and status for 24 caverns in BC dome.....	26
Table 8: Range of operating pressures measured at the wellhead for SPR caverns at BC.	29
Table 9: Recent workover dates for SPR caverns.....	30
Table 10: Material parameters of Bayou Choctaw salt used in the analyses.....	43
Table 11: Material properties of the lithologies around salt dome used in the analyses.	43
Table 12: Failure and dilatancy criteria data for Bayou Choctaw Salt.	45
Table 13: Applicable software and version number	49
Table 14: File naming convention for Bayou Choctaw SPR caverns calculations.....	50

NOMENCLATURE

BC	Bayou Choctaw
BH	Big Hill
BMSL	Below Mean Sea Level
CGZ	Clay and Gypsum Zone
DOE	U.S. Department of Energy
DILFAC	DILatant damage FAcTOR
FEM	Finite Element Method
GAZ	Gypsum-Anhydrite Zone
MCS	Minimum Compressive Stress
MMB	Million barrels
RF	elastic modulus Reduction Factor
SMF	Structural Multiplication Factor
SNL	Sandia National Laboratories
SPR	Strategic Petroleum Reserve
UTP	Union Texas Petroleum
WIPP	Waste Isolation Pilot Plant
UTM	Universal Transverse Mercator
WH	West Hackberry

1. INTRODUCTION

1.1. Objective

Recent advances in the state-of-art in geomechanics modeling have enabled 3D analyses to be performed. Three dimensional analyses capture the actual geometry and layout of a cavern field and result in more realistic simulations. The complexities within the Bayou Choctaw (BC) cavern field require such advanced simulations as the field has a long history of development resulting in 24 caverns of various shapes, depths, and states. This report attempts to model these conditions and addresses the resulting performance and stability issues.

1.2. Background

The US Strategic Petroleum Reserve (SPR) stores crude oil in 62 caverns located at four different sites in Texas and Louisiana (Figure 1). The reserve contains approximately 700 million barrels (MMB). Most of the caverns were solution mined by the Department of Energy (DOE) and are typified as cylindrical in shape and emplaced at approximately the same depth. The exceptions to this are caverns acquired by the DOE. Of the six SPR caverns at BC five were acquired. The geometry, spacing, and depths of the caverns are irregular. Geotechnical concerns arise due to the close proximity of the some of the caverns to each other (e.g., Caverns 15 and 17) or to the edge of salt (e.g., Cavern 20). In addition to the SPR caverns at BC, nine other caverns, which store various hydrocarbons and operated by private industry, exist. Nine abandoned caverns, one of which collapsed (Cavern 7) and another (Cavern 4) is believed to be in a quasi-stable condition, exist.

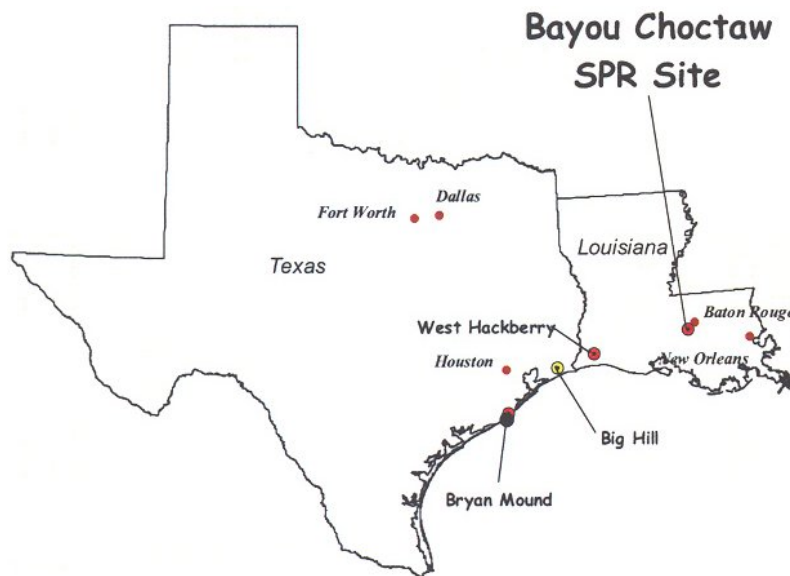


Figure 1: Location of SPR Sites.

1.3. Report Organization

Section 2 introduces the Bayou Choctaw (BC) site by summarizing the location, the history, and the geological description. Section 3 presents an overview of the geomechanical model and cavern model including cavern geometry and layout, model history, and thermal condition. Also included in Section 3 are descriptions of the constitutive models used in the analyses. Section 4 provides the discretized finite element mesh for twenty four caverns array considering five leaches. Section 5 presents back-fitting analysis to determine the unmeasured parameters by calibrating them to best match the field data. Section 6 provides the failure criteria for checking the structural stability of salt dome and allowable strains for wells and surface structures. Section 7 lists the computer codes used for this study, including the finite element code, JAS3D. Section 8 describes the results such as cavern deformation, storage loss with time, subsidence, integrity of cavern wells, checking the cavern stability by dilatant damage criteria and a tensile failure criterion. Section 9 describes the analysis result for alternative model history (Scenario 2), and its effect on the structural integrity of SPR caverns. Finally, Section 10 provides the discussion and conclusions.

2. SITE DESCRIPTION

The BC salt dome, located in south-central Louisiana near Baton Rouge (Figure 1), was discovered in 1926. Since then over three hundred oil and gas wells have been drilled on and around the dome, as well as numerous shallow holes drilled into the caprock. Since 1937, Allied Chemical Corporation has drilled over twenty brine wells on the dome. In 1976, the Department of Energy (DOE) purchased eleven of these leached caverns and was storing a total of approximately twenty two million barrels of crude oil in three of the caverns (numbered 15, 18, and 19), forming part of the Strategic Petroleum Reserve (SPR) Program [Hogan, 1980].

Since 1980, SPR caverns 18, 19, and 20 have been enlarged substantially; Union Texas Petroleum (UTP) Caverns 6 and 26 have been constructed, and Caverns 101 and 102 have been leached by DOE. Cavern 102 was traded to UTP in a swap for Cavern 17, now used for SPR oil storage. In 1992 UTP converted its brine Cavern 24 to natural gas storage. UTP had leached in 1993 along the northeast dome edge [Neal et al., 1993].

Data from the 300 oil and gas wells were used to construct contour maps and cross sections of the salt dome and the overlying caprock. Figure 2 shows a plan view of the BC site with salt contour lines defining the approximate location of the salt dome edge. The locations of the six SPR caverns, nine UTP caverns, one inactive cavern, and seven abandoned caverns are included. A vertical cross section through Cavern 7 and Cavern 19 provides a geologic representation near the middle of the dome as shown Figure 3.

The surface and near surface sediments overlying the BC dome are of Pleistocene through Holocene age. The oldest sediments consist of proglacial sands and gravels with some clay layers. These sediments are overlain by alternating sequences of sand, silts and clays [Hogan, 1980].

Two distinct zones are found in the caprock at BC: an upper zone, termed the clay and gypsum zone (CGZ); and the lower zone, called the massive gypsum-anhydrite zone (GAZ). The CGZ is composed of layers of gypsum intercalated with clay. The proportion of clay to gypsum is highly variable, with generally more clay than gypsum. The GAZ is predominantly gypsum-anhydrite with minor amounts of clay, sand and gypsum [Hogan, 1980].

The top of the BC salt dome lies between 600 and 700 ft below the surface. The east flank dips gently downward to 1,500 feet where the dip increases to approximately 80° between 2,000 and 6,000 ft. The west flank of the dome is overhung between 1,000 and 5,000 ft. Below 6,000 to 8,000 ft, the slope of the salt surface diminishes to about 60° [Hogan, 1980].

The lithology surrounding the salt dome contains up to 30,000 ft of silts, sands, shales, limestones and evaporites. These sediments were deposited in a variety of sedimentary environments including desert basin, evaporating flat, ocean basin and delta [Hogan, 1980].

Figure 4 shows three dimensional representation of the BC salt dome constructed by digitally putting together the separate models of the flank and top of salt. A view from directly overhead is shown in Figure 5. The outline of salt dome is generally oval in plan view. The transition from steeply dipping flanks to the relatively flat-lying dome crest occurs between depths of 1,000 to

2,000 ft in the eastern portion of the dome and quite abruptly at approximately 1,000 ft in the west. A visualization of the caprock overlying the BC salt dome is presented in Figure 6. The average thickness of the caprock is approximately 150 ft, however in some locations it can be in excess of 400 ft [Rautman and Stein, 2004].

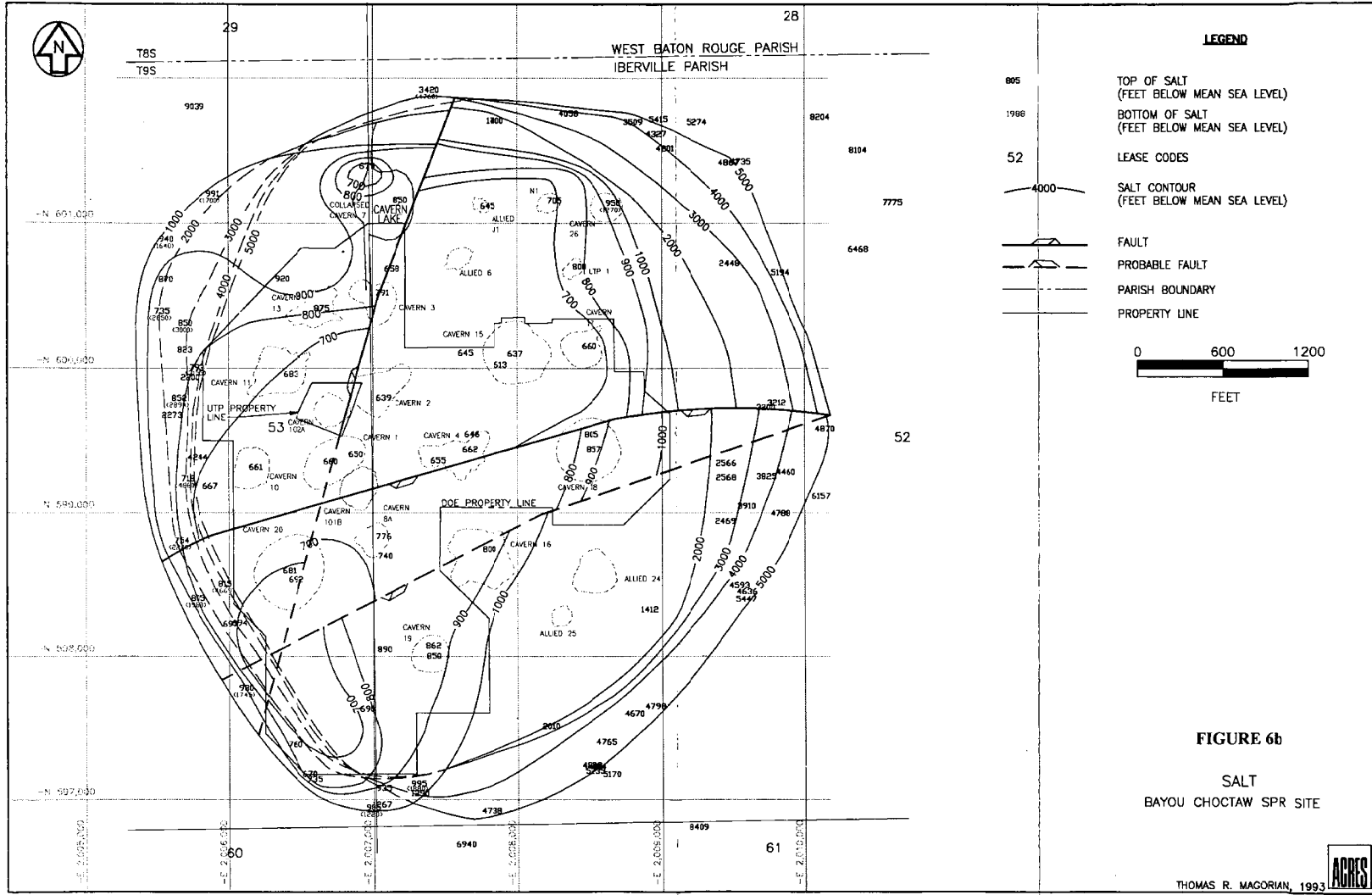


Figure 2: Bayou Choctaw site plan view [Neal et al., 1993]

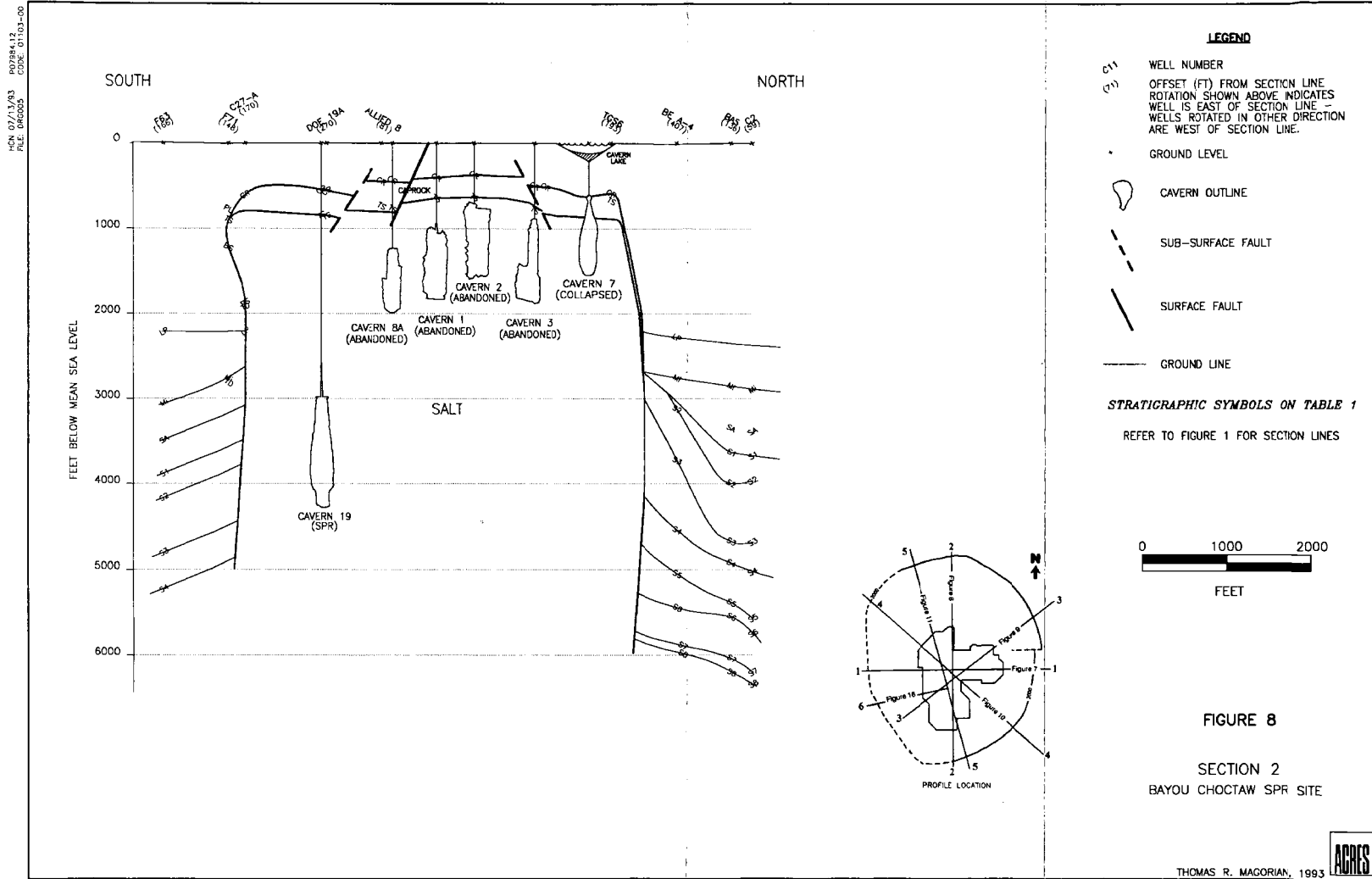


Figure 3: Cross-section through Cavern 7 and Cavern 19 [Neal et al., 1993]

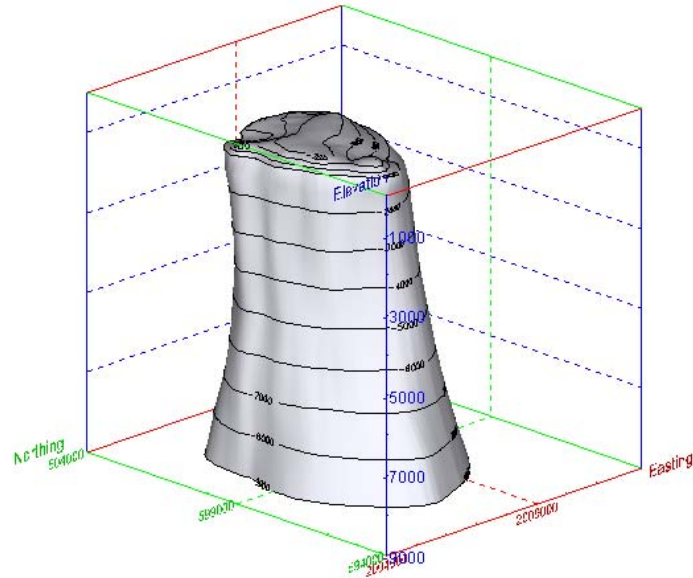


Figure 4: Three dimensional representation of the Bayou Choctaw salt dome [Rautman and Stein, 2004].

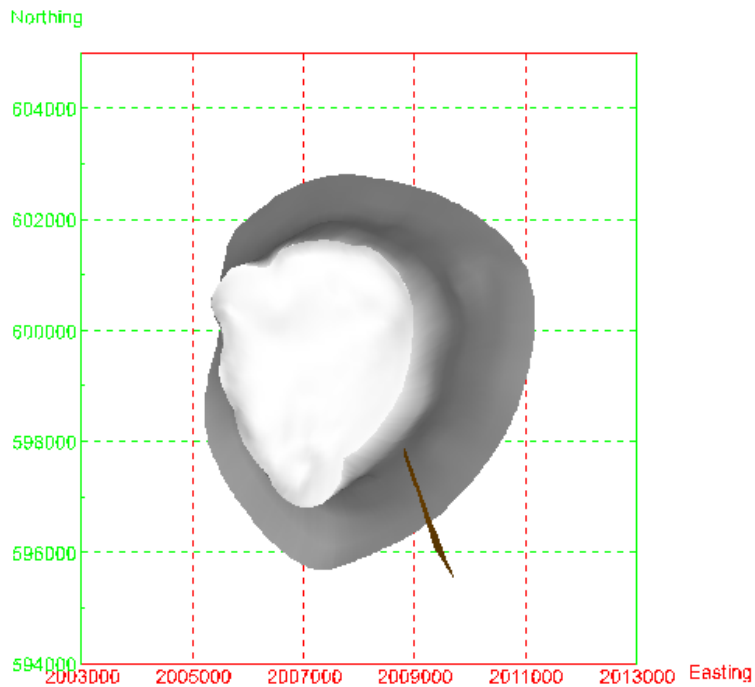


Figure 5: Geometry of the Bayou Choctaw salt dome as viewed from directly overhead (elevation=90°) [Rautman and Stein, 2004].

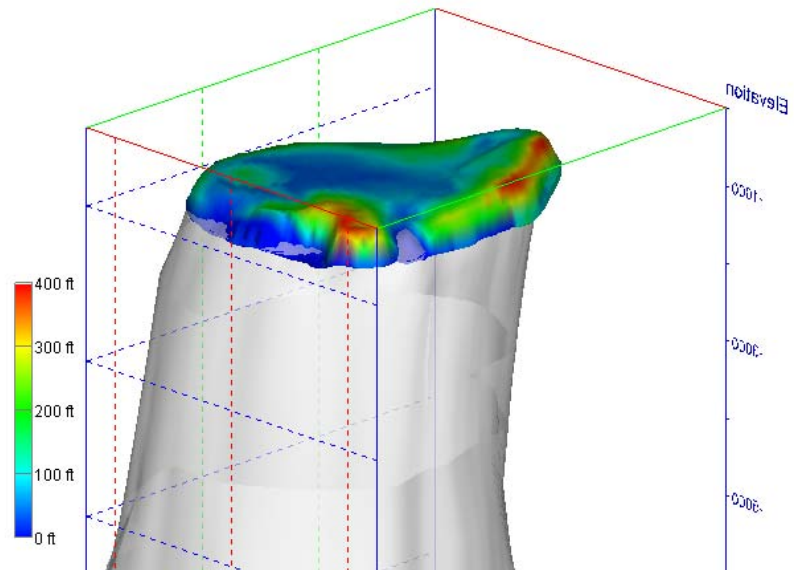


Figure 6: Oblique view of the thickness of the caprock on top of the Bayou Choctaw salt dome (gray). View is from azimuth 315°, elevation 20° above the horizontal [Rautman and Stein, 2004].

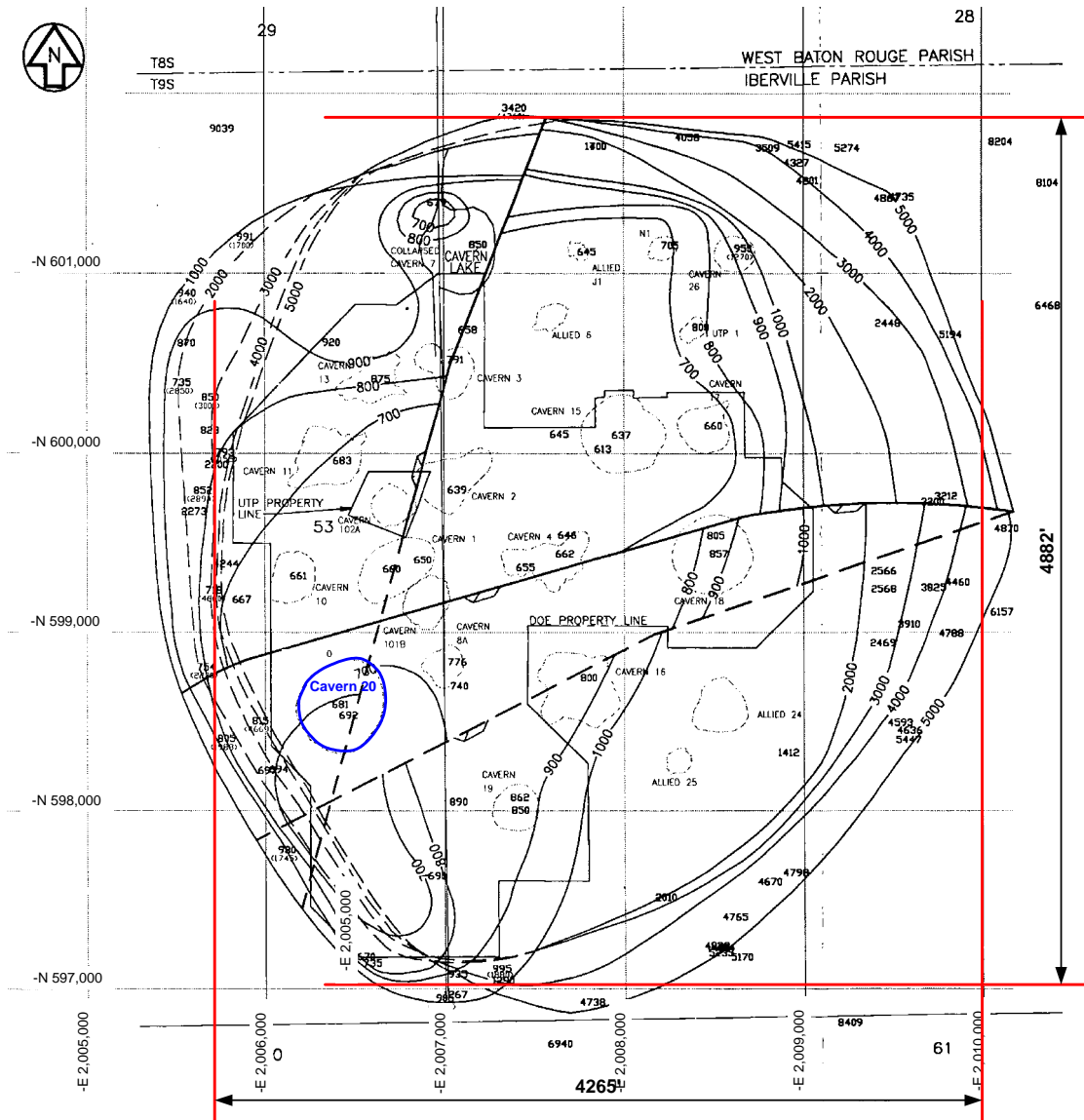


Figure 8: Major diameter and minor diameter of salt dome for modeling.

The horizontal section of the dome forms an ellipse as shown Figure 2. The major and minor radii are obtained using the 4,000 ft contour, which is half of the model depth, by hand measuring the distances in Figure 8. Cavern 20 is closest to the dome edge. The structural integrity of the web between Cavern 20 and the edge will be checked in this simulation. The elevation of Cavern 20 is approximately 4,000 ft below the surface. Thus, the 4,000 ft contour was selected to get the radii of salt dome. The major and minor radii are measured to be 4,882 ft and 4,265 ft, respectively. The geometric parameters of the dome are estimated from Figure 7 and Figure 8 as listed in Table 1.

Table 1: Geometric parameters of the salt dome at Bayou Choctaw

UTM Coordinate of West Edge at 4000 ft BMSL	E	2,005,738	ft
UTM Coordinate of East Edge at 4000 ft BMSL	E	2,010,000	ft
UTM Coordinate of South Edge at 4000 ft BMSL	N	597,000	ft
UTM Coordinate of North Edge at 4000 ft BMSL	N	601,881	ft
UTM Coordinate of Center at 4000 ft BMSL	E	2,007,869	ft
UTM Coordinate of Center at 4000 ft BMSL	N	599,440	ft
Major Diameter at 4000 ft BMSL		4,881	ft
Minor Diameter at 4000 ft BMSL		4,262	ft
Avg. Elevation Top Salt		-650	ft
Avg. Elevation Top Caprock		-500	ft
Height of Salt Dome		7,350	ft
Thickness of Caprock		150	ft
Thickness of Overburden		500	ft
Height of Surrounding Rock		7,500	ft

Note: BMSL –Below Mean Sea Level

UTM – Universal Transverse Mercator

3.1.2. Salt constitutive model

The creep response from a core specimen of BC salt from a deep borehole in Well 19A was determined using an incremental stress and temperature change procedure [Wawersik and Zeuch, 1984]. This material was medium grained, with the maximum grain size of 0.75 in. The principal impurity in the salt was uniformly distributed anhydrite crystals. The anhydrite concentration in this specimen was probably no more than 4.2%, based on dissolution of specimen remains. As a consequence, the BC salt appears to be more creep resistant than the WIPP (Waste Isolation Pilot Plant) clean salt by about a factor of 0.17. BC salt is classified as hard salt; while BH and WH salt are classified as soft salts [Munson, 1998].

A power law creep model is used for the salt creep constitutive model, which considers only secondary or steady-state creep. The creep strain rate is determined from the following effective stress law:

$$\dot{\epsilon} = A \left(\frac{\sigma}{\mu} \right)^n \exp \left(- \frac{Q}{RT} \right) \quad (1)$$

where, $\dot{\epsilon}$ = creep strain rate,

σ = effective or von Mises stress,

μ = shear modulus, $E/2(1+\nu)$, where E is Young's modulus and ν is Poisson's ratio
 T = absolute temperature,
 A, n = creep constants determined from fitting the model to creep data,
 Q = effective activation energy,
 R = universal gas constant.

The geomechanical properties of BC salt are not entirely known for modeling. The BC field data for the creep constants, the stress exponent, and the thermal constant do not exist. To augment this lack of material data, the material properties of other salts are considered.

The elastic and creep constants measured at the WIPP and WH sites are given in Table 2. The properties assume a homogeneous material. The elastic modulus was reduced from the value measured in the laboratory to account for large scale discontinuities and fracturing of the caprock [Preece and Foley, 1984]. Using a reduced modulus has been shown to simulate the transient response of salt around underground excavations [Morgan and Krieg, 1988]. The elastic modulus reduction factor (RF) is known to vary from salt to salt [Munson, 1998]. Limited creep testing of SPR salts [Wawersik and Zeuch, 1984] showed considerable variability in creep rates (up to an order of magnitude difference). Therefore, the RF and the secondary constants of salt will be determined by calibrating those to best match the measured volume closure of caverns at the BC site through back-fitting analyses. Details are provided in Section 5.

Table 2: Material properties of halite measured at the WIPP and WH site

Parameter		Unit	Value	Site	References
Young's modulus (E)		psi	4.496×10^6	WIPP	Krieg, 1984
Density (ρ)		lb/in ³	0.083	WIPP	Krieg, 1984
Poisson's ratio (ν)		-	0.25	WIPP	Krieg, 1984
Bulk modulus (K)		psi	3.002×10^6	WIPP	Krieg, 1984
Two mu (2μ)		psi	1.798×10^6	WIPP	Krieg, 1984
Secondary Constants	Creep Constant (A)	Pa ^{-4.9} /s	5.79×10^{-36}	WIPP	Krieg, 1984
	Stress Exponent (n)		4.9	WH	Wawersik and Zeuch, 1984
	Thermal Constant (Q)	cal/mol	12000	WH	Wawersik and Zeuch, 1984

3.1.3. Material properties of lithologies around the salt dome

The surface overburden layer, which is mostly comprised of sand, is expected to exhibit elastic material behavior. The sand layer is considered isotropic, and has no assumed failure criteria. The required model parameters for the overburden are not available for BC, so the McCormick Ranch Sand properties used in the WH analysis [Ehgartner and Sobolik, 2002] were used instead. These properties are listed in Table 3.

The caprock layer, consisting of gypsum, anhydrite and sand, is also assumed to behave elastically. Samples of caprock from core holes at BC were tested by Dames and Moore [1978] to determine physical properties. The tested samples were from the massive gypsum-anhydrite unit at depths of 602 ft and 645 - 648 ft in Core Hole 1 and 558 - 642 ft in Core Hole 2 [Hogan, 1980]. The caprock parameters used in this analysis are listed in Table 4.

The sedimentary rocks surrounding the salt dome are assumed to be isotropic, homogeneous elastic sandstone. The required model parameters of the surrounding rocks are also not available either. In lieu of this information density and Poisson's ratio were assumed to be the same as that of California mine sandstone [Lama and Vutukuri, 1978]. Young's modulus of this sandstone is assumed to have the wide range from 5.802×10^4 to 1.105×10^7 psi [Carmichael, 1984] because it is an important parameter in the structural analysis and varies greatly from site to site. The mechanical properties used in the present analysis are listed in Table 5.

Table 3: Assumed material properties of sandy overburden [Ehgartner and Sobolik, 2002]

Parameter	Unit	Value
Density	lb/in ³	0.068
Young's Modulus	psi	1.45×10^4
Poisson's Ratio		0.33

Table 4: Material properties of caprock [Hogan, 1980]

Parameter	Unit	Value
Density	lb/in ³	0.084
Young's Modulus	psi	2.277×10^6
Poisson's Ratio		0.288

Table 5: Material properties of the rocks surrounding the salt dome (sandstone) [Lama and Vutukuri, 1978; Carmichael, 1984]

Parameter	Unit	Value
Density	lb/in ³	0.090
Young's Modulus	psi	5.802×10^4 to 1.105×10^7
Poisson's Ratio		0.33

3.2. Cavern Model

3.2.1. Cavern geometry and layout

The cavern shapes and locations vary widely as shown in Figure 2 and Figure 3. Since the six SPR caverns and eighteen other caverns have structural interactions, a model including all caverns in the dome should be considered to investigate the SPR structural behavior.

Fifteen active and nine abandoned caverns exist at BC, producing a total cavern volume of some 164 million barrels (MMB). This includes 81 MMB in six SPR caverns, 31 MMB in nine UTP caverns, and about 52 MMB in abandoned caverns. Cavern 7 collapsed in 1954 and was filled with overburden material. The total cavern volume is important since the void space affects total creep closure (and consequent subsidence) in the BC salt mass. Creep closure in the BC caverns is relatively small when compared with other domes.

Table 6 lists the geotechnical parameters for the twenty four caverns considered in the present simulation [Neal et al., 1993; Stein, 2005]. The X and Y coordinates of the center of each cavern were calculated by subtracting Universal Transverse Mercator (UTM) coordinates of the center of the dome listed in Table 1 from UTM coordinates of each cavern collected by Stein [2005], i.e. the origin of the coordinates system used in the modeling is the center coordinates of the dome. The geometric parameters for Cavern 7 are estimated from Figure 3 because those are unknown. Information regarding drill date, cavern condition and present use for all caverns in BC dome is presented as Table 7 [Hogan, 1980; Neal et al., 1993; Stein, 2005].

The schematics of six operating SPR caverns are shown in Figure 9. A set of visualizations of the SPR caverns in the dome is presented in Figure 10. Digital sonar-survey data were used to generate the visualizations. The shapes of caverns will be simplified to the cylindrical shapes using the geometric parameters in Table 6. The schematics of nine operating UTP cavern are also shown in Figure 11.

The faults shown in Figure 2 and Figure 3 are ignored in the analysis because the faults did not extend to the deep salt beyond the top of abandoned caverns thus the faults can not affect the structural behavior of the SPR caverns. And, by ignoring the shear zone, the analyses of overburden and the cap rock layers are able to be simplified.

The thickness of the web between Caverns 15 and 17 is 156.6 ft as derived from Figure 9. The distance from Cavern 20 to the edge of the dome is conservatively estimated to be 175 ft [Ehgartner et al., 2003].

Table 6: Geometric parameters for 24 caverns considered in the simulation [Neal et al., 1993; Stein, 2005; Hogan, 1980; Ehgartner et al., 2003]

Cavern Number	X Coordinate of Center	Y Coordinate of Center	Gross Volume	Elevation of Cavern Top	Elevation of Cavern Bottom	Cavern Height	Diameter Average	Last Sonar Date
	ft	ft	MMB	ft	ft	ft	ft	mmm-yyyy
Cavern 1	-1002	-27	8.42	-950	-1810	860	250.0	1977
Cavern 2	-817	369	9.02	-715	-1590	875	260.0	1977
Cavern 3	-821	1082	5.01	-890	-1875	985	200.0	1977
Cavern 4	-212	12	5.98	-620	-1710	1090	280.0	1980
Allied 6	-192	1353	0.82	-1195	-1562	367	126.4	Nov-1990
Cavern 7	-786	1679	4.01	-440	-1560	1120	160.0	Unknown
Cavern 8	-811	-604	3.12	-1235	-1976	741	200.0	1980
Cavern 10	-1706	-118	6.40	-990	-1902	912	200.0	1980
Cavern 11	-1458	521	9.50	-1030	-1800	770	280.0	1978
Cavern 13	-1241	969	4.31	-1103	-1880	777	240.0	1977
Cavern 15	92	669	16.45	-2605	-3296	691	412.0	Mar-1993
Cavern 16	-68	-675	10.49	-2612	-3228	616	349.1	Mar-1989
Cavern 17	573	736	12.17	-2600	-4023	1423	238.0	Mar-1993
Cavern 18	609	43	17.44	-2125	-4219	2094	244.0	Jun-1993
Cavern 19	-477	-1362	12.67	-2935	-4228	1293	260.0	Jun-1993
Cavern 20	-1561	-936	9.17	-3830	-4225	395	514.0	Mar-1993
Allied 24	664	-798	5.59	-3100	-4337	1237	179.1	Apr-1992
Allied 25	451	-1167	7.08	-3575	-5790	2215	151.2	Jun-1992
Cavern 26	747	1669	0.71	-3076	-3470	394	113.2	Sep-1991
Cavern 101	-951	-325	13.06	-2550	-4830	2280	201.0	Jun-1993
Cavern 102	-1169	270	4.20	-2640	-5339	2699	105.5	Oct-1984
Allied J1	-92	1682	0.75	-2854	-3945	1091	69.9	Jul-1989
Allied N1	358	1686	0.49	-2670	-3590	920	61.9	Jan-1987
UTP 1	369	1223	1.41	-2360	-3502	1142	94.0	Aug-1989

Table 7: Drill date, use and status for 24 caverns in BC dome [Hogan, 1980; Neal et al., 1993; Stein, 2005]

Cavern Number	Date Drilled	Use/Product	Status
Cavern 1	Jan-37	Unknown	Abandoned
Cavern 2	Jan-34	Unknown	Abandoned
Cavern 3	Jan-34	Unknown	Abandoned
Cavern 4	Jan-35	Unknown	Inactive
Allied 6	Jan-43	Propylene	UTP
Cavern 7	Jan-42	Unknown	Collapsed
Cavern 8	Jan-44	Unknown	Abandoned
Cavern 10	Jan-47	Unknown	Abandoned
Cavern 11	Jan-47	Unknown	Abandoned
Cavern 13	Jan-48	Unknown	Abandoned
Cavern 15	Jan-53	Petroleum	SPR
Cavern 16	Jan-54	Ethylene	UTP
Cavern 17	Jan-55	Petroleum	SPR
Cavern 18	Jan-67	Petroleum	SPR
Cavern 19	Jan-67	Petroleum	SPR
Cavern 20	Jan-70	Petroleum	SPR
Allied 24	Jan-79	Natural gas	UTP
Allied 25	Jan-79	Brine	UTP
Cavern 26	Jan-90	Brine	UTP
Cavern 101	Jan-90	Petroleum	SPR
Cavern 102	Jan-81	Ethane	UTP
Allied J1	Jan-72	Ethane/Propane	UTP
Allied N1	Jan-72	Ethylene	UTP
UTP 1	Jan-67	Ethylene	UTP

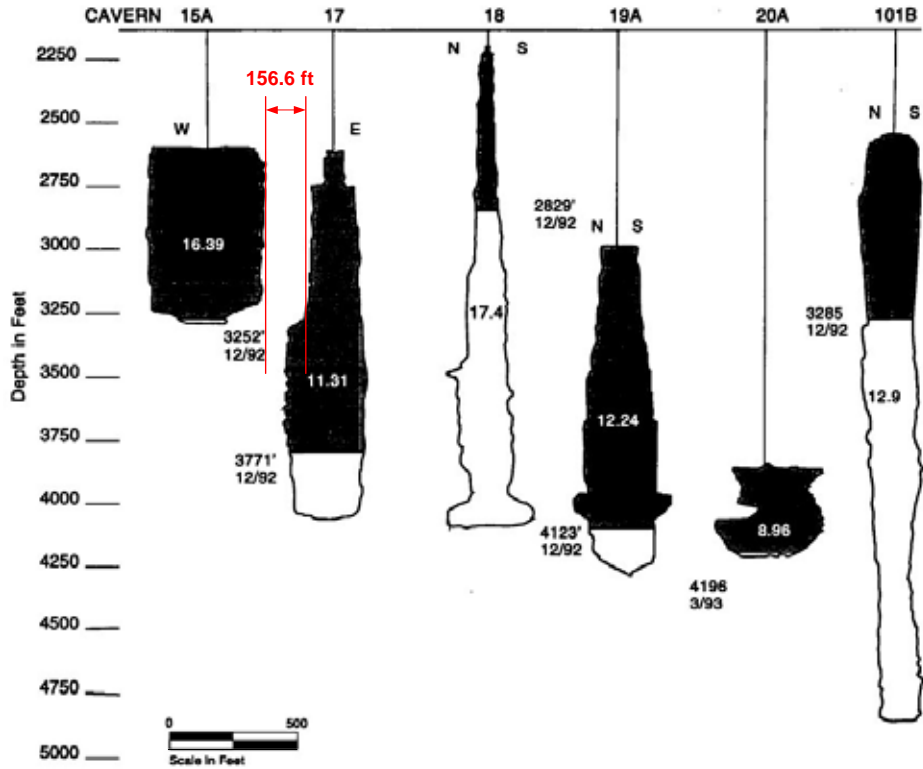


Figure 9: Schematic diagram of the SPR caverns (not in true relationship to one another spatially, except for Cavern 15 and 17) [Neal et. al, 1993].

- Note:
- 1) Refer to Figure 2 for locations.
 - 2) Cavern volumes (in MMB) are from 1992 data and estimation. These numbers are different from those listed in Table 6.
 - 3) Oil/Brine depths in feet.
 - 4) Vertical and horizontal scales are equal.

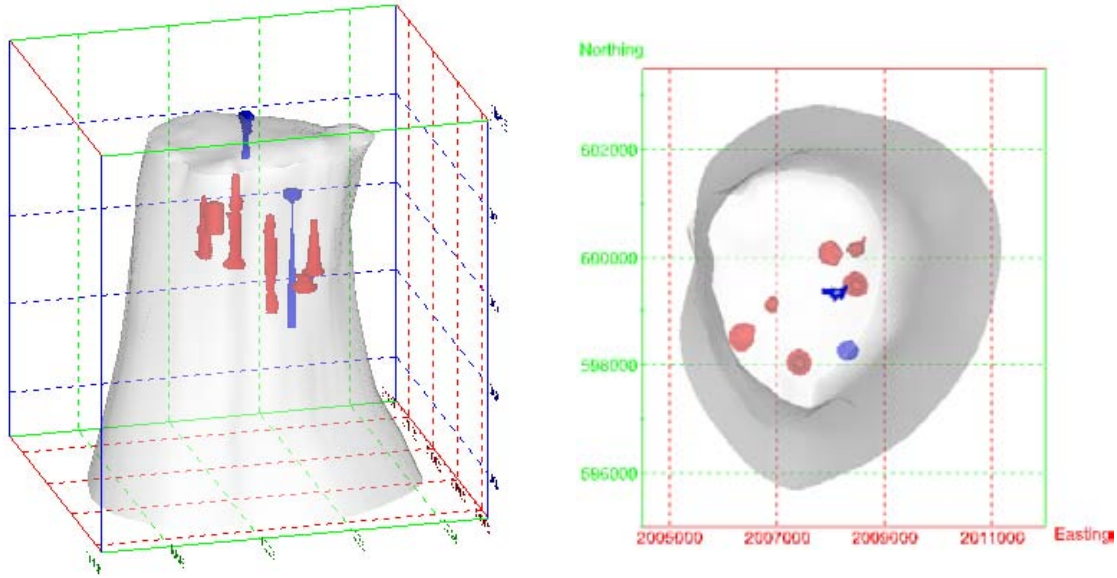


Figure 10: Visualizations of the six SPR caverns (in red) in the dome [Rautman and Stein, 2004].

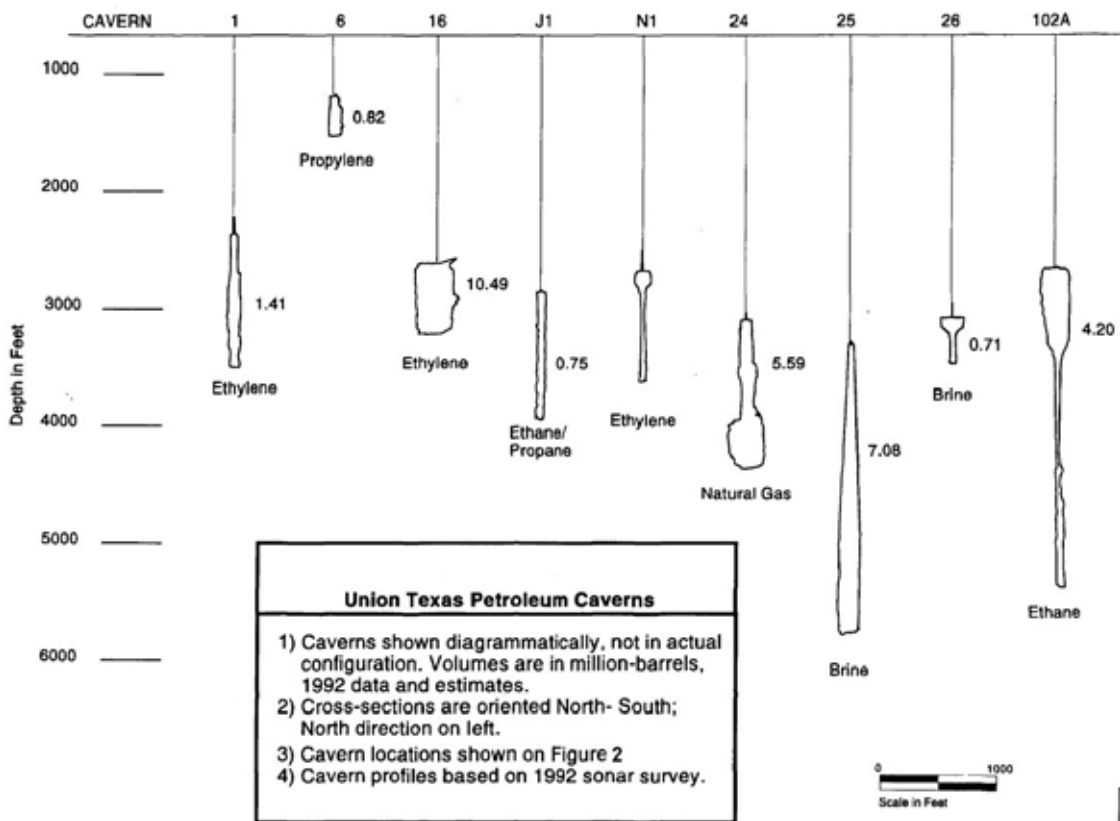


Figure 11: UTP caverns shown diagrammatically, not in actual configuration.

3.2.2. Model history

As listed in Table 7, the drill dates of the caverns varied from 1934 to 1990. The last sonar dates to measure the shape of caverns were between 1977 and 1993, as listed in Table 6. For the purposes of the present simulation, it is assumed that all caverns were drilled twenty-one years ago (i.e., 1985) to simplify the model history. This simulation start time was chosen because it is the average of the sonar measurement dates. The sonar measurement dates represent a time when the cavern geometry had been measured with surety and therefore give a baseline from which volume changes can be determined.

The analysis simulates caverns that were leached to full size over a one year period by means of gradually switching from salt to fresh water in the caverns. It was assumed that the SPR caverns were filled with petroleum and non-SPR caverns were filled with brine at year one, and then permitted to creep for twenty years to reach the preset twenty-one year age for the caverns to be simulated. Subsequently, every 5 years after twenty-one year, the SPR caverns were instantaneously leached. Modeling of the leaching process of the caverns was accomplished by deleting elements along the walls of the caverns so that the volume increased by 15% with each leach. The good salt quality at BC should provide a leach of 15 percent. Leaching is assumed to occur uniformly along the entire height of the cavern. However, leaching is not permitted in the floor or roof of the caverns. The 5-year period between each drawdown allows the stress state in the salt to return to a steady-state condition, as will be evidenced in the predicted closure rates. The simulation executed by right before 6th leach to investigate the structural behavior of the dome for 46 years, during which creep closure to occur in all caverns.

The pressure conditions applied to the caverns were based on an average wellhead pressures listed in Table 8. Cavern 15 operates over a range of pressures from 815 to 990 psi under normal conditions. The pressure starts at 815 psi, then, due to creep and thermal expansion of fluids, the pressure gradually rises to 990 psi. At that time the brine is removed from the cavern to reduce the pressure down to 815 psi again. Thus, on average, a pressure of 903 psi is used for Cavern 15 wellhead pressure operating under normal conditions. In the same manner, the pressures of 903, 715, 925, 850, and 913 psi are used for the normal operating wellhead pressures of Cavern 17, 18, 19, 20, and 101, respectively.

Table 8: Range of operating pressures measured at the wellhead for SPR caverns at BC.

Cavern	Operating Pressure Range (psi)		
	Low	High	Average Pressure
Cavern 15	815	990	903
Cavern 17	815	990	903
Cavern 18	690	740	715
Cavern 19	900	950	925
Cavern 20	825	875	850
Cavern 101	825	1000	913

According to the recent workover dates listed in Table 9, workovers on the five SPR caverns were performed from 12/10/2000 to 7/25/2003. Workover durations for the five caverns varied from 22 days to 36 days. However, Caverns 15 and 17 are currently operated as a gallery, maintaining equal pressures at all times including the workover periods. Thus Caverns 15 and 17 were workovered together and workovers followed on Caverns 19, 18, and 101B in order. Figure 12 shows the well head histories of each SPR cavern. Rather than complicating the analyses, the following assumptions were made based on the actual field conditions for the six SPR caverns:

- A constant pressure is applied for the majority of the time, with pressure drops periodically included.
- For workover conditions, zero wellhead pressure is used.
- The workovers on the Caverns 15 and 17 are performed one year after switching from brine to petroleum. Cavern 19 is workovered 1 month after the workover of Caverns 15 and 17 have been completed. The workover of Cavern 18 starts as soon as the workover of Cavern 19 has been completed. Then, Cavern 20 is workovered 2.5 years later. Finally, Cavern 101 is workovered as soon as the workover of Cavern 20 has been completed. This workover cycle is repeated every 5 years.
- Workover durations are 1 month for all caverns
- For both normal and workover conditions, the caverns are assumed to be full of oil with a pressure gradient of 0.37 psi/ft of depth.

Table 9: Recent workover dates for SPR caverns.

Cavern	Starting Date	Ending Date
Cavern 15	12/10/2000	1/1/2001
Cavern 17	12/31/2000	1/25/2001
Cavern 18	2/25/2001	3/14/2001
Cavern 19	1/30/2001	2/20/2001
Cavern 20	Unknown	Unknown
Cavern 101	6/20/2003	7/25/2003

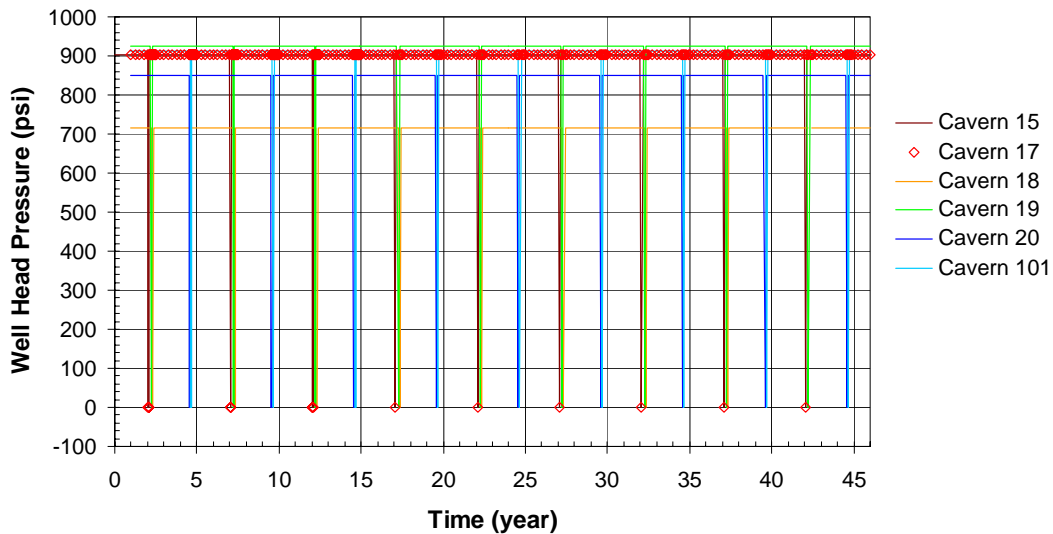


Figure 12: Well head histories of each SPR cavern.

Figure 13 shows the schematic diagram of a typical salt cavern with the inlet and outlet tubes and valves. In the case of SPR caverns, the brine and water valves are closed and a well head pressure is applied to the cavern through the oil tube during the normal operation. Thus the pressure due to the oil head plus the well head is applied on the walls of cavern. All valves are open during the workover, thus the interface of brine and oil rises slowly because brine is heavier than oil. The pressure applied on the cavern wall is conservatively assumed to be the oil head with a pressure gradient of 0.37 psi/ft.

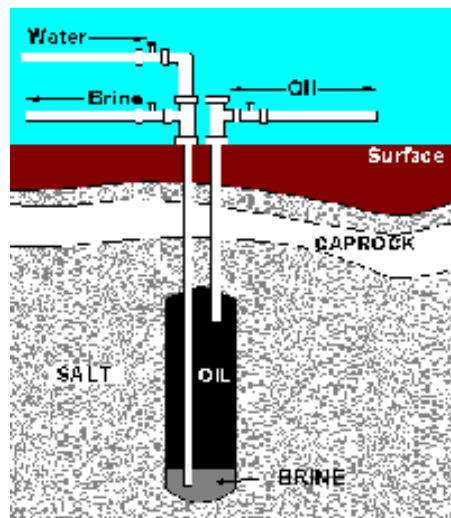


Figure 13: Schematic diagram of a typical SPR cavern with the inlet and outlet tubes and valves.

In the case of non-SPR caverns, except Cavern 7, the oil and water valves are closed and the brine valve is open. Thus the pressure due to brine head with a pressure gradient of 0.52 psi/ft is applied on the cavern walls. Cavern 7 was drilled in 1942 to a depth of 1,951 ft. It collapsed in

1954 and was filled by overburden material, which has an assumed density and Poisson's ratio as listed in Table 3. Thus the pressure gradient of 0.4 psi/ft is applied on the wall and 0.812 psi/ft is applied on the floor and roof.

3.3. Thermal conditions

The finite element model includes a depth-dependent temperature gradient which starts at 84.02 °F (28.90 °C) at the surface and increases at the rate of 0.0138 °F/ft (0.0251 °C/m). The temperature profile is based on the average temperature data recorded in well logs from BC prior to leaching [Ballard and Ehgartner, 2000]. The temperature distribution is important because the creep response of the salt is temperature dependent. Radial temperature gradients due to cavern cooling effects of the cavern product are not considered in these calculations. Previous 2D cavern studies have shown the predicted cavern deformation to be insensitive to the developed radial thermal gradients [Hoffman, 1992].

4. MESH GENERATION

The location and depth of caverns in the BC salt dome are irregular as shown Figure 2 and 3. Symmetry of the modeled region cannot be assumed in the present model as was possible in previous simulations of West Hackberry and Big Hill [Ehgartner and Sobolik, 2002; Park et. al, 2005]. Therefore, a three dimensional mesh was constructed which allows each cavern to be configured individually (see Figure 14 through 17).

Figure 14 shows the overview of the finite element mesh of the stratigraphy and cavern field at BC. The mesh has been separated to show the individual material blocks. The X-axis of model is in the EW (East-West) direction, Y-axis is in the NS (North-South) direction, and Z-axis is the vertical direction. Four material blocks are used in the model for the overburden, caprock, salt dome, and surrounding rocks.

The surrounding rock block surrounds the caprock and salt dome block, and the salt dome block contains 24 caverns. The caprock contains the upper part of Cavern 7 because Cavern 7 collapsed, becoming filled mainly with sand up to the caprock layer. The caprock is made of gypsum, anhydrite, and sand. The surrounding rock is sedimentary rock that consists of sandstone and shale. For simplifying the mesh, the surrounding rocks are assumed to be made of entirely sandstone because Young's moduli of sandstone and shale are similar [Carmichael, 1984].

Figure 15 shows the mesh for the salt dome and the caprock in the surrounding rock block. An elliptical shape is applied to the section of the dome as an approximation for the actual shape of the dome. As mentioned in Section 3.1.1, the lower boundary of the salt dome is considered to extend 8,000 ft below the surface. Since the overburden is 500 ft thick and the caprock is 150 ft thick, the height of the salt dome is assumed to be 7,350 ft. The major and minor diameters of the salt dome are 4,882 ft and 4,265 ft, respectively. Figure 16 shows the cavern layout within the salt dome. The center of each cavern matches the center of each cavern shown in Figure 2. Each SPR cavern is modeled as having five cylindrical layers to be removed to account for the drawdown activities. The diameter of the SPR caverns will be increased by 7.24% per drawdown by deleting elements in the cylindrical layers at 21 years, and subsequently every 5 year.

Figure 17 shows the cavern geometry and the elevation of the caverns. The shapes of all caverns are simplified by cylindrical shapes using the geometrical parameters in Table 6. The caverns can be classified by two groups. One group is above 2,000 ft depth and the other group is below 2,000 ft depth. All the caverns in the upper group are abandoned except Cavern 6. The caverns in the lower group are operated by DOE and UTP.

Figure 18 shows the assembled mesh and the boundary conditions used for the BC model. The salt dome is modeled as being subjected to a regional far-field stresses acting from an infinite distance away. The lengths of the confining boundaries are 24,410 ft in the NS direction and 21,325 ft in the EW direction. These lengths are about five times the major or minor diameter of the salt dome, respectively. This ratio (5) is far better than the generally accepted ratio (3 to 4) between the maximum dimensions/minimum excavation sizes. The model consists of 409,248 nodes and 398,090 elements.

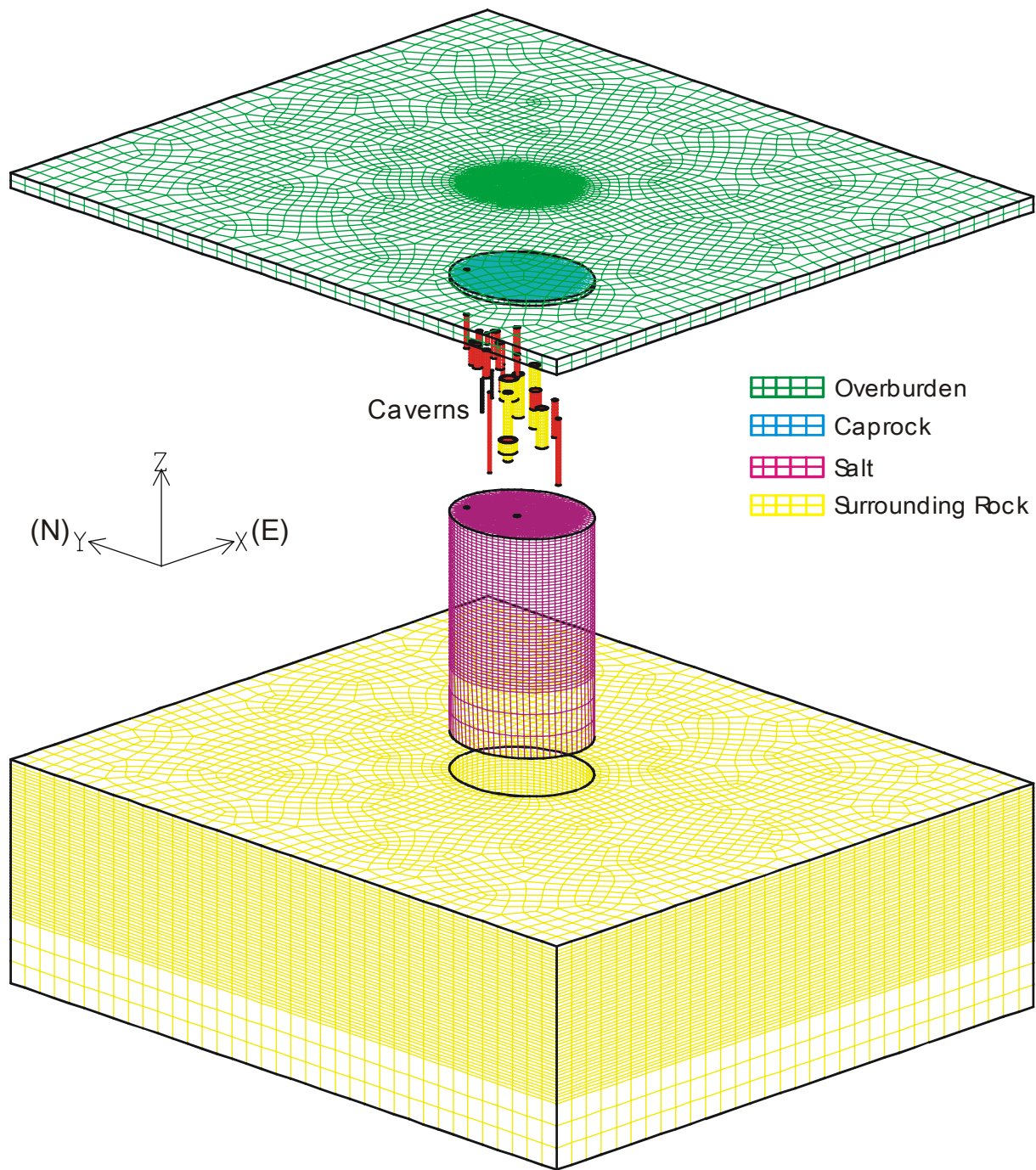


Figure 14: Overview of the finite element mesh of the stratigraphy and cavern field at Bayou Choctaw.

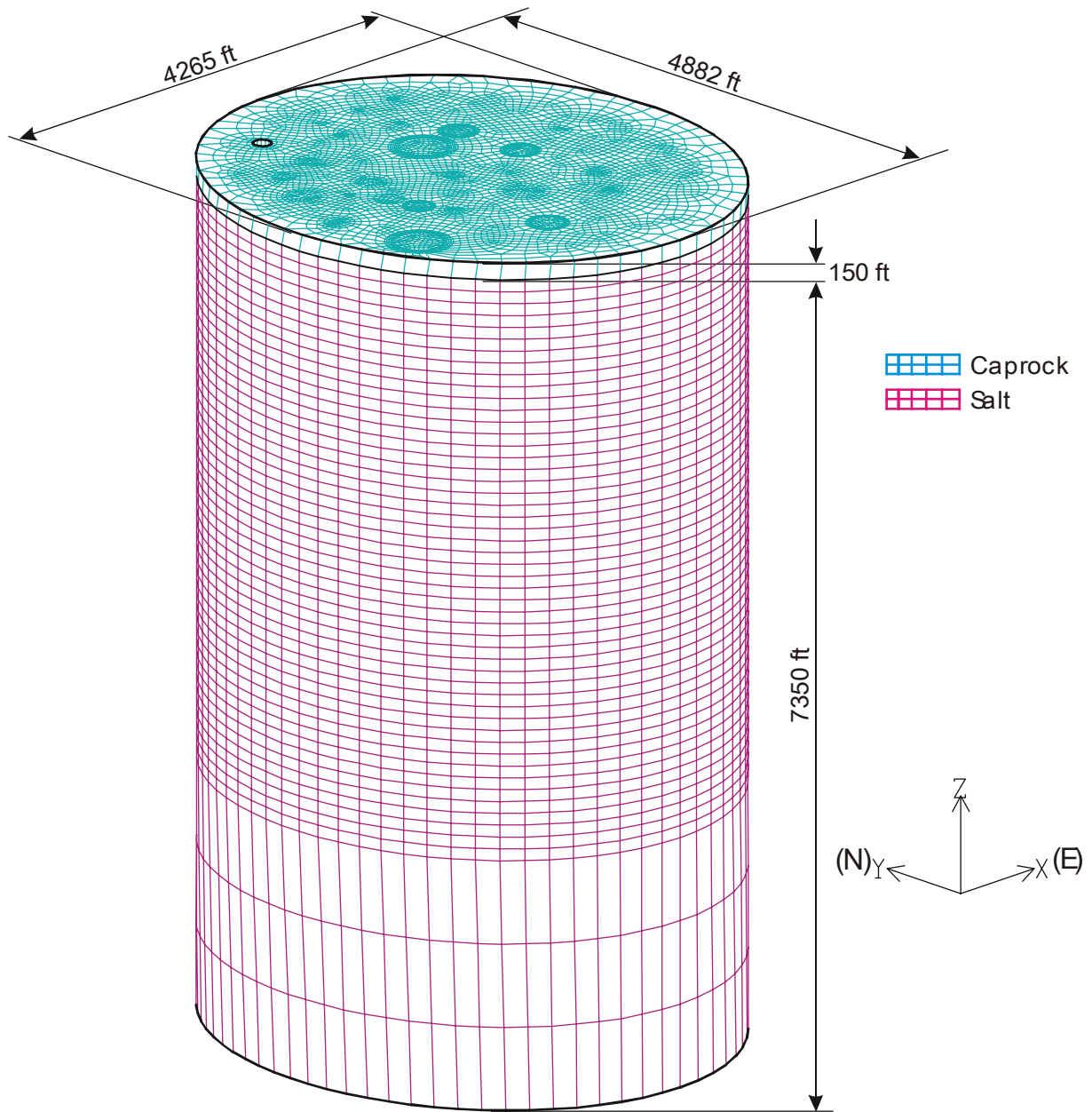


Figure 15: Mesh for salt dome and caprock

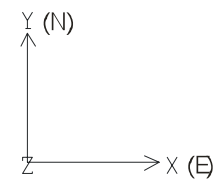
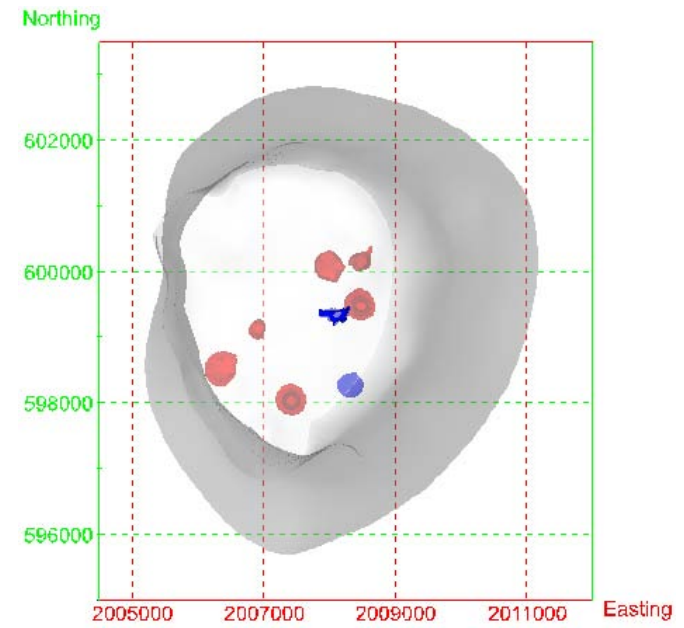
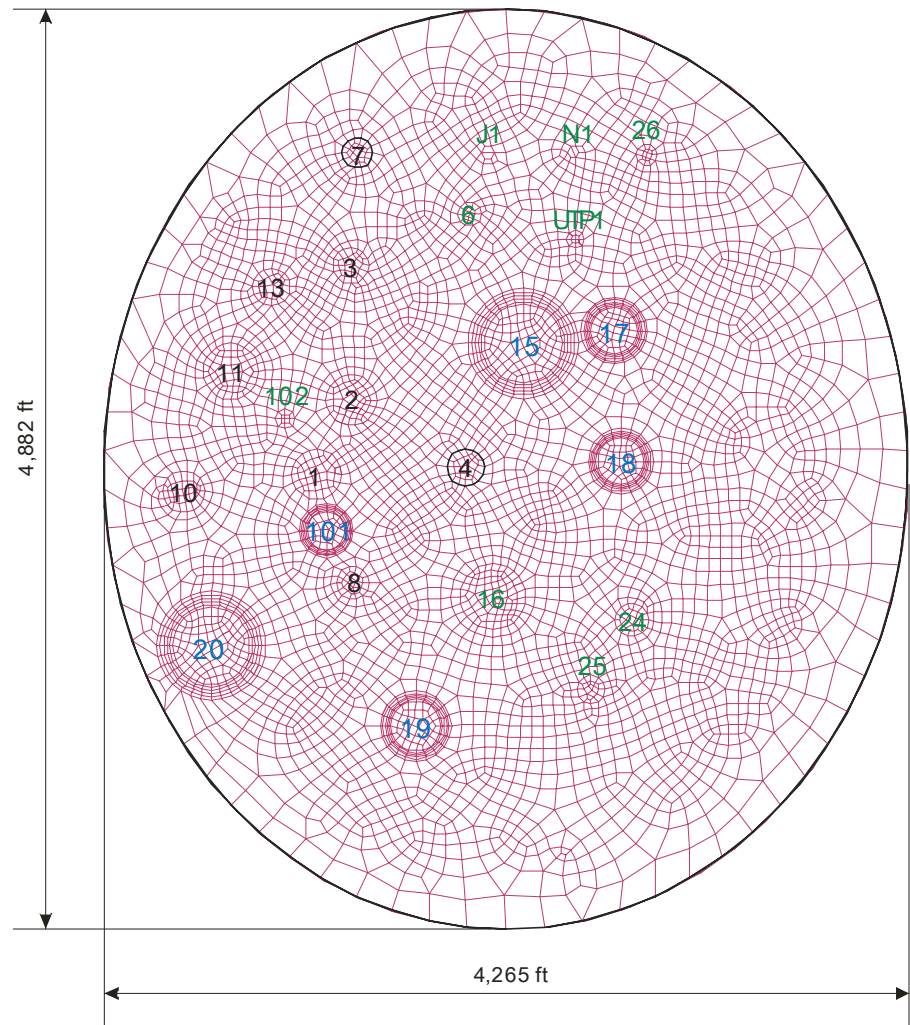


Figure 16: Cavern layout in the salt dome mesh as compared with the actual salt dome. The six SPR caverns are shown in red.

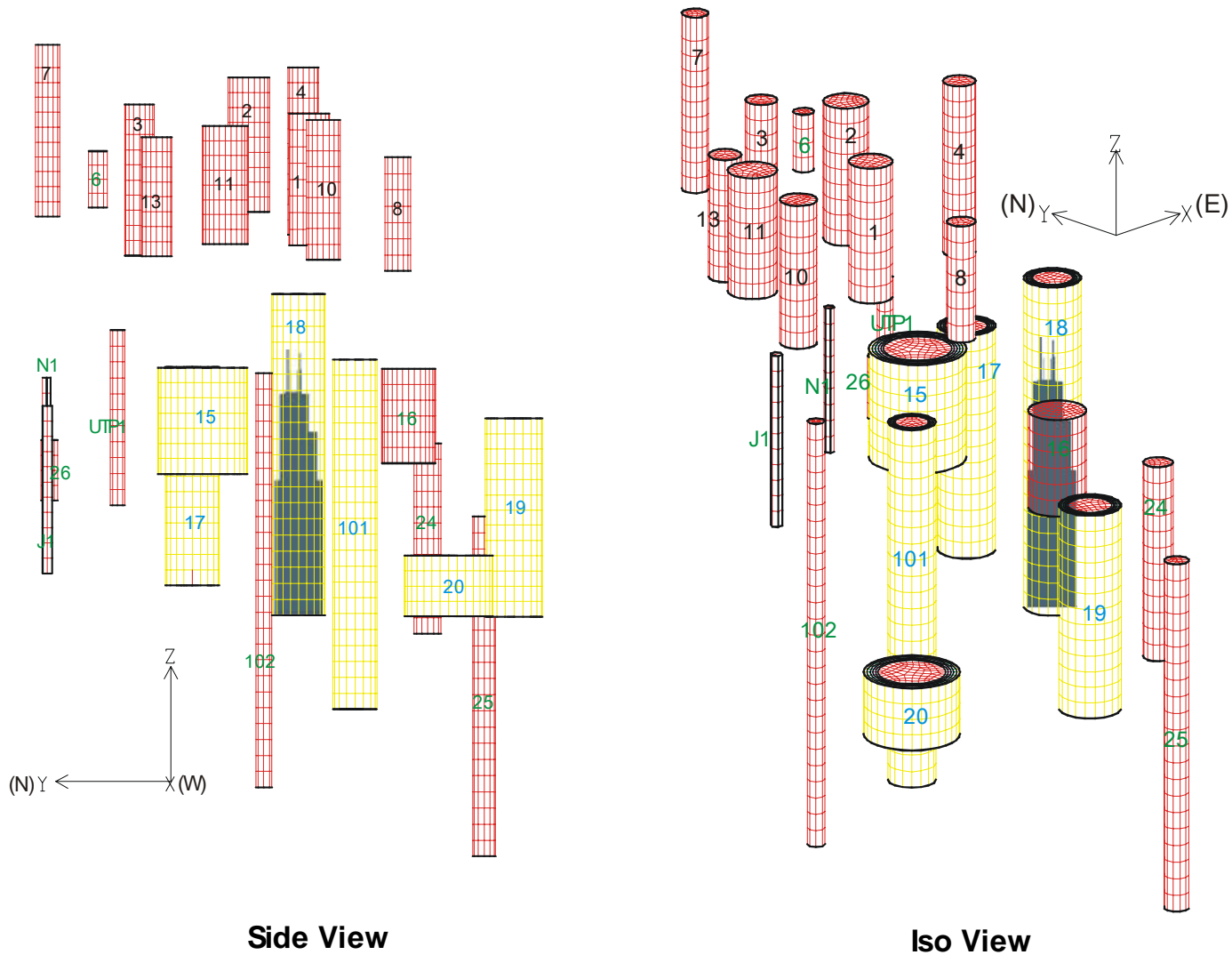


Figure 17: Various views of the cavern geometry within the Bayou Choctaw salt dome. For comparison purposes to show how large caverns are, a silhouette of the Sears Tower is shown inside Cavern 18.

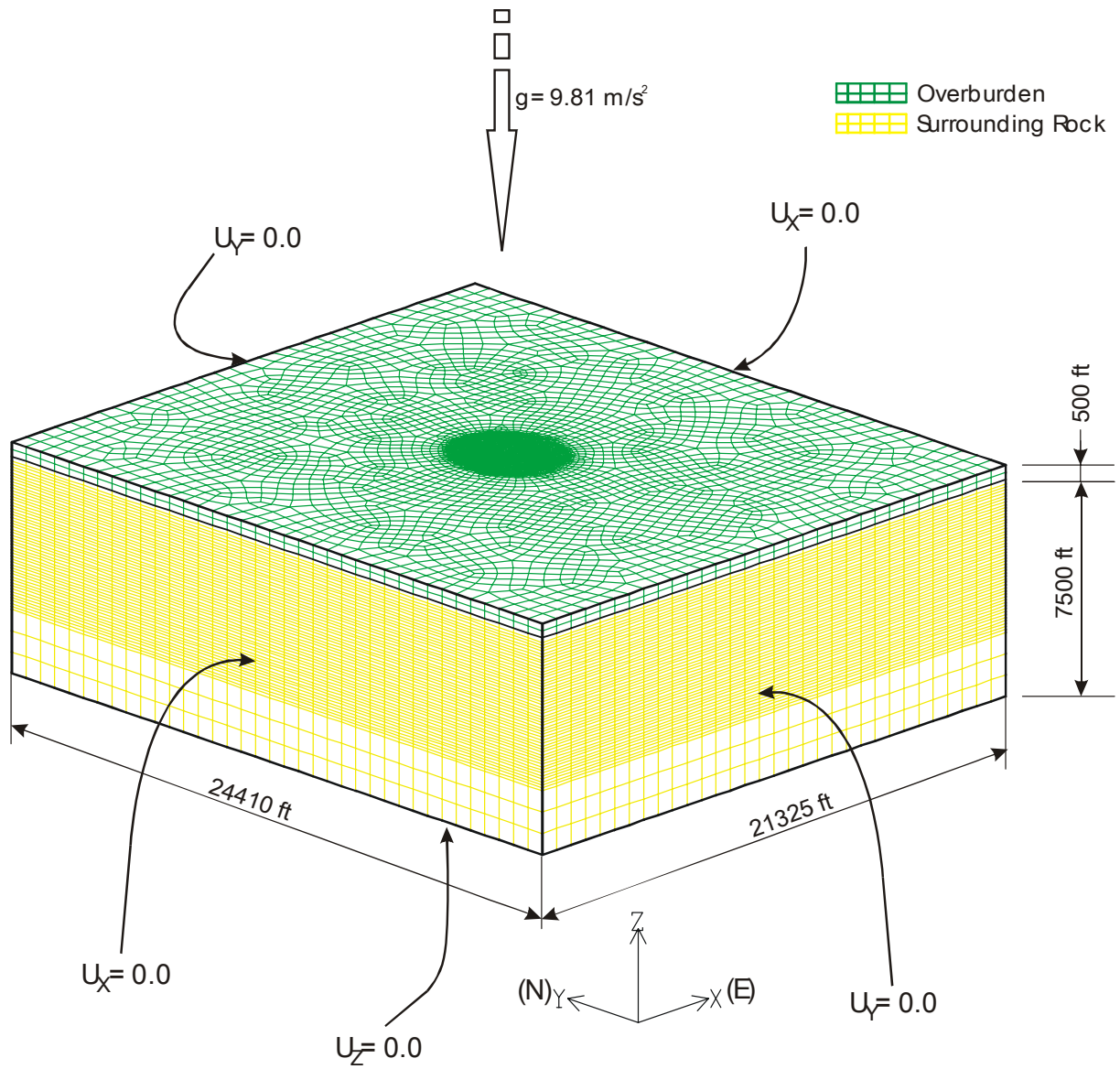


Figure 18: Finite mesh discretization and boundary conditions at Bayou Choctaw.

5. BACK-FITTING ANALYSIS

5.1. Field Data

Volume closure data have been collected from the six SPR caverns in the BC salt dome. Through the back-fitting analysis, the elastic modulus reduction factor (RF) and the secondary constants of the salt can be estimated based on the field data.

Figure 19 shows the normalized volumetric decrease of each SPR cavern since its development. The results were obtained using the latest version of CAVEMAN, a code for SPR cavern pressure analysis [Ballard and Ehgartner, 2000]. These results are based on the measured cavern pressures at the wellhead over the last 52 years [Ehgartner, 2004c]. There are no data measured between 15 and 20 years after the completion of the SPR caverns.

These data were integrated to get the average normalized cavern closure of the six SPR caverns as shown Figure 20. The average volumetric closure in the field was calculated to be 0.041% per year [Ehgartner, 2004c].

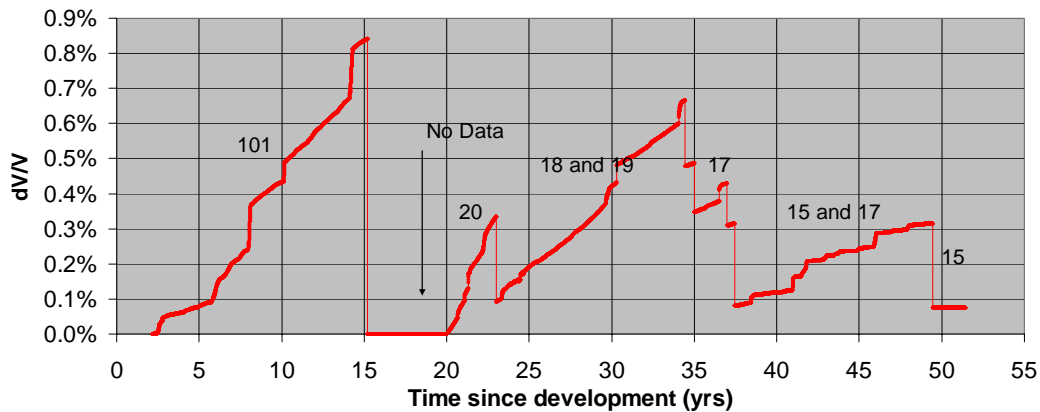


Figure 19: Normalized volume decrease of each SPR cavern in the BC salt dome.

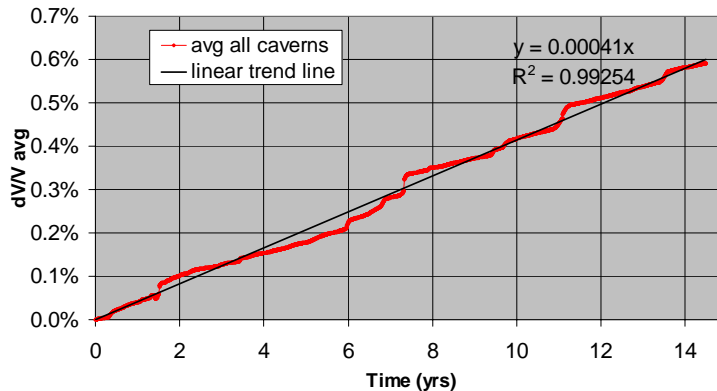


Figure 20: Normalized average decrease in storage volume for the six SPR caverns in the BC salt dome.

5.2. Selection of Parameters to Calibrate

As mentioned in Section 3.1.2, RF and the secondary constants of salt can be estimated by back-calculation to best match the measured closure data. RF is defined as follows:

$$E_B = E_{WIPP} / RF \quad (2)$$

where, E_B = Back-fitting Young's modulus of salt

E_{WIPP} = Measured Young's modulus of salt at WIPP site

An earlier predecessor of the JAS3D code, SANCHO, which had been used to simulate the salt behavior, had difficulties in treating stiff equations such as those used to describe a transient creep response. In the solution method used in SANCHO, the finite element advancement of the calculation produced considerable error, causing the code not to converge. In an attempt to obtain a solution, the time step was typically reduced. However, time step reduction results in extremely long run times, often without a result or a satisfactory solution. As a result, Morgan and Krieg [1988] introduced an artifact into the code as an approximation to transient response. This addition facilitated the calculations significantly. The approximation uses a reduction of the elastic modulus by an arbitrary amount, 12.5, which was chosen by back-fitting the WIPP South Drift data [Munson, 2004]. The RF of BC salt was assumed to be the same as for the WIPP salt [Munson, 1998]. Thus, a RF value of 12.5 is used herein.

The secondary constant of salt creep (A in Equation (1)) is controlled by the Structural Multiplication Factor (SMF). The factor is defined as follows:

$$A_B = SMF \cdot A_{WIPP} \quad (3)$$

where, A_B = Back-fitting creep constant of salt

A_{WIPP} = Measured creep constant of salt at WIPP site in Table 2

The salt at BC has higher purity than that of WH in it, so the creep closure rate is expected to be different. SMF also can be adjusted to match the volume closure of the caverns.

The rock surrounding the salt dome is a sedimentary rock that mostly consists of sandstone and shale. The Young's modulus of sandstone/shale has large uncertainty which range is 5.802×10^4 to 1.105×10^7 psi [Carmichael, 1984]. For simplifying the back-fitting analysis, a median value of the Young's modulus of sandstone, 5.076×10^6 psi, was assumed. The overburden made of sand is assumed to be similar to that found at WH. Young's modulus of caprock is taken to be 2.277×10^6 psi as discussed in Section 3.1.3. The Poisson's ratio of overburden, caprock, and surrounding rock are taken to be 0.33, 0.29, and 0.33, respectively as discussed in Section 3.1.3.

5.3. Results of Back-fitting Analysis

Figure 21 shows the predicted decrease in storage volume of Cavern 101 compared with the field data as shown Figure 19 for 16 years since switching from brine to oil. The green, blue and sky blue lines indicate the normalized volume closure when SMF is 0.2, 0.12, and 0.1, respectively.

Larger SMF values yield larger volume closure rates. The peaks correspond to the workover activities, which were initially performed 3.5 years after switching from brine to oil for one month. This cycle has been repeated for every five year as mentioned in 3.2.2.

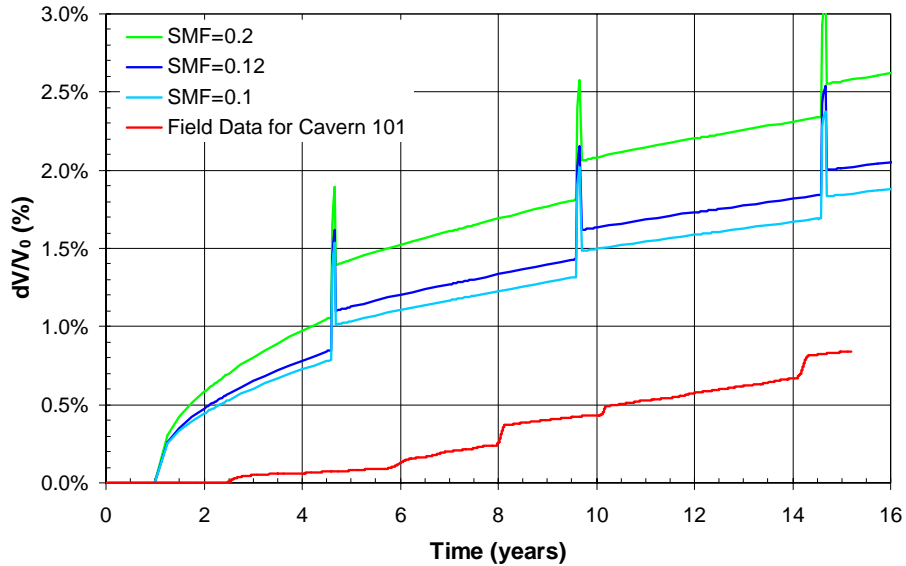


Figure 21: Predicted volumetric closure normalized by cavern volume for Cavern 101 with the field data as shown Figure 19.

Based on experience from a number of back-fitting analyses to match the field data, SMF has a strong relationship with the volumetric closure of caverns in salt dome [Park et al., 2005]. To determine SMF, attention needs to be focused on the periods between the workovers in order to compare the model predicted volumetric closure rates with the actual field data. Thus, the data between the workovers obtained by the analysis are superposed over the field data line by adjusting time as shown Figure 22. When SMF is 0.12, the predicted closure rate matches the field data best for the longest interval between workovers from 10 to 14 years.

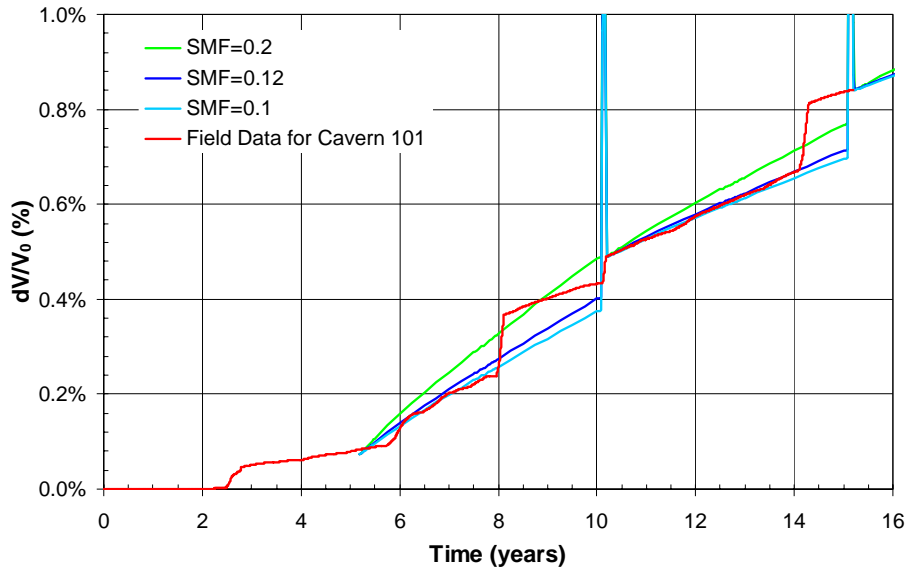


Figure 22: Superposed volumetric closure rate for comparing with the field data.

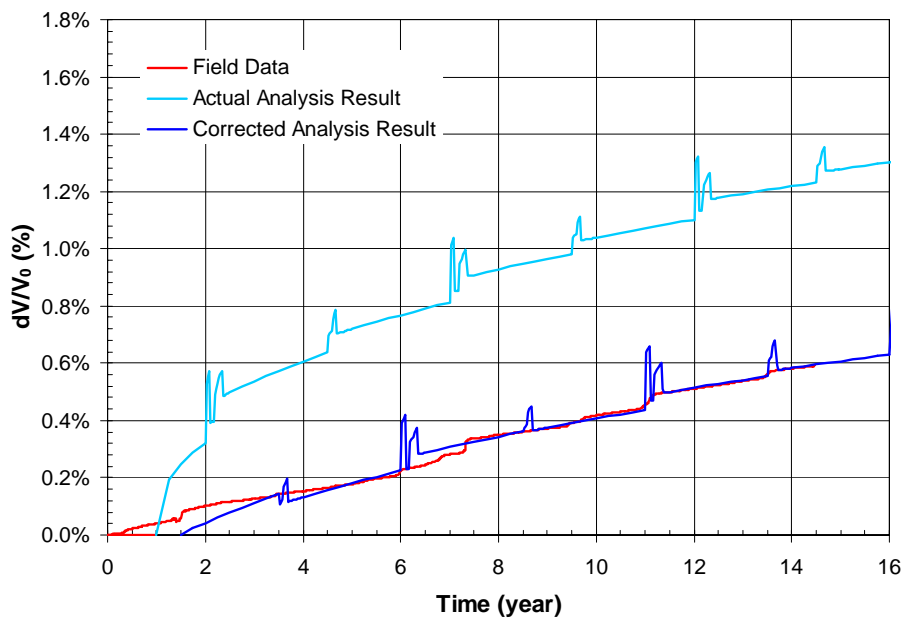


Figure 23: Uncorrected and corrected normalized average decreases in storage volume for the six SPR caverns with the field data as shown Figure 20 for SMF of 0.12.

Figure 23 shows uncorrected and corrected decreases in storage volume for the six SPR caverns from the analyses with field data as shown Figure 20, for 16 years since switching from brine to oil, when SMF is 0.12. As discussed in Section 3.2.2, the peaks appear during the workover of the caverns. The predicted data are corrected by adjusting time and dV/V_0 (where V_0 is initial volume and dV is volume reduction) for comparing with the compiled field data because the

drilled dates of the six caverns are different (see Table 7). The line plotted using the corrected data match the field data well.

Using a SMF of 0.12, the calibrated creep constant (A_c) was calculated to be 0.695×10^{-36} from Equation (3). The predicted closure rates for both Cavern 101 and the six SPR caverns agree well with the measured values. In the case of WH site, SMF was determined to be 7.5 (Creep constant $A = 43.4 \times 10^{-36}$) [Ehgartner and Sobolik, 2002]. Therefore, the creep rate of BC salt appears to be much slower than WH salt.

The material properties, including calibrated values (bold font), in Table 10 and Table 11 are used as input data in the present analyses.

Table 10: Material parameters of Bayou Choctaw salt used in the analyses.

Parameter	Unit	Value	References
Young's modulus (E)	psi	4.496×10^6	Krieg, 1984
Density (ρ)	lb/in ³	0.083	Krieg, 1984
Poisson's ratio (ν)	-	0.25	Krieg, 1984
Elastic modulus reduction factor (RF)	-	12.5	Morgan and Krieg, 1988
Bulk modulus (K)	psi	2.397×10^5	Calculated using E and ν
Two mu (2μ)	psi	2.878×10^5	Calculated using E and ν
Creep constant (A)	Pa ^{-4.9} /s	5.79×10^{-36}	Krieg, 1984
Structure multiplication factor (SMF)	-	0.12	Back-fitting analysis
Calibrated creep constant	Pa ^{-4.9} /s	0.695×10^{-36}	Back-fitting analysis
Stress exponent (n)	-	4.9	Krieg, 1984
Thermal constant (Q)	cal/mol	12000	Krieg, 1984
Universal gas constant (R)	cal/(mol-K)	1.987	
Input thermal constant (Q/R)	cal/mol	6039	

Table 11: Material properties of the lithologies around salt dome used in the analyses.

	Unit	Overburden	Caprock	Surrounding Rock
Young's modulus	psi	1.450×10^4	2.277×10^6	5.076×10^6
Density	lb/in ³	0.068	0.090	0.090
Poisson's ratio	-	0.33	0.29	0.33

Intentionally left blank

6. FAILURE CRITERIA

6.1. Structural Stability of Salt Dome

Potential damage to or around the SPR caverns was evaluated based on two failure criteria: dilatant damage and tensile failure.

Dilatancy, defined as an increase in volume under compressive stress [Jaeger and Cook, 1979], is attributed to micro-fracturing or changes in the pore structure of the salt, resulting in an increase in permeability. A dilatant damage criterion is used to delineate potential zones of damage in the salt formation surrounding the SPR facility.

Two reports [Price, et. al, 1981; PB-KBB Inc, 1978] contain strength data relative to BC salt as listed in Table 12.

Table 12: Failure and dilatancy criteria data for Bayou Choctaw Salt.

Well	Depth (ft)	Confining Stress (psi) σ_2, σ_3	Axial Stress (psi) σ_1	I_1 (psi)	$\sqrt{J_2}$ (psi)	Temp (°F)	Reference
Testing to Failure							
CH-1	714.1	0	2900	2900	1674	ambient	PB-KBB, 1978
CH-1	715.85	2500	15800	20800	7679	ambient	PB-KBB, 1978
CH-1	716.4	3500	12000	19000	4907	ambient	PB-KBB, 1978
CH-1	716.7	5000	17900	27900	7448	ambient	PB-KBB, 1978
CH-1	722.2	750	9450	10950	5023	ambient	PB-KBB, 1978
CH-1	722.9	5000	17000	27000	6928	ambient	PB-KBB, 1978
19A	2581	0	3740	3740	2159	72	Price, 1981
19A	2579	500	5480	6480	2875	140	Price, 1981
19A	2576	2000	8440	12440	3718	140	Price, 1981
Dilatancy Limits							
19A	2582	14.5	230	259	124	72	Price, 1981
19A	2579	500	1760	2760	727	140	Price, 1981

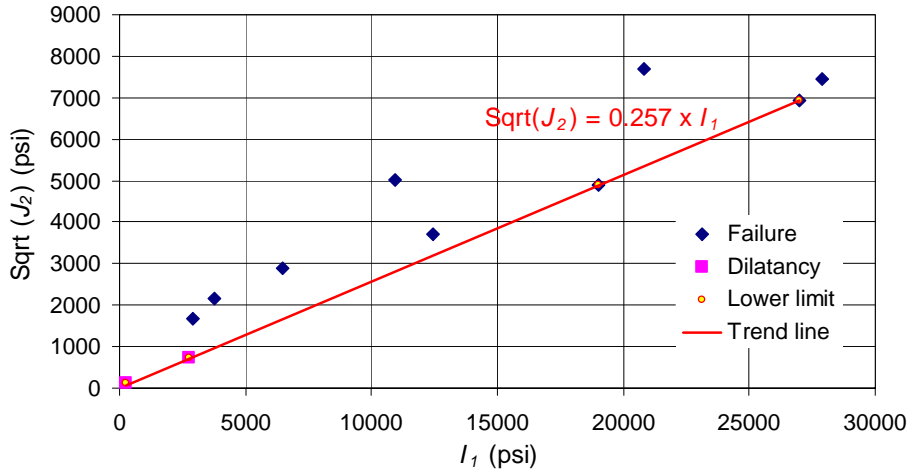


Figure 24: Dilatancy criteria for Bayou Choctaw salt with field data.

The compression data can be plotted in terms of the stress invariants as shown Figure 24. To determine a dilatant damage criterion, four lower bound data are chosen for conservatism.

In this study, the following dilatancy criterion as shown in Figure 24 is used.

$$D = \frac{0.257 \cdot I_1}{\sqrt{J_2}} \quad (4)$$

where, D = damage factor

$I_1 = \sigma_1 + \sigma_2 + \sigma_3 = 3\sigma_m$: the first invariant of the stress tensor.

$\sqrt{J_2} = \sqrt{\frac{(\sigma_1 - \sigma_2)^2 + (\sigma_2 - \sigma_3)^2 + (\sigma_3 - \sigma_1)^2}{6}}$: the square root of the second invariant of the deviatoric stress tensor

σ_1 , σ_2 , and σ_3 are the maximum, intermediate, and minimum principal stresses, respectively.

σ_m is the mean stress.

Where $D \leq 1$, the shear stresses in the salt (J_2) are large compared to the mean stress (I_1) and dilatant behavior is expected. Where $D > 1$, the shear stresses are small compared to the mean stress and dilatancy is not expected. Account for the stability of the caverns may be controlled by weaker dirty salts and the variability in the measured strength and dilatancy values, 20% uncertainty of safety factor at least is required for this criterion. Therefore an allowable safety factor against dilatancy is assumed to be 1.2 in this study.

For purpose of these analyses, the tensile strength of the salt is conservatively assumed to be zero in order to check the tensile failure. Tensile cracking in rock salt initiates perpendicular to the largest tensile stress direction. The potential for tensile failure exists if the maximum principal stress is numerically zero or tensile. To calculate the dilatancy damage and tensile failure

potential in salt, the post-processing code ALGEBRA is used with the JAS3D output file to determine spatial locations of dilatant damage.

It should be emphasized that the above dilatancy criterion is not used in the present study to quantify damage, but merely to identify regions with a high potential for damage even though the estimates are considered conservative for the reason stated above. This criterion identifies regions where the deviatoric stress is high and the mean stress is low, a state of stress conducive to dilation. No comprehensive constitutive model exists at this time which can predict damage evolution in a reasonable computation time for a 3D problem of this magnitude. Hence, the post-processed dilatation criterion was used as a conservative engineering approach to estimate possible regions of salt damage. Much can be inferred from this approach [Ehgartner and Sobolik, 2002].

6.2. Allowable Strains for Well and Surface Structures

The physical presence of wells and surface structures are not included in the finite element model, but the potential for ground deformation to damage these structures can be conservatively estimated by assuming that they will deform according to the predicted ground deformation.

At wells locations, subsidence will primarily induce elongation of the axis of the well. Under these conditions, the cemented annulus of the wells may crack, forming a horizontal tensile fracture that may extend around the wellbore. Vertical fluid migration is not expected under these conditions, however horizontal flow could occur. The allowable strain for purposes of this study is assumed to be 2 millistrains in compression and 0.2 millistrains in tension [Thorton and Lew, 1983]. The benefit of the steel casings in reinforcing the strength of the cement, especially under elongation, is not accounted for in this simplistic evaluation.

Structural damage on the surface is typically caused by large accumulated surface strains due to subsidence. These strains can cause distortion, damage, and failure of buildings, pipelines, roads, bridges, and other infrastructure. Surface strains will accumulate in structures over time, which increases the possibility of damage in older facilities. The criteria vary in some countries depending on application [Peng, 1985]. For purposes of this study, the allowable strain is taken to be 1 millistrain for both compression and tension.

Intentionally left blank

7. COMPUTER CODES AND FILE NAMING CONVENTION

7.1. Computer Codes

The finite element code used in the present calculations, JAS3D [Blanford, 2001], uses an eight-node hexahedral Lagrangian uniform strain element with hourglass stiffness to control zero energy modes. A nonlinear conjugate gradient method is used to solve the nonlinear system of equations. This efficient solution scheme is considerably faster than the direct solvers which are used in most commercial codes and is a product of decades of research and development into nonlinear large strain finite element analyses. JAS3D includes at least 30 different material models. Two material models were chosen for use in the model described in this report: an elastic model for the overburden material (sand), caprock, and sandstone; and a power law creep model for the salt. Related preprocessing, mesh generation, and post processing codes were used in conjunction with JAS3D. Applicable software and version numbers used in this analysis are listed in Table 13.

Table 13: Applicable software and version number

Code Name	Version	Uses
APREPRO	1.78	Preprocessor
CUBIT	10.0B	Mesh generation
EMERGE	1.50	Adds temperature to the mesh
JAS3D	2.2.A	FEM solver
ALGEBRA2	1.26	Postprocessor
BLOT II-2	1.50	Postprocessor

7.2. File Naming Convention

These calculations are performed on Sandia National Laboratories' Compaq Tru64 workstation (ELO), on which UNIX V.1.5B is installed. The general path for any of these subdirectories is 'ELO: //home/bypark/bcspr/'. The files related to the mesh generation, the FEM solver, and the volume calculations exist in the subdirectories of ~/bcspr/mesh/coar/, ~/bcspr/solv/coar/, and ~/bcspr/volc/coar/, respectively. The files related to Scenario 1, Scenario 2, and the failure of Cavern 7 exist in the subdirectories of ~/bcspr/solv/coar/scn1/, ~/bcspr/solv/coar/scn2/, and ~/bcspr/solv/coar/cav7/, respectively. All the files that remain within each subdirectory are listed and described in Table 14. *Input Files* are files that should be obtained from ELO in order to run the programs; *Intermediate Files* are created during the execution; *Output files* are created as a result of execution and which are stored in ELO. *Intermediate files* are typically output files created by one program and used as input to another program. Table 14 also lists the names of the *user defined subroutines*, and the names of any *executables* needed to run the entire analysis from grid generation through post processing.

Table 14: File naming convention for Bayou Choctaw SPR caverns calculations (* means wild card)

File Names	Description
Input Files	
24cav5l_coar.jou	CUBIT journal file for mesh generation
24cav5l_coar.g0	3D GENESIS mesh generated using CUBIT
24cav5l_coar.g	3D GENESIS mesh contains the temperature data at each node and used for the execution of JAS3D
24cav5l_coar.nod	ASCII node data of coordinates
emerge.inp	Emerge input file for merging the temperature data into the mesh
spr_bc*.alg	ALGEBRA script for computing the subsidence, principal stresses, safety factor against dilatant damage, safety factor for shear failure
bc_24cav5l_*.i	JAS3D input files
Intermediate Files	
24cav5l_coar.th	Binary temperature data of each node
tempz_bc_24cav5l_coar.f	FORTRAN file for calculating the temperature at each node
*.blk	BLK file for compiling FORTRAN files
usrpbc_24cav5l.o	Objective file from compiling FORTRAN file
User Defined Subroutines	
usrpbc_24cav5l.f	User-supplied subroutine to provide an internal pressure state in the caverns
volcav.f	User-supplied subroutine to calculate the volume change of each cavern as a function of time
Output files	
temp_check_coar.dat	ASCII data for checking the temperature at each node
*.ps	Post script file
24cav5l_bc_smax_mindil_minshr_*.dat	ASCII data of the principal stresses, safety factor against dilatant damage, safety factor for shear failure
bc_24cav5l_*.e	EXODUS output files
bc_24cav5l_*.ea	EXODUS output files manipulated using ALGEBRA script
volcav_*.csv	Excel output from the volume calculation of caverns with time
bc_24cav5l_*.o	ASCII output file
*.log	Log file during execution
Executables	
a.out	Calculates the temperature at each node
jas3d	Baseline
Makefile	Commands to compile volcav.f
volcav	Calculates the volume change of each cavern with time
volcav.run	Commands to run volcav

8. ANALYSES RESULTS

8.1. Cavern Deformation

Creep closure decreases cavern volume over time and is more pronounced near the bottom of the caverns. The flow of salt can be illustrated by displacements vectors at each node. Figure 25 through 27 show the deformed cavern shapes and displacement vectors around the SPR caverns at 21 years.

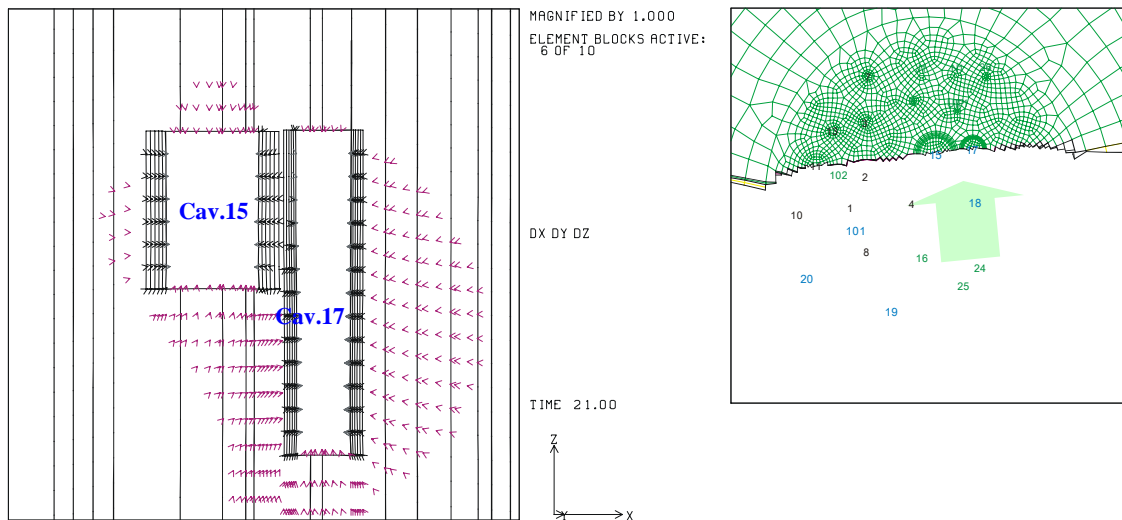


Figure 25: Displacement vectors around Caverns 15 and 17 at 21 years

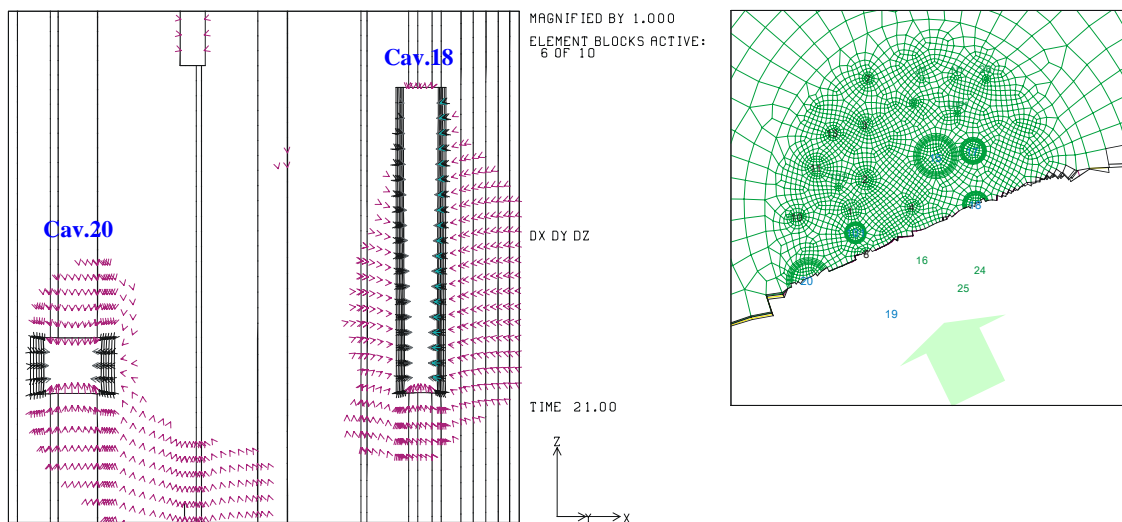


Figure 26: Displacement vectors around Caverns 18 and 20 at 21 years

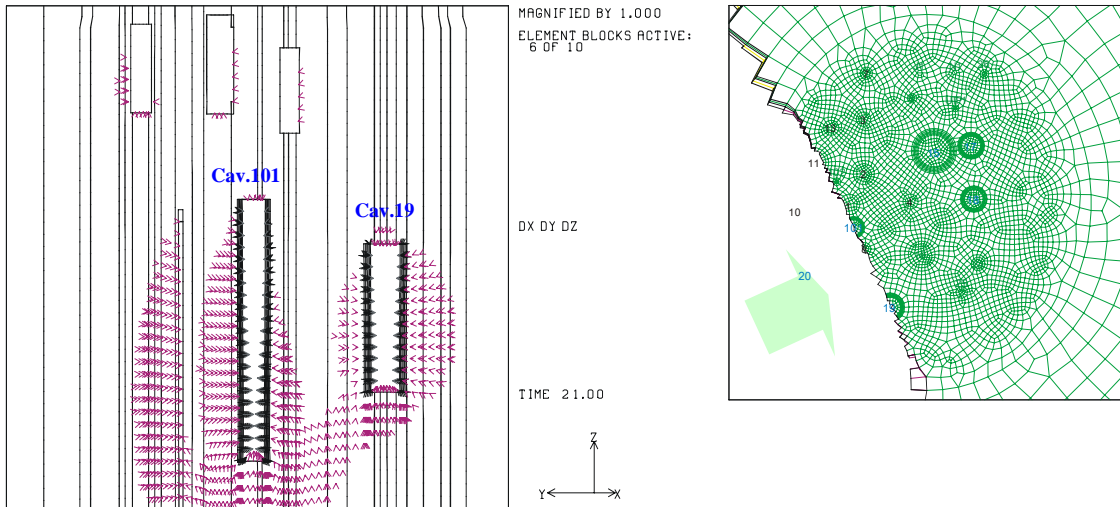


Figure 27: Displacement vectors around Caverns 19 and 101 at 21 years

The salt flows are primarily downward near the roofs of the caverns, upward near the floors, and lateral in the pillar. The largest displacements occur in the floors of the caverns. The predicted displacements in the center of the floor are more than twice those predicted near the edge of the floor. This produces an upward curvature in the floor. The lateral salt deformation causes the outer cavern walls to shift inward over time.

Figure 28 through 30 show the quantified vertical displacements around SPR caverns at 21 years. Positive displacements are directed upward.

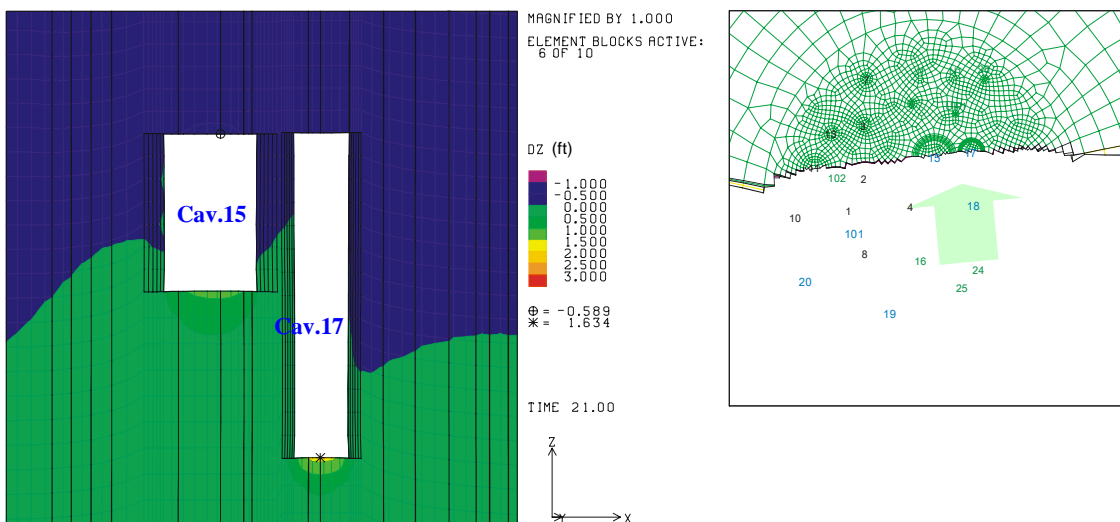


Figure 28: Vertical displacement contours around Cavern 15 and 17 at 21 years

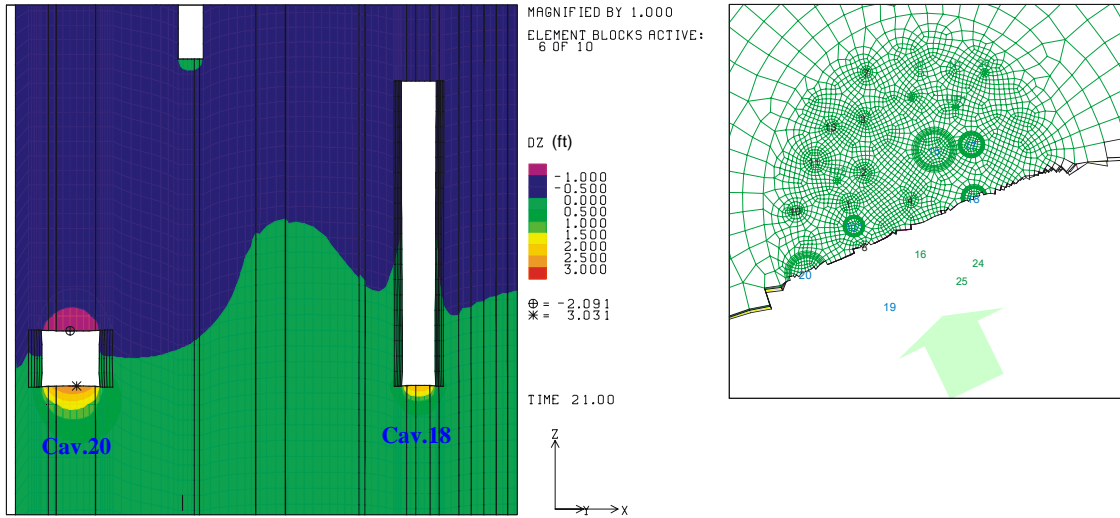


Figure 29: Vertical displacement contours around Cavern 18 and 20 at 21 years

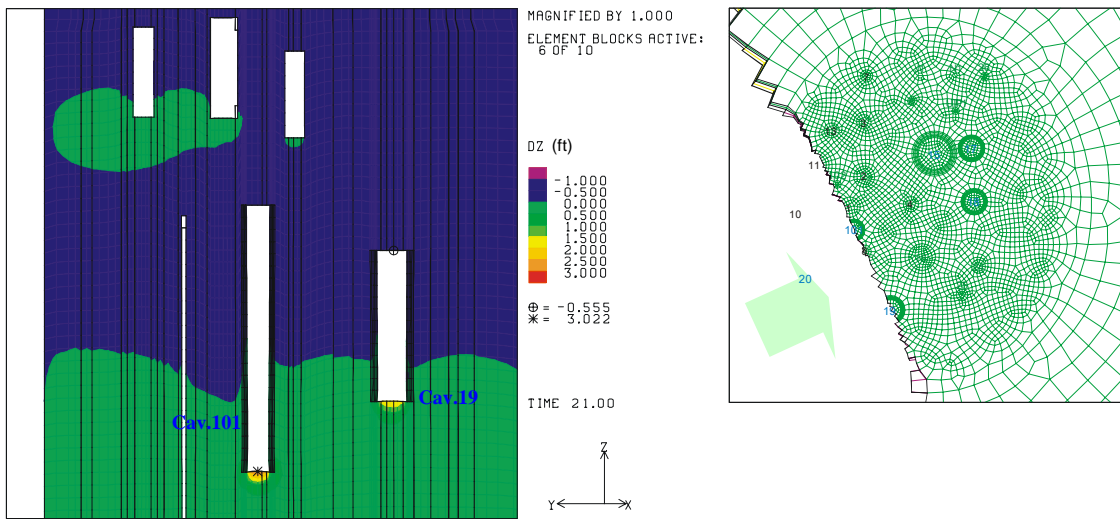


Figure 30: Vertical displacement contours around Cavern 19 and 101 at 21 years

Note that the numerous vertical lines in the Figures 25 through 30 are the element edges which are visible because the cross-sectional cut. The element sides are not necessarily parallel to the cross-sectional cut, which is not flat.

8.2. Storage Loss

Figure 31 shows the decrease in overall storage volume in the six SPR caverns over 46 years of time. Because the caverns are initially leached at the beginning of the analysis, then again at 21 years, and every 5 years thereafter, the percentage of closure is normalized by the volume immediately following each leach. The overall storage volume decreases by about 0.3% every 5

years. The impact of workover pressure is also evident in Figure 31 by the abrupt change in normalized volumetric closures that occur each month following leaching.

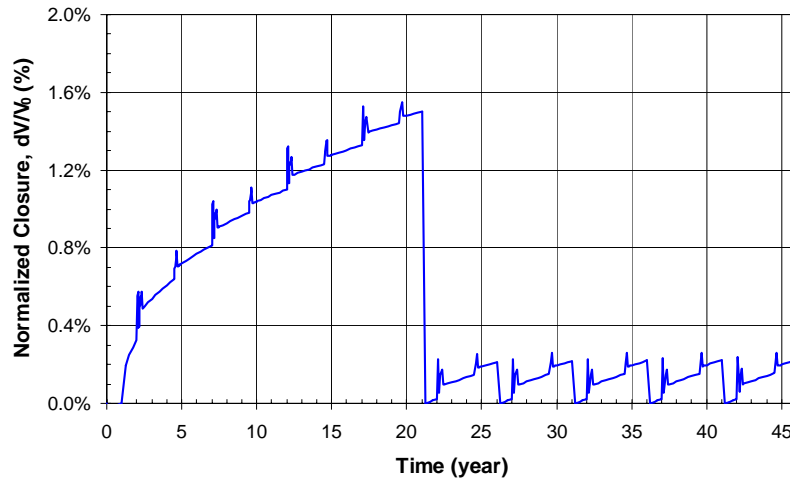


Figure 31: Predicted overall volumetric closure normalized to overall storage volume for the six SPR caverns immediately following each leach.

Figure 32 shows the volumetric closure of each cavern normalized by the cavern volume immediately following each leach. The closure rate of Cavern 101 is largest and the rates decrease in the order of Cavern 20, 19, 18, 17 and 15. The bottom elevation of Cavern 101 is -4,830 ft while that of Cavern 15 is -3,296 ft. This implies that the closure rate depends on the elevation of cavern bottom. Figure 33 shows the volume change of each cavern due to leaching and salt creep closure over time.

Figure 34 shows the predicted volume change for each non-SPR cavern with time. The volume changes of Cavern 16, 24, 25, and 102 are larger than that of the others because their bottom elevations are deeper.

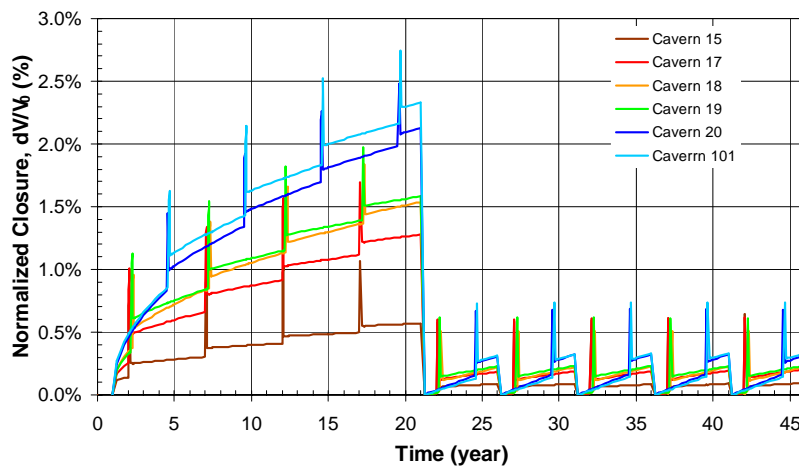


Figure 32: Normalized volumetric closure of each cavern with time. The volumes were normalized by the volume of the cavern immediately following each leach.

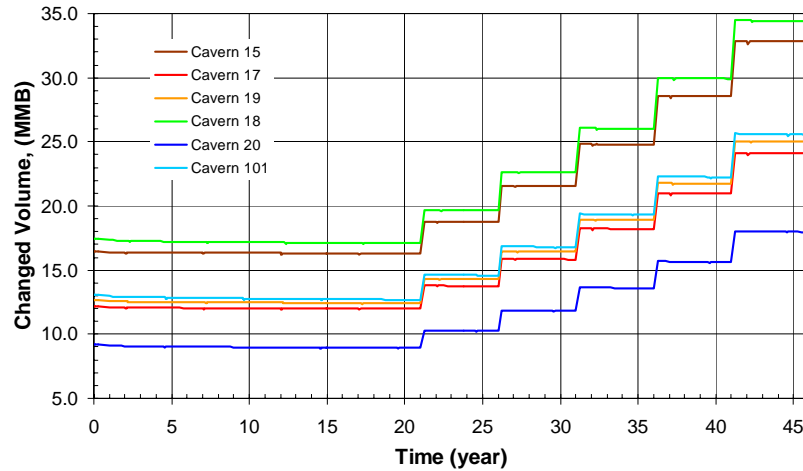


Figure 33: Volumetric changes of each cavern due to leaching and salt creep closure over time

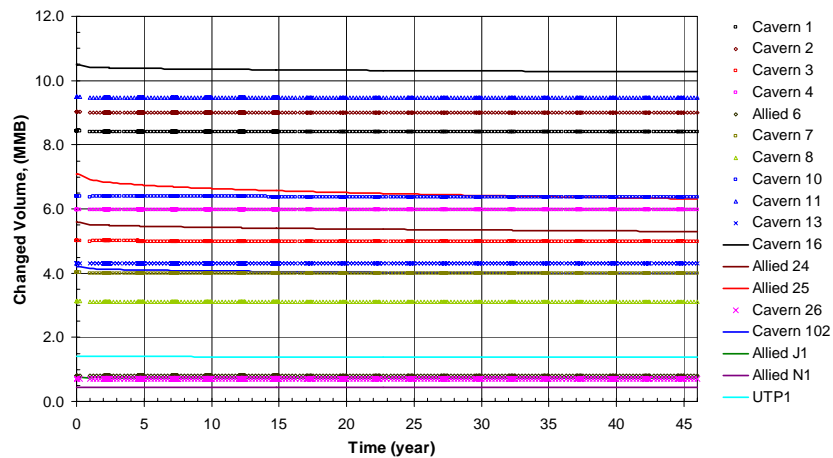


Figure 34: Predicted volume change for each non-SPR cavern over time

8.3. Subsidence

The subsidence above the central axis of the caverns is plotted as a function of time in Figure 35. The magnitude of subsidence slowly increases with time as a result of creep and cavern size. The subsidence above Caverns 4, 16, 18 and 15 is larger than that above the other caverns. The locations of these caverns are near the center of the dome as shown Figure 16. This suggests that the amount of subsidence depends on the location at which the subsidence is calculated, and subsidence contributed by other caverns is compounded.

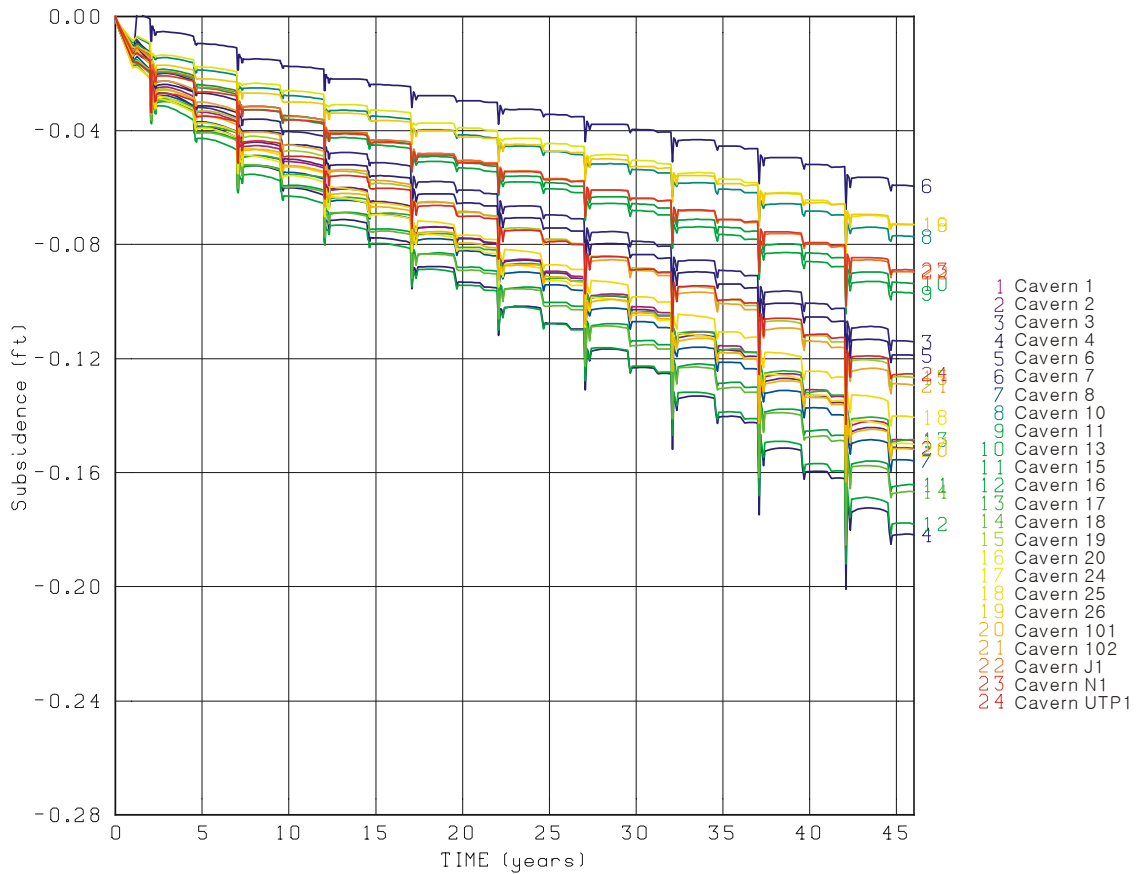


Figure 35: Predicted subsidence on the surface near the center of each cavern.

Figure 36 through 38 show the vertical ground displacements immediately before the first leach and before the 6th leach. The amount of subsidence is predicted to extend to greater distances over time. The surface subsidence is similar in magnitude to the subsidence at the surface, but increases with depth from the surface to the top of the caverns. The difference between subsidence at the surface and top of caverns results in well strains, which are discussed in the next section, but are predicted here to be greater over the locations of the caverns.

Note that the numerous vertical lines in the figures (left) are the visible element edges, as mentioned in Section 8.1, caused by the mesh being cut.

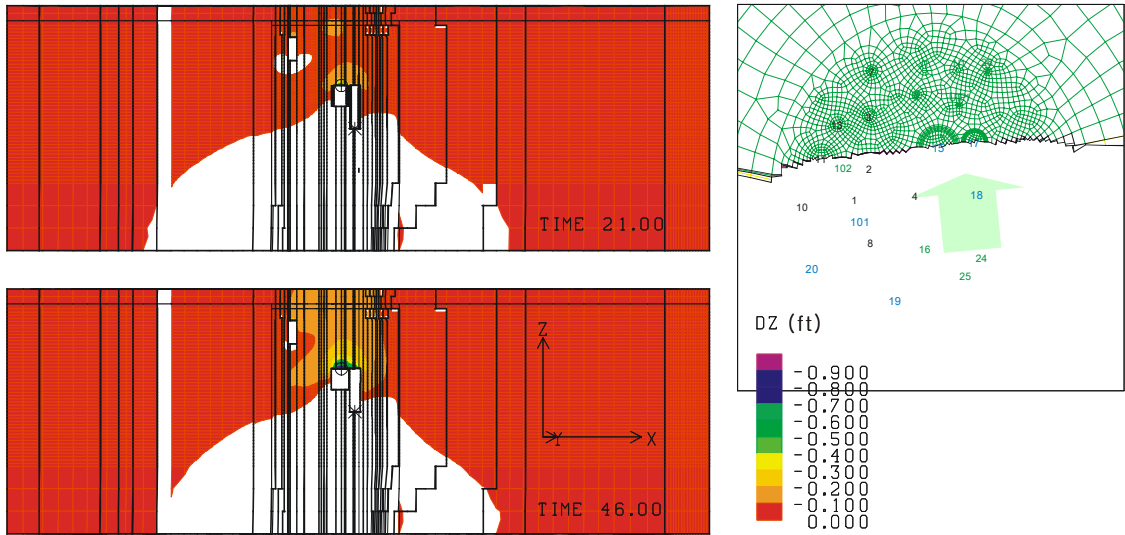


Figure 36: Vertical displacement contours prior to 1st leach (upper left) and immediately before 6th leach (lower left) for the section through Cavern 15 and Cavern 17

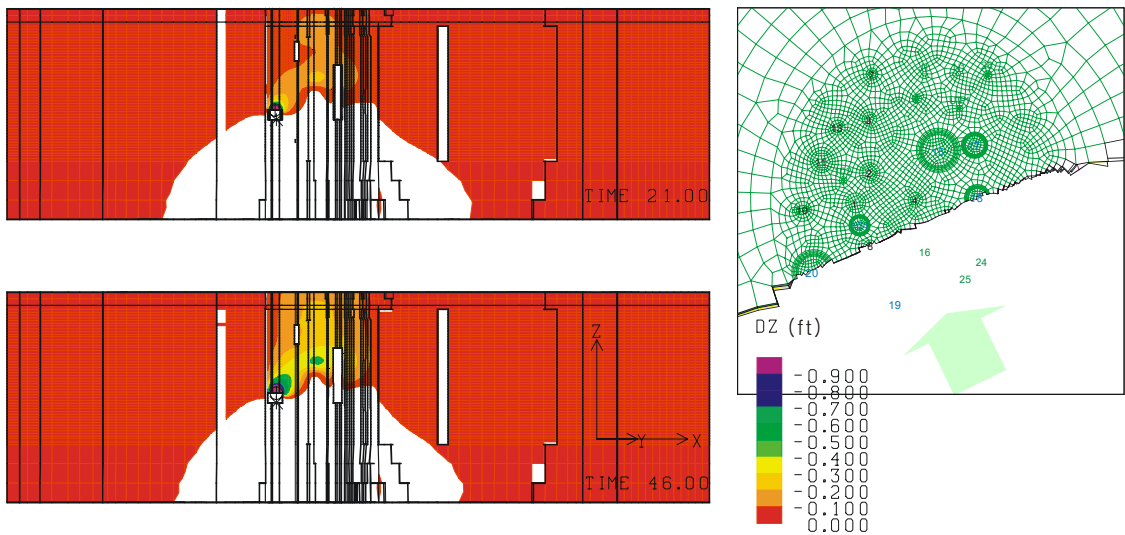


Figure 37: Vertical displacement contours prior to 1st leach (upper left) and immediately before 6th leach (lower left) for the section through Cavern 20 and Cavern 18

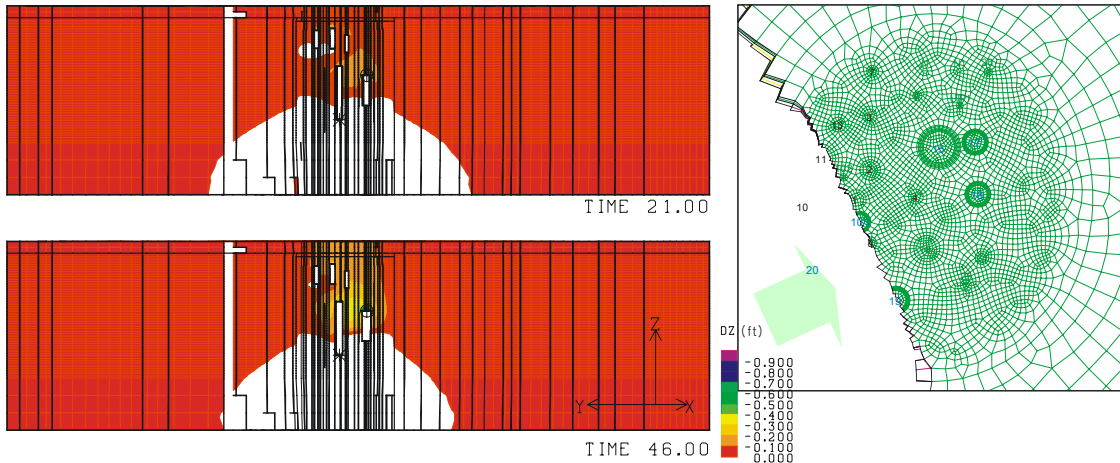


Figure 38: Vertical displacement contours prior to 1st leach (upper left) and immediately before 6th leach (lower left) for the section through Cavern 101 and Cavern 19

Figure 39 shows the calculated surface strain at 21 years after development of the cavern, prior to the initial leach, and 46 years, after the 5th leach. At both times, in comparison to the allowable 1 millistrain identified in Section 6.2, accumulated strain is below the limiting value and thus structural damage should not occur. There is not a marked increase in surface strains due to cavern enlargement.

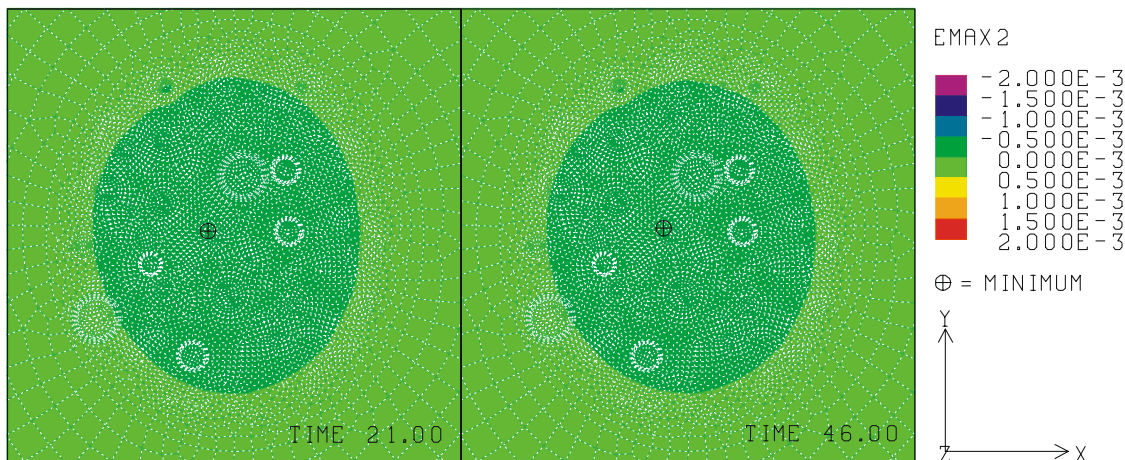


Figure 39: Predicted radial surface strains prior to leaching (left) and after the 5th leaching (right)

8.4. Cavern Wells

The calculated vertical ground strains are shown in Figure 40 through 42 at 21 years (prior to 1st leach) and after the 5th leach. Of interest are the magnitudes in the proximity of the cavern wells. The predicted strains near cavern wells are larger than 0.2 millistrains in tension. As discussed in Section 6.2, yielding is predicted in the cemented casing which extends from the surface to typically about 100 ft above the cavern roof. The collapse strength of the steel component of the

cemented steel is reduced as the cemented casing stretches. However, the steel casing will not be completely yielded until about 2 millistrains.

The predicted strains above the cavern roofs of Caverns 15, 17, 18, 19, and 101 at 21 years are less than yield, with a possible exception near the bottom of the deepest cemented casing. This is typically about 100 ft above the cavern roof. The predicted strains above the cavern roofs of Caverns 15, 17, 18, and 101 after 46 years are also less than yield.

The predicted strains over 100 ft above the cavern roof of Cavern 20 at 21 years and both Cavern 19 and 20 at 46 years are larger than yield. Since the cemented casing deformation will be controlled by the creep of salt, no large localized deformations will occur because the creep rate will be very small and less than that of the cavern due to the backpressure the casing exerts on the salt and the relatively shallow depth of the casing in salt.

Again, the vertical lines in the plots are the edges of the model elements, as mentioned in Section 8.1.

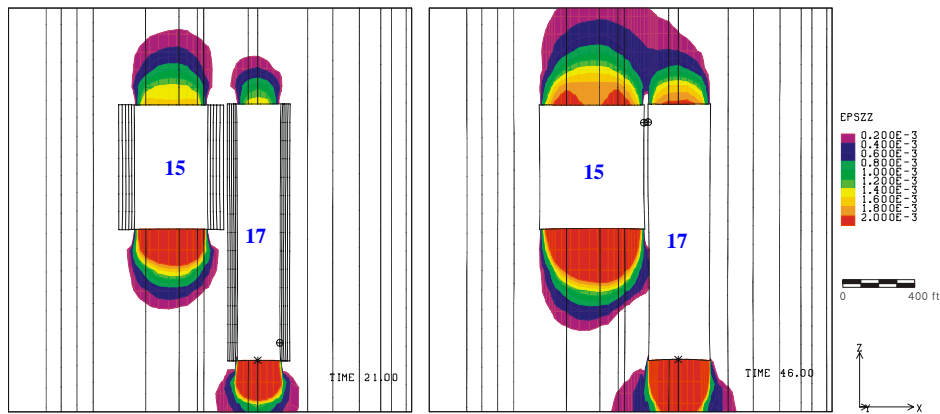


Figure 40: Vertical strains near Caverns 15 and 17 prior to 1st leach (left) and after the 5th leach (right).

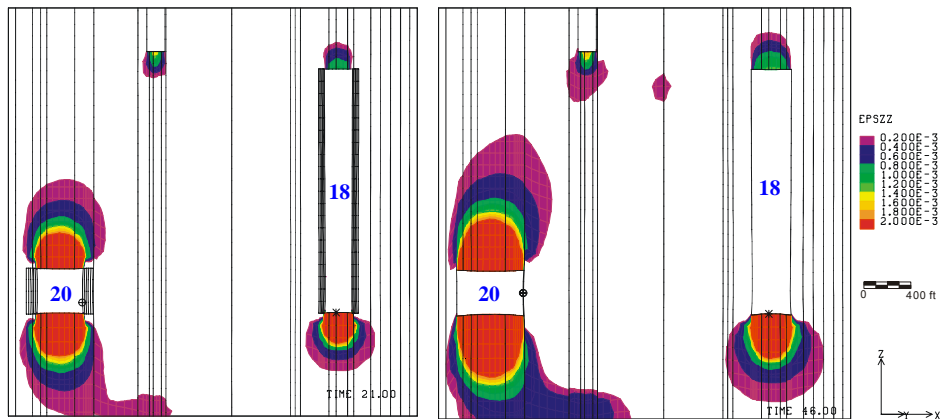


Figure 41: Vertical strains near Caverns 18 and 20 prior to 1st leach (left) and after the 5th leach (right).

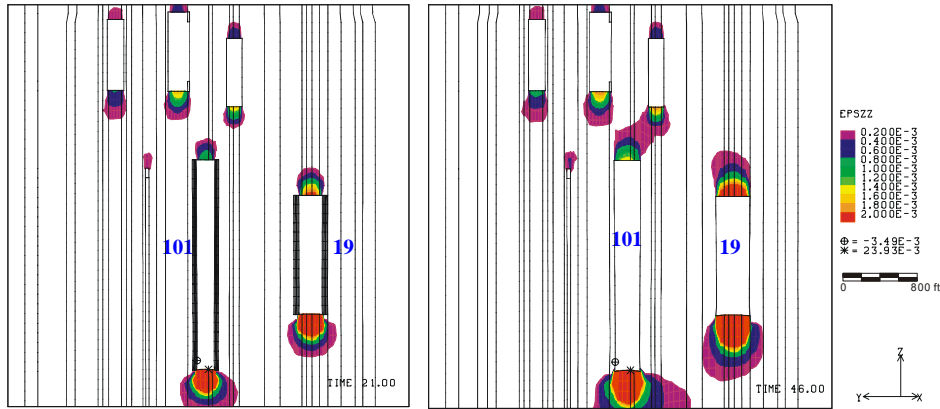


Figure 42: Vertical strains near Caverns 19 and 101 prior to 1st leach (left) and after the 5th leach (right).

8.5. Cavern Stability

As discussed in Section 6.1, the stability of the caverns was evaluated by examination for any tensile stresses and by calculation of the safety factors against dilatant damage.

8.5.1. Minimum compressive stress

Figure 43 shows the minimum compressive stress (MCS) histories for the BC salt dome and for only the caverns below 2,000 ft. The MCS in the entire salt dome is calculated as -300 psi at 1 year when the brine in the SPR caverns was switched to oil. Note that the minus sign (-) indicates a compressive stress. The most critical location was found to be in the top of the salt dome as shown in Figure 44. Having the MCS on the top of the dome is not of interest because all SPR caverns are located below 2000 ft. The data for 'Below 2000 ft' in Figure 43 means that the data above 2000 ft is screened out to show the detailed change of MCS around the SPR caverns.

Figure 45 shows the MCS contours around Caverns 18 after 4th leach at 37.33 years when the smallest compressive stress (-694 psi) is predicted to occur during workover of the cavern (See Figure 43). The MCS on the upper wall of Cavern 18 is predicted to be smaller than that at any other locations below 2000 ft because the roof elevation of Cavern 18 is higher than that of other SPR caverns (See Figure 17). Again, the numerous vertical lines in the figures are the element edges as mentioned in Section 8.1.

All stresses around the caverns at all times were found to be compressive (<0 psi). Thus, all caverns are structurally stable against tensile failure throughout the entire simulation time because the potential for tensile failure exists if the MCS is numerically zero or plus (i.e. tensile) as mention in Section 6.1. From a compressive stress stability view point, the upper walls near the roofs of the caverns appear to be the areas of greater concern than other locations based on this analysis.

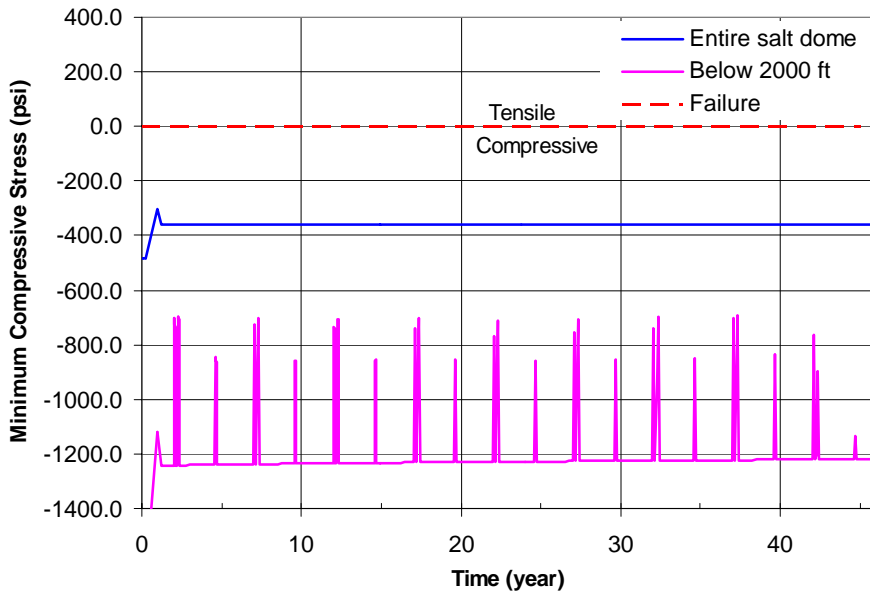


Figure 43: Minimum compressive stress as a function of time

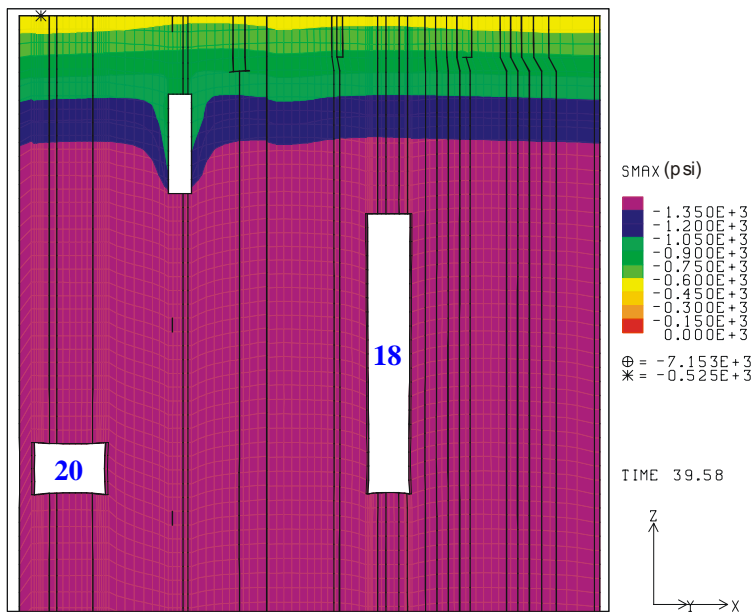


Figure 44: Minimum compressive stress contours around Caverns 18 and 20 during workover of Cavern 18 after 5th leach.

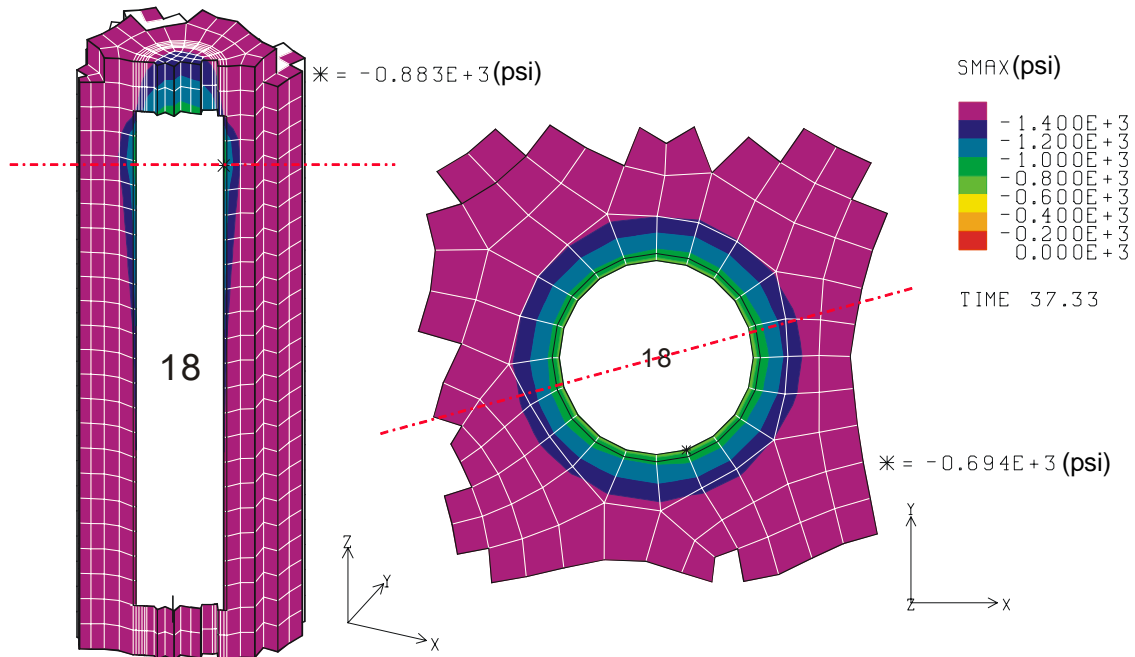


Figure 45: Minimum compressive stress contours around Caverns 18 during workover after 4th leach. The left diagram is of the vertical cross-section through the center of the cavern and the right diagram is of the horizontal cross-section. The red lines show where the mesh was cut.

8.5.2. Minimum safety factor against dilatant damage

The minimum safety factor against dilatant damage (DILFAC) is plotted in Figure 46 over time. The influence of workovers is seen by the reduction in safety factor from 2.04 to approximately 0.93 in the entire salt dome. The dilatancy criterion of Equation (5) in Section 6.1 is used. The area for potential dilatant failure is indicated in the contour where DILFAC is less than 1.2.

The web between Caverns 15 and 17, and the web formed by Cavern 20 and the edge of the dome are anticipated to be the weakest areas in the salt dome. The DILFAC at 37.08 years is calculated to be 1.2 along the wall of Caverns 15 and 17 as shown Figure 46. This implies that the web between the caverns is expected to fail during first workover after 4th leach.

The DILFAC distribution around Caverns 15 and 17 during workover of caverns after 5th leach is provided in Figure 47. The DILFAC in the web between Caverns 15 and 17 appears less than 1.2 at 42.08 years in Figure 47. The weakest area in the web appears at approximately three quarters-height of Cavern 15.

The lowest DILFAC on the wall of Cavern 20 is predicted to be 1.67 at 4.53 years, during the first workover of the cavern after the initial leach as shown in Figure 46. The web formed by Cavern 20 and the edge of the dome at this time appears structurally stable from the DILFAC point of view (Figure 48). The web still appears stable after the 5th leach is completed as shown Figure 49. This implies that the web thickness formed by Cavern 20 and the dome edge does not affect the structural stability. The sides in Cavern 20 including the roof, floor, and the right side

of wall move to inward with time. However the left side of wall remains approximately parallel to the dome edge because the stiff surrounding sandstone prevents the salt creep closure (Figure 49). Therefore the web becomes structurally more stable even though the web thickness decreases.

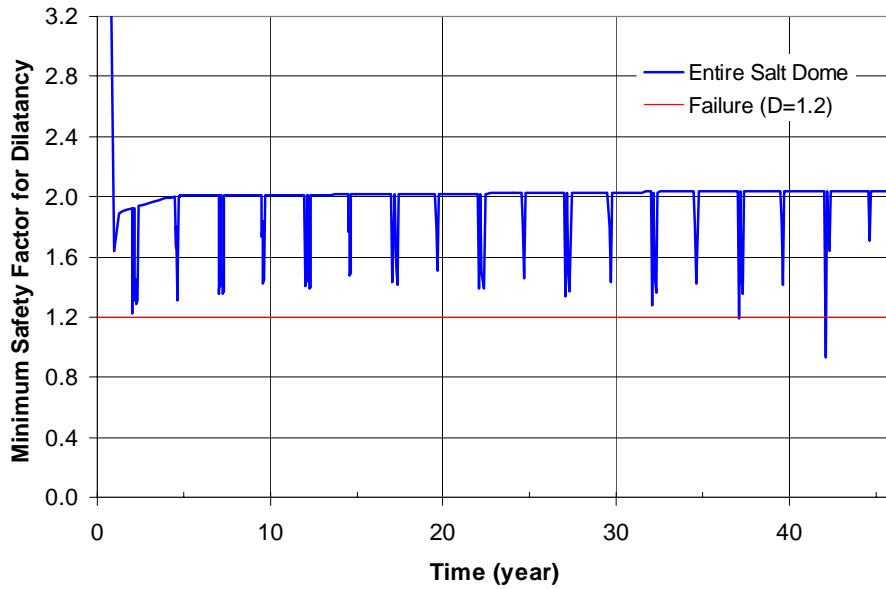


Figure 46: Minimum safety factor against dilatant damage

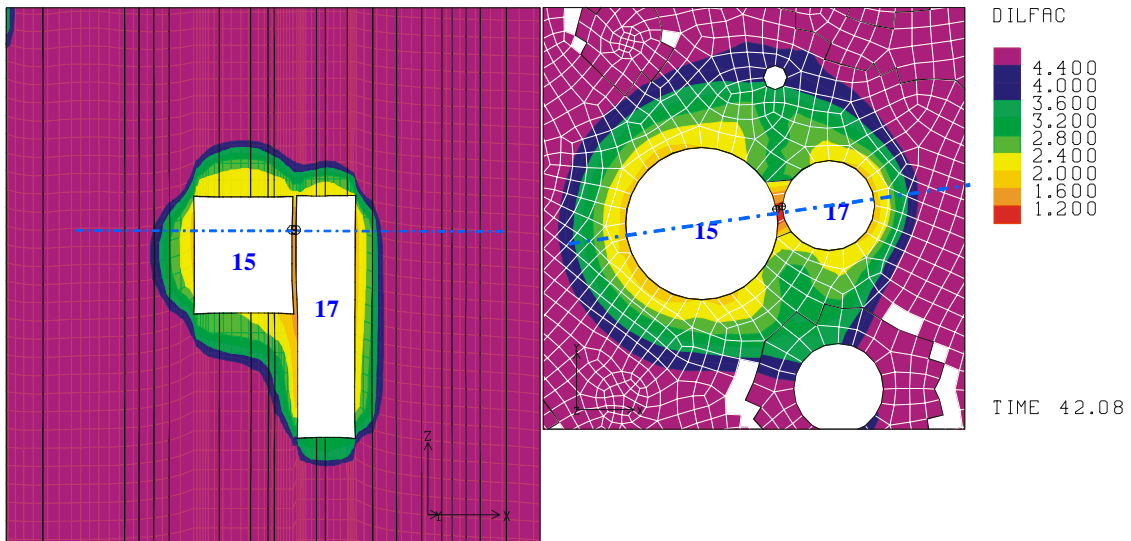


Figure 47: Safety factor contours against dilatant damage during workover of Caverns 15 and 17 after 5th leach, vertical cross-section through the centers of caverns (Left) and horizontal cross-section at the elevation where minimum safety factor occurs (Right). The blue lines show where the mesh was cut.

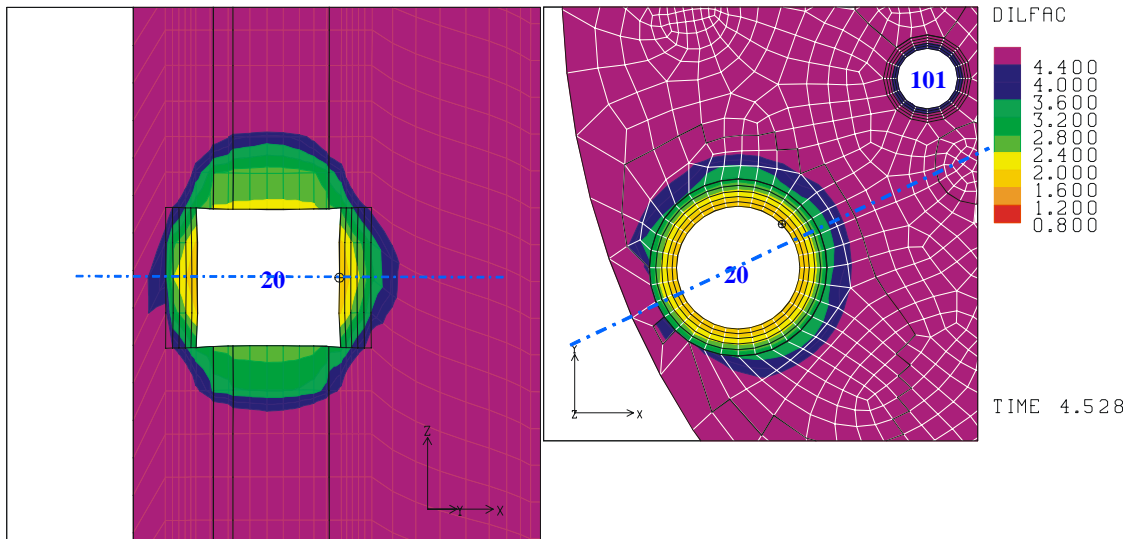


Figure 48: Safety factor contours against dilatant damage during first workover of Cavern 20 after initial leach, vertical cross-section through the centers of Caverns 18 and 20 (Left) and horizontal cross-section at the elevation where minimum safety factor occurs (Right). The blue lines show where the mesh was cut.

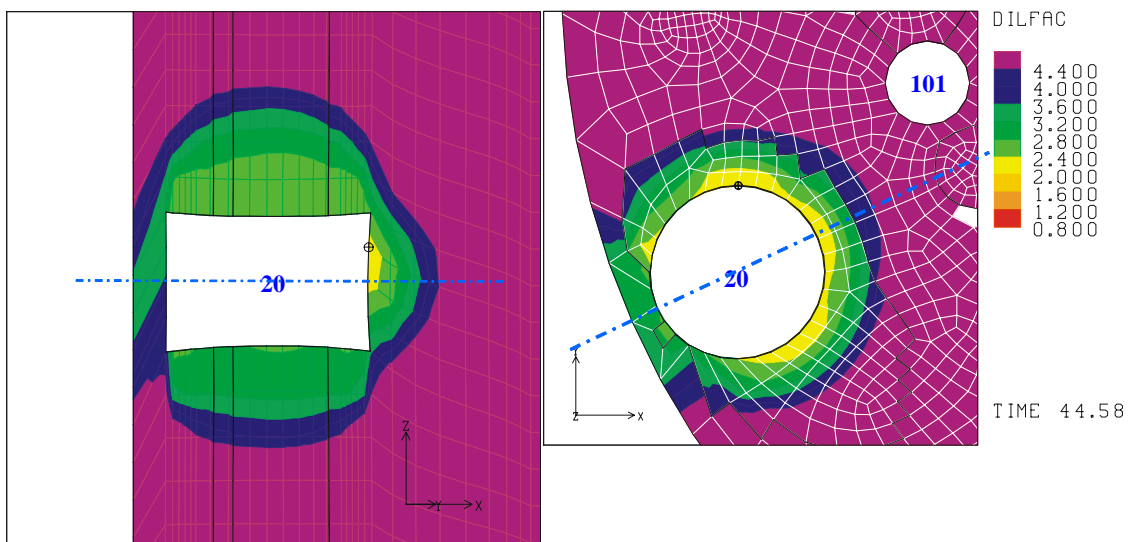


Figure 49: Safety factor contours against dilatant damage during workover of Cavern 20 after 5th leach, vertical cross-section through the centers of Caverns 18 and 20 (Left) and horizontal cross-section at the elevation of mid-height of Cavern 20 (Right). The blue lines show where the mesh was cut.

8.6. Stability of Caverns 7 and 4

As discussed in Section 3.2.2, Cavern 7 was drilled in 1942 and collapsed 12 years afterwards. Cavern 7 was filled with brine when it collapsed. The MCSs around the cavern in the caprock were predicted in an attempt to determine the reason why the cavern collapsed at the caprock layer.

It is necessary to investigate the structural stability around Cavern 4 because the salt volume around under the cavern is being considered as a location of new SPR cavern. If Cavern 4 will potentially collapse during leaching of a new cavern, the location will have to be removed from the list of candidates. Thus the examinations of a MCS around Cavern 4 are also provided in this section.

Figure 50 and 51 show the MCS contours at the top of the salt dome and the top of the caprock respectively at 12 years since initial leach. Figure 52 shows the MCS contours on the vertical cross-section through the centers of Caverns 7 and 4. Caverns 4 and 7 were filled with brine. All stresses on the salt dome are below the tension limit, 0 psi. Thus the caverns should not collapse into the salt dome. However, the stresses around the perimeter of Cavern 7 in the caprock as shown Figure 51 and 52 are larger than 0 psi, i.e. the tensile failure can occur around Cavern 7 in the caprock layer.

Figure 53 shows the MCS contours on the caprock at 1, 13, 21, and 46 years in simulation time. The stresses around Cavern 4 are not only less than 0 psi throughout the entire simulation time, but they gradually decrease. That is, the compressive stresses around the perimeter of Cavern 4 increase with time. Thus Cavern 4 will be structurally stable against tensile failure.

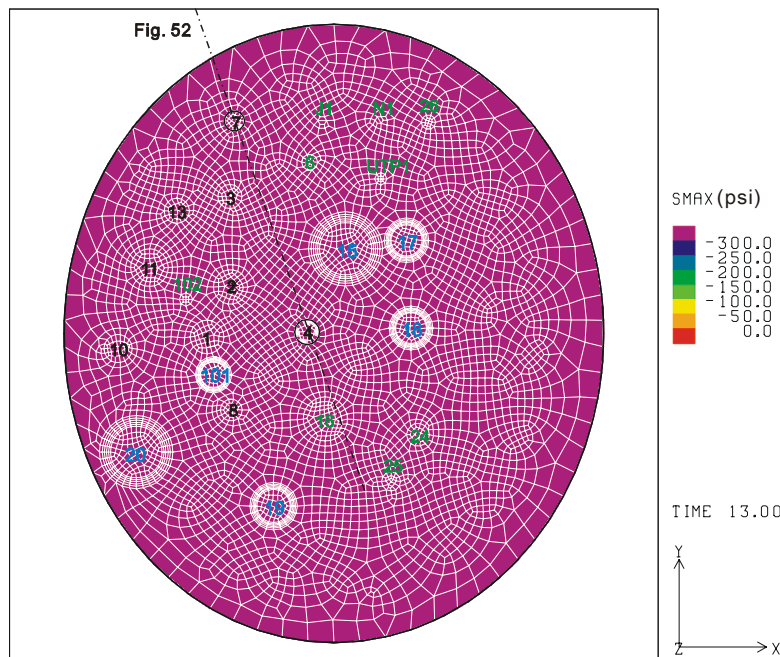


Figure 50: Contour plots of minimum compressive stress on the top of the salt dome at 12 years since initial leach. The line shows where the mesh was cut for Figure 52.

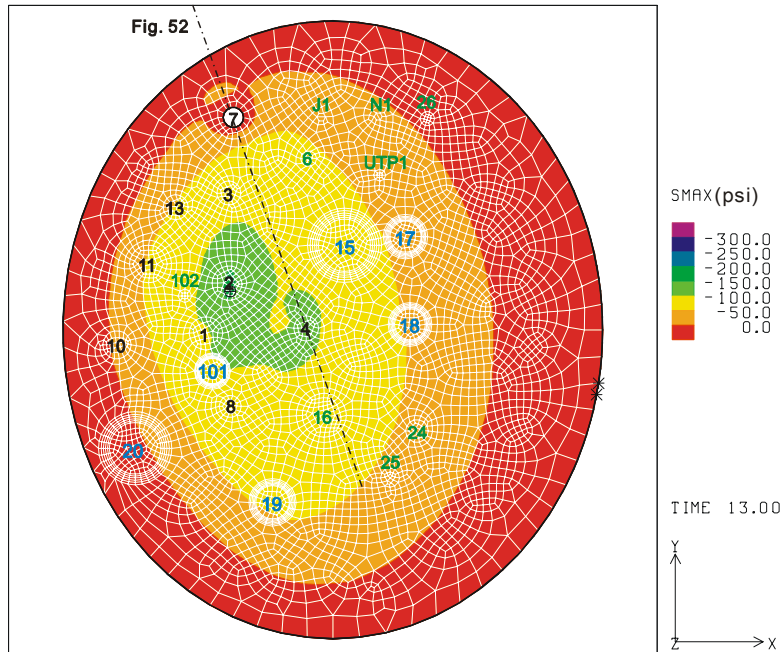


Figure 51: Contour plots of minimum compressive stress of the caprock at 12 years since initial leach. The line shows where the mesh was cut for Figure 52.

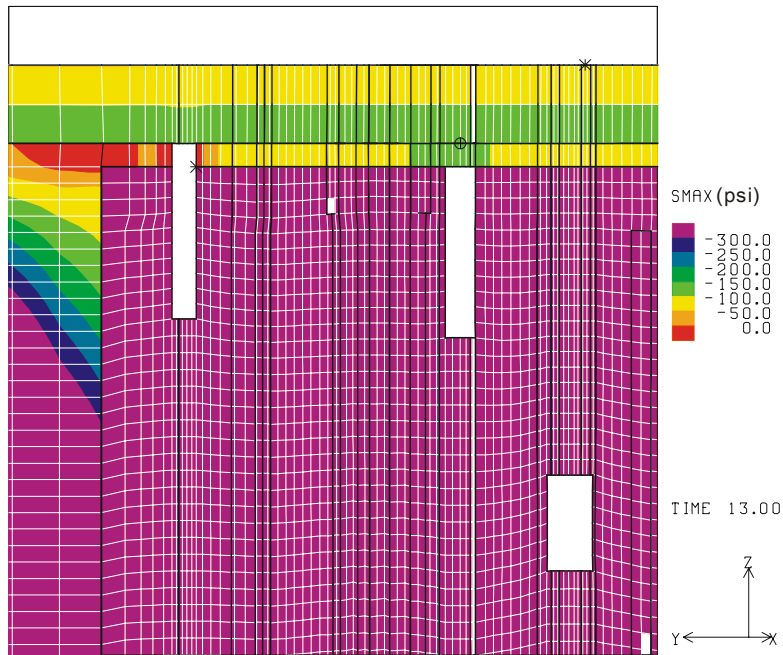


Figure 52: Contour plots of minimum compressive stress on the section through Caverns 7 and 4 at 12 years since initial leach.

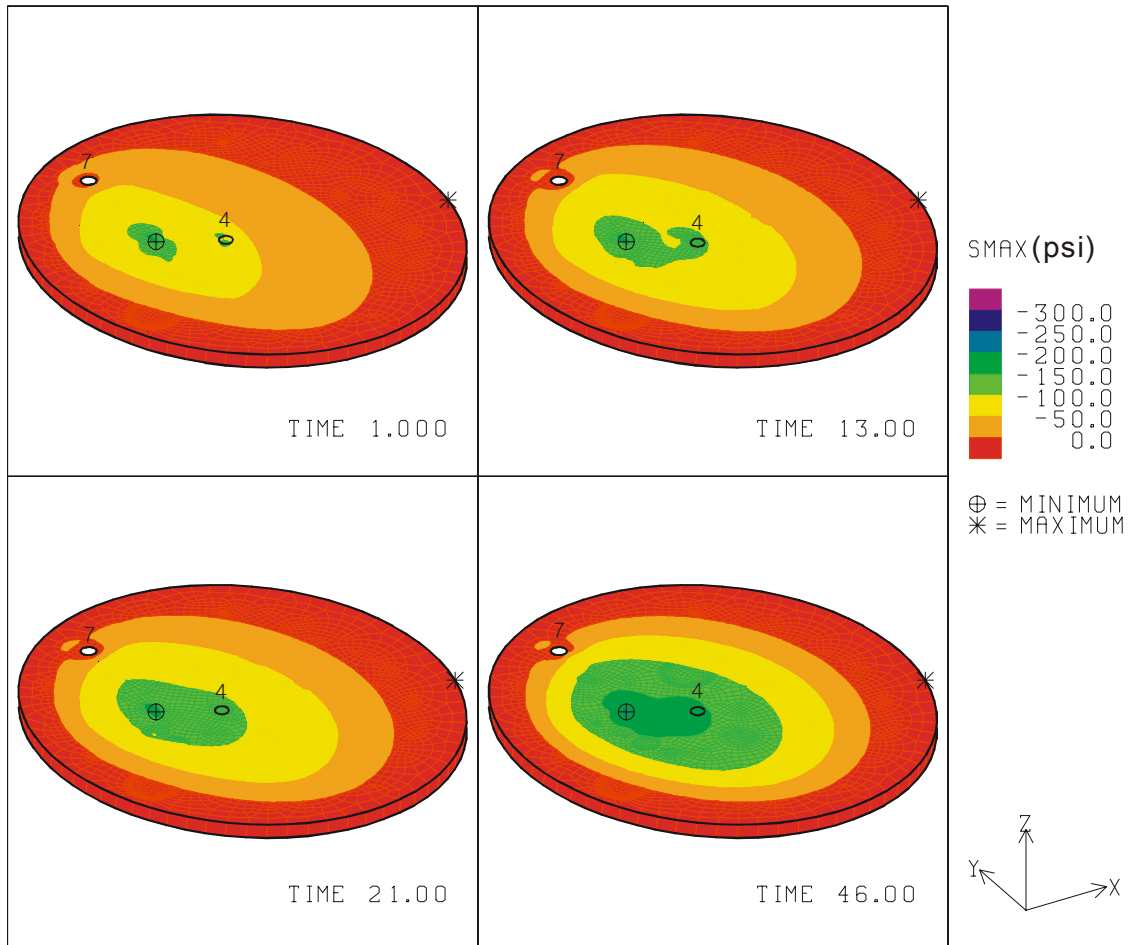


Figure 53: Contour plots of the minimum compressive stress on the caprock at 1, 13, 21, and 46 years.

Intentionally left blank

9. ALTERNATIVE ANALYSIS (SCENARIO 2)

9.1. Objectives

In general, SPR caverns are most likely to become structurally unstable when a workover is in progress. In this analysis, the workover is simulated by means of an internal pressure change in the SPR caverns. An alternative model history was performed for the WH and BH analyses [Ehgartner and Sobolik, 2002; Park et. al, 2005] which accounts for the duration of the workovers. This alternative history, Scenario 2, is used to investigate the structural stability of the caverns as workover progresses.

9.2. Model History

The original model history (or Scenario 1), discussed in Section 3.2.2, is based on the workover dates listed Table 9. Figure 54 shows the well head histories of each SPR cavern for Scenarios 2. To consider the effect of the duration in the workover process rather than the original scenario, following order and durations of workovers are used:

- The workover order is Caverns 15 and 17 at one year after switching from brine to oil. Cavern 19 workover is at year 2; Caverns 18 and 20 at year 3; and Cavern 101 at year 4. This cycle is repeated every 5 year until the end of the simulation.
- All workover durations are 3 months.
- Other workover conditions follow the original history as described in Section 3.2.2.

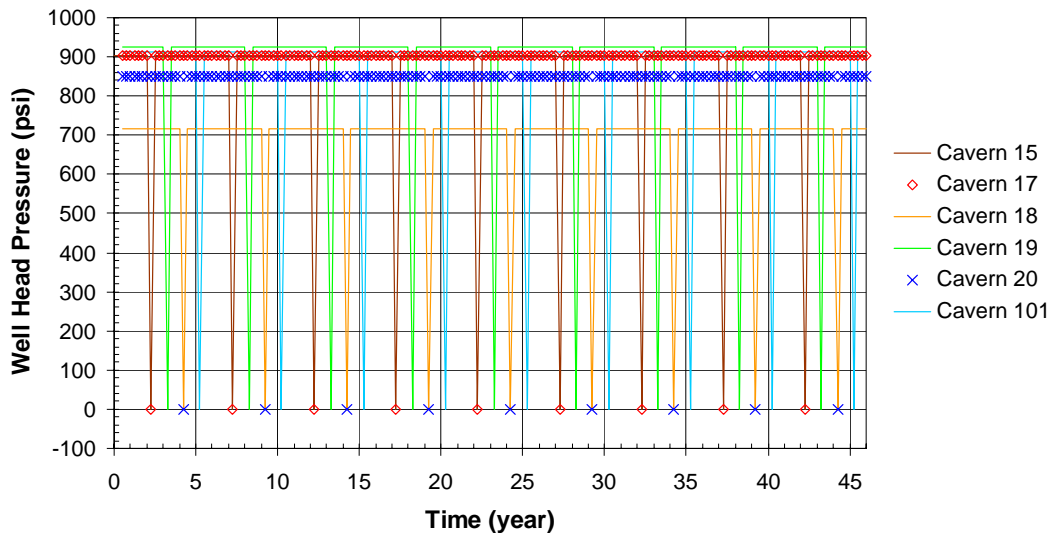


Figure 54: Well head histories of each SPR cavern for Scenario 2.

9.3. Analysis Prediction

9.3.1. Storage loss

Figure 55 shows the decrease in overall storage volume of the six SPR cavern over time for the alternative workover history (Scenario 2). We observe the predicted normalized volume closure using Scenario 2 is larger than the one using Scenario 1. The cause of increased normalized volume closure is due to the increased workover duration from 1 to 3 months. The overall storage volume based on Scenario 1 is reduced 1.55% at 19.7 years. Based on Scenario 2, the reduction is 2.0% at 20.25 years. After twenty one years, the maximum normalized volume closure during workover process is about 0.26% based on the original scenario. Based on Scenario 2, this maximum value is 0.36%. The maximum values appear at different times during the different workover processes.

Figure 56 shows the normalized volumetric closure of each cavern immediately following each leach for Scenario 2. As mentioned above, the predicted normalized closure volume of each cavern is larger than those from Scenario 1 (see Figure 32). Figure 57 shows the volume change of each cavern due to salt creep closure and leach over time for Scenario 2.

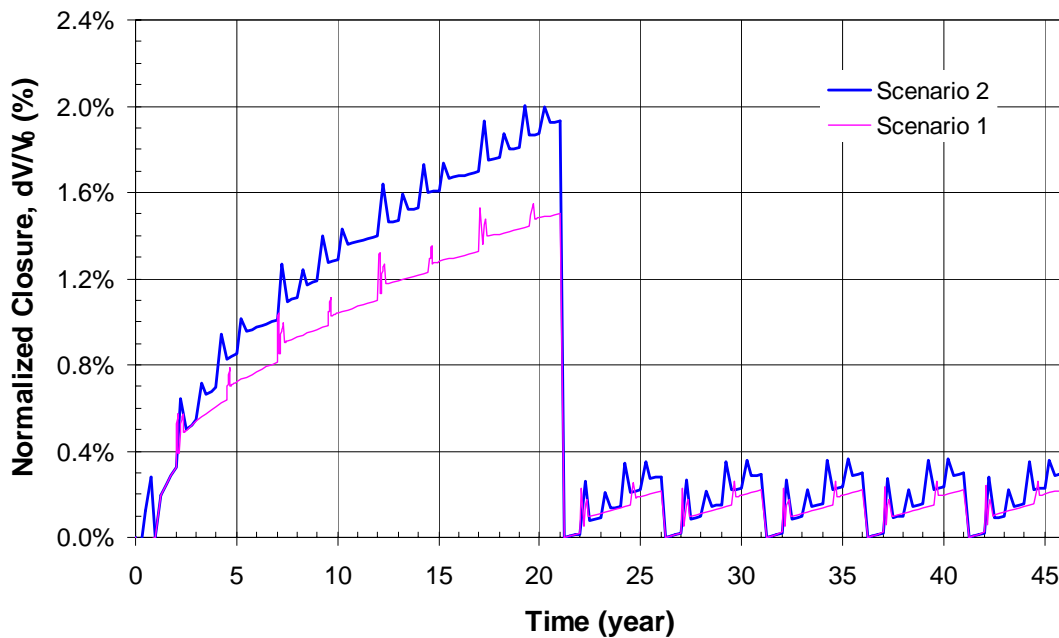


Figure 55: Predicted total volumetric closure normalized to overall storage volume for the six SPR caverns immediately following each leach for Scenario 2 and original workover history.

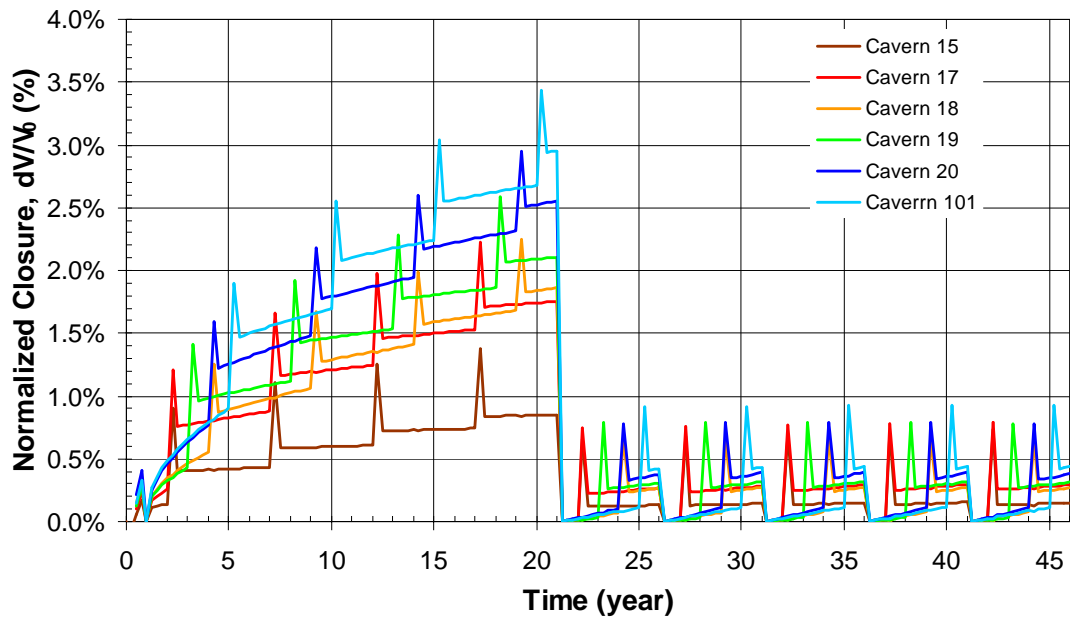


Figure 56: Volumetric closure of each SPR cavern, normalized by cavern volume, immediately following each leach for Scenario 2

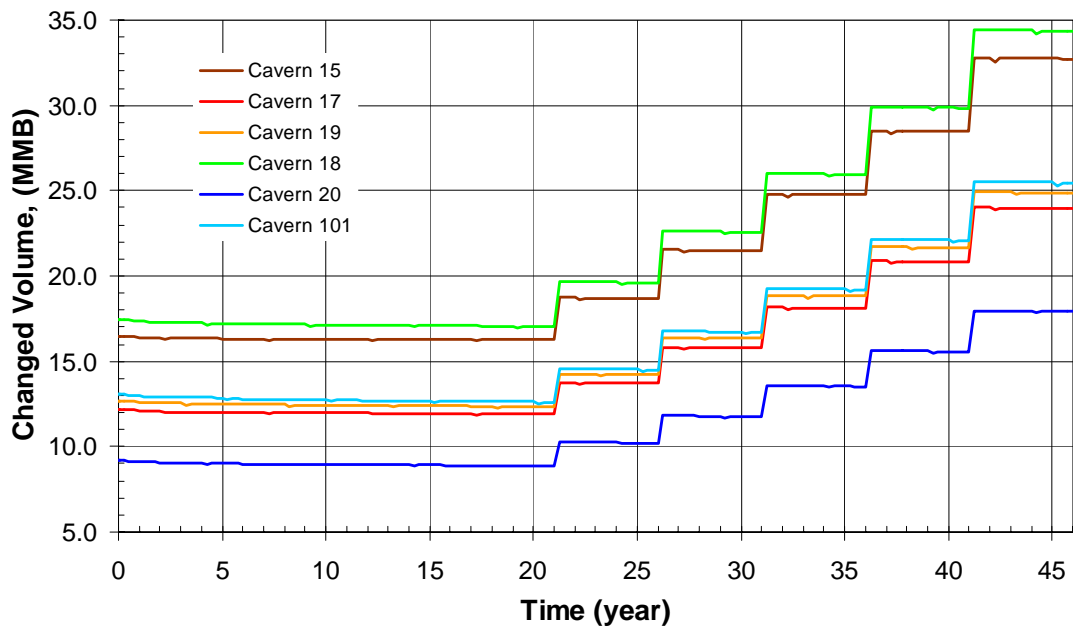


Figure 57: Volume change of each cavern due to salt creep closure and leach over time for Scenario 2.

9.3.2. Subsidence

The subsidence above the caverns for Scenario 2 is plotted as a function of time in Figure 58. When compared with Figure 35, it is seen that the subsidence tendencies are similar to that for

Scenario 1 except for the magnitude of subsidence. The magnitudes of subsidence above all SPR caverns for Scenario 2 are larger than those for the original scenario because the workover durations are increased from 1 to 3 months. The longer duration of workover results in low pressures in the caverns for a longer period of time than in Scenario 1. The low pressures in the caverns allow for larger subsidence to occur because of the lack of backpressure to withstand subsidence.

The calculated surface strains at 21 year and 46 year for Scenario 2 are shown in Figure 59. These strains appear similar to those in Figure 39 based on Scenario 1. We could not observe marked difference in surface strains due to the changed workover order and workover duration. The accumulated strains, based on Scenario 2 at current day and after the 5th leach, are below the allowable 1 millistrain. Thus, structural damage on the surface above the salt dome may not occur.

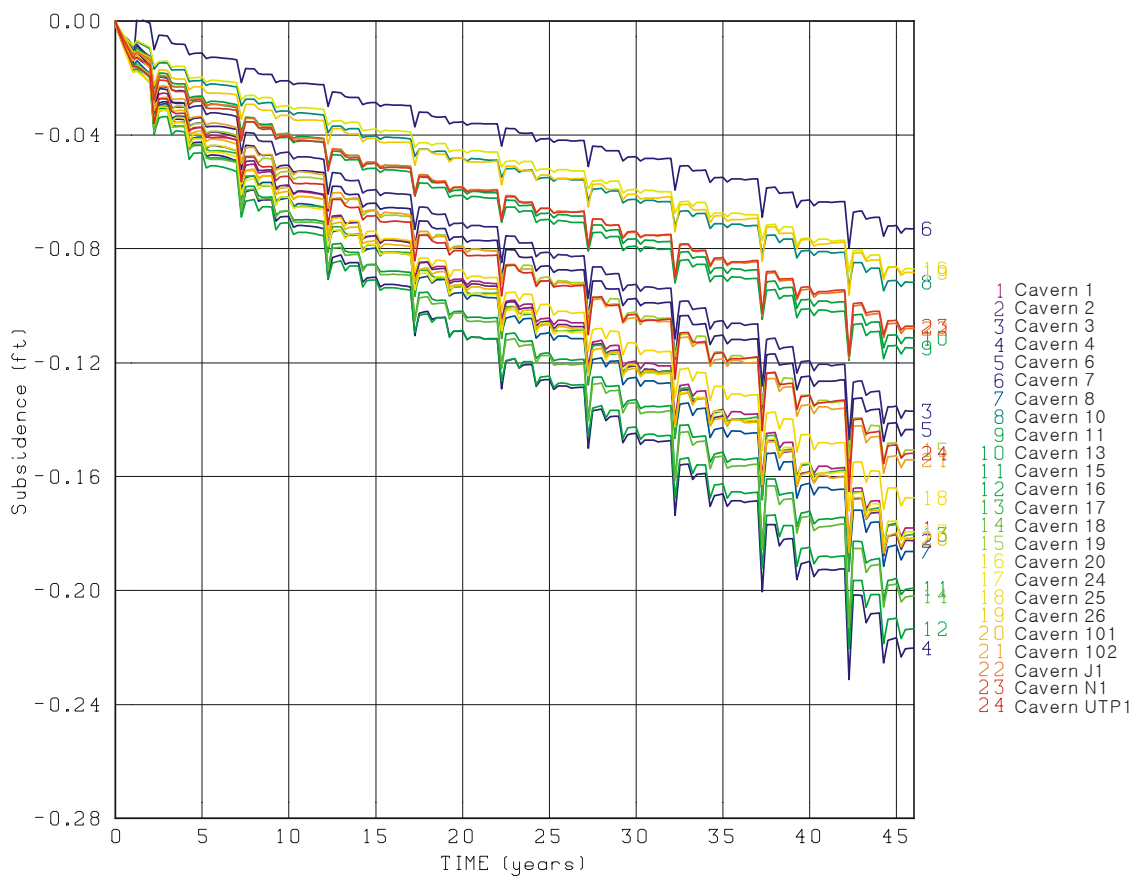


Figure 58: Predicted subsidence near the center of each cavern on the surface for Scenario 2

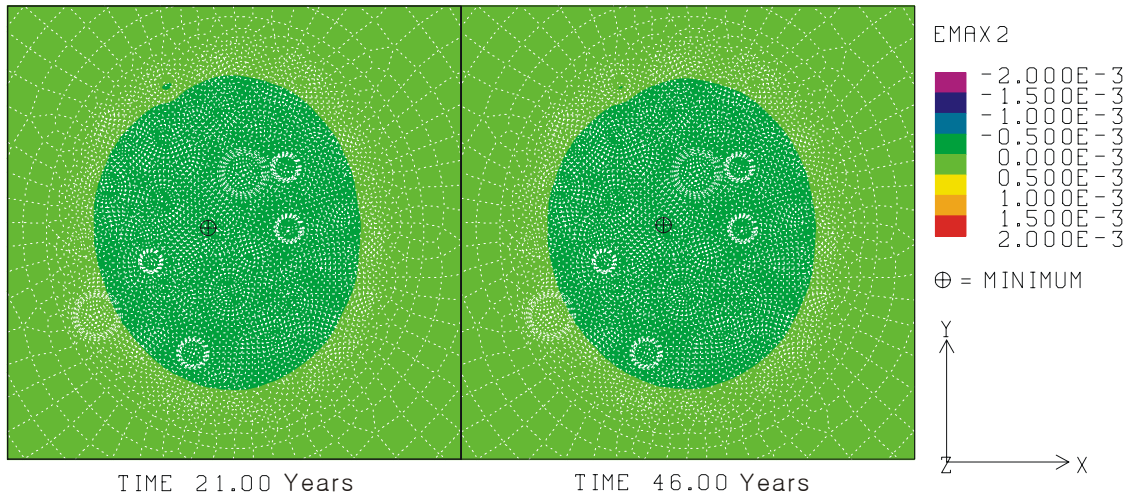


Figure 59: Predicted radial surface strains prior to leach (left) and after 5th leach (right) for Scenario 2

9.3.3. Cavern wells

The predicted vertical ground strains based on Scenario 2 are shown in Figure 60 through 62 at year 21 (prior to any leach) and after the 5th leach. In comparison with Figure 40 through 42, the strains for Scenario 2 are again larger than those for the Scenario 1. This result can be attributed to the relatively longer time period of low pressure condition in Scenario 2 during workover.

The predicted strains within 100 ft above the cavern roofs of Caverns 19 and 20 at 21 year and Caverns 15, 17, 19, and 20 at 46 year are larger than the strain at yield (2 millistrain) as mentioned in Section 6.2. As discussed in Section 8.4, yielding of the casing in the salt may be of little consequence since salt creep will control the deformation.

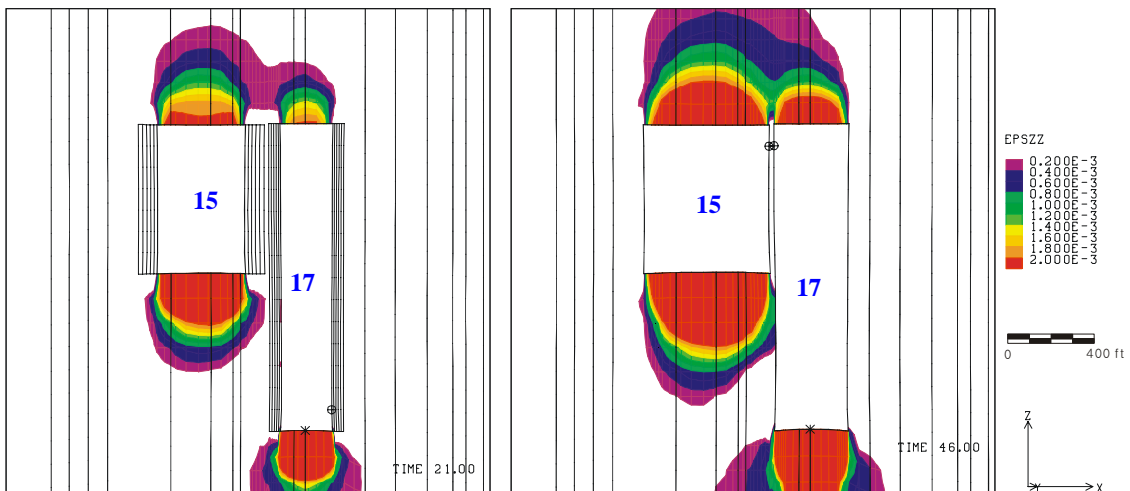


Figure 60: Vertical ground strains near Caverns 15 and 17 for Scenario 2 prior to the 1st leach at 21 years (left) and after the 5th leach (right).

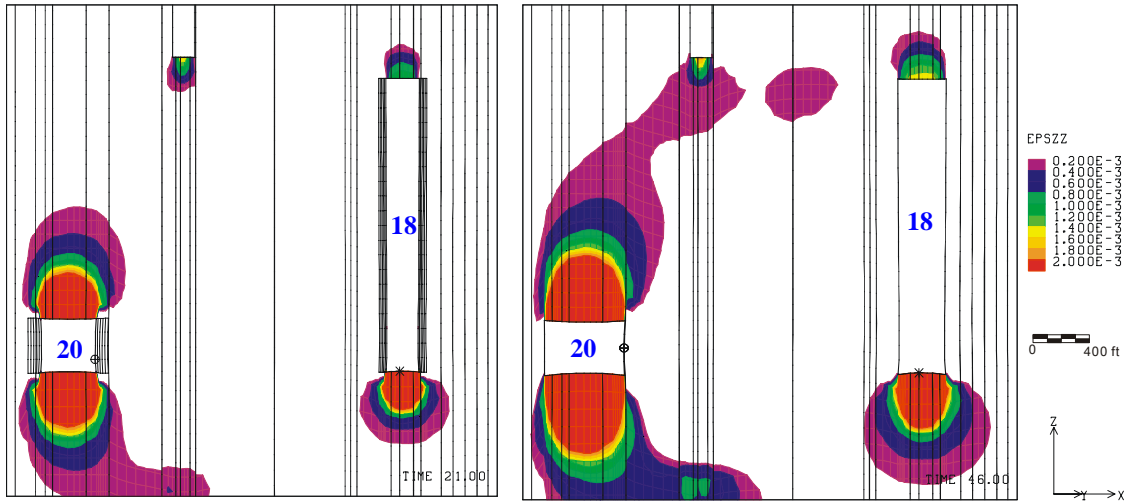


Figure 61: Vertical ground strains near Caverns 18 and 20 for Scenario 2 prior to the 1st leach at 21 years (left) and after the 5th leach (right).

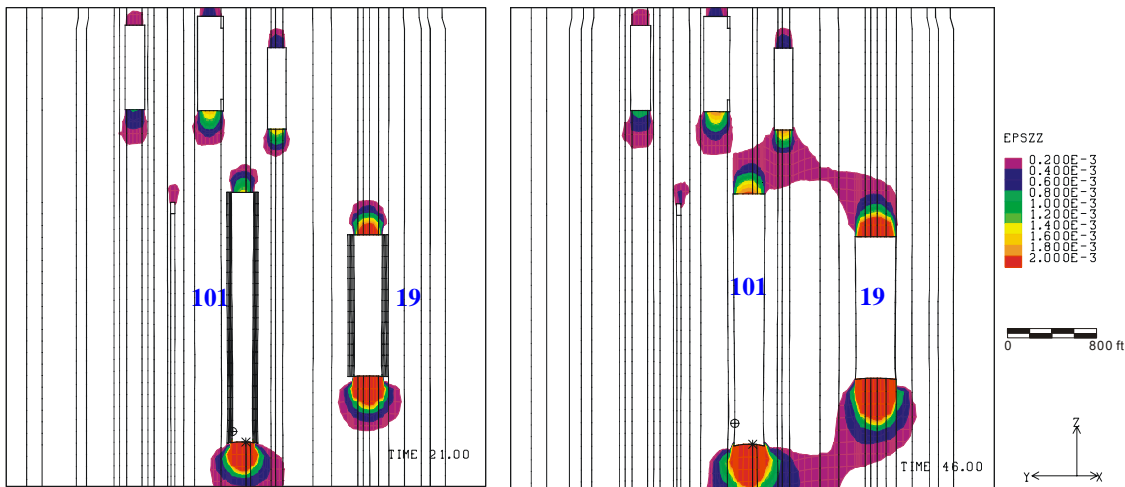


Figure 62: Vertical ground strains near Caverns 19 and 101 for Scenario 2 prior to the 1st leach at 21 years (left) and after the 5th leach (right)

9.4. Alternative Workover History Effect on Cavern Stability

9.4.1. Minimum compressive stress

Figure 63 shows the MCS as a function of time for the alternative workover history (Scenario 2). The smallest compressive stress below 2,000 ft is predicted to be -468 psi at 42.5 years, which is less than the MCS of -694 psi at 37.33 years for the original scenario as shown Figure 43. Figure 64 shows the MCS contour around Caverns 15 and 17 at 42.5 years during workover of the caverns after 5th leach. Figure 65 shows the MCS contours on the cross-section through the centers of Caverns 20 and 18 at 44.25 years during workover of the caverns after 5th leach.

The compressive stress in the upper web between Caverns 15 and 17 appears smaller than that at any other locations below 2,000 ft. Thus, if Scenario 2 is used for the workovers, the critical location against tensile failure will be the web between Cavern 15 and 17 rather than the upper wall of Cavern 18 for Scenario 1 (See Figure 45). As mentioned in Sections 3.2.2 and 9.2, the workover duration is 3 months for Scenario 2, versus 1 month for the original scenario. The longer duration potentially yields greater damage in the web between Caverns 15 and 17 from a compressive stress stability view point.

All stresses around the caverns were found to be compressive (< 0 psi). Thus, all caverns are structurally stable against tensile failure throughout the entire simulation time. From a compressive stress stability view point, the upper web between Cavern 15 and 17 appears to be the area of greater concern for Scenario 2.

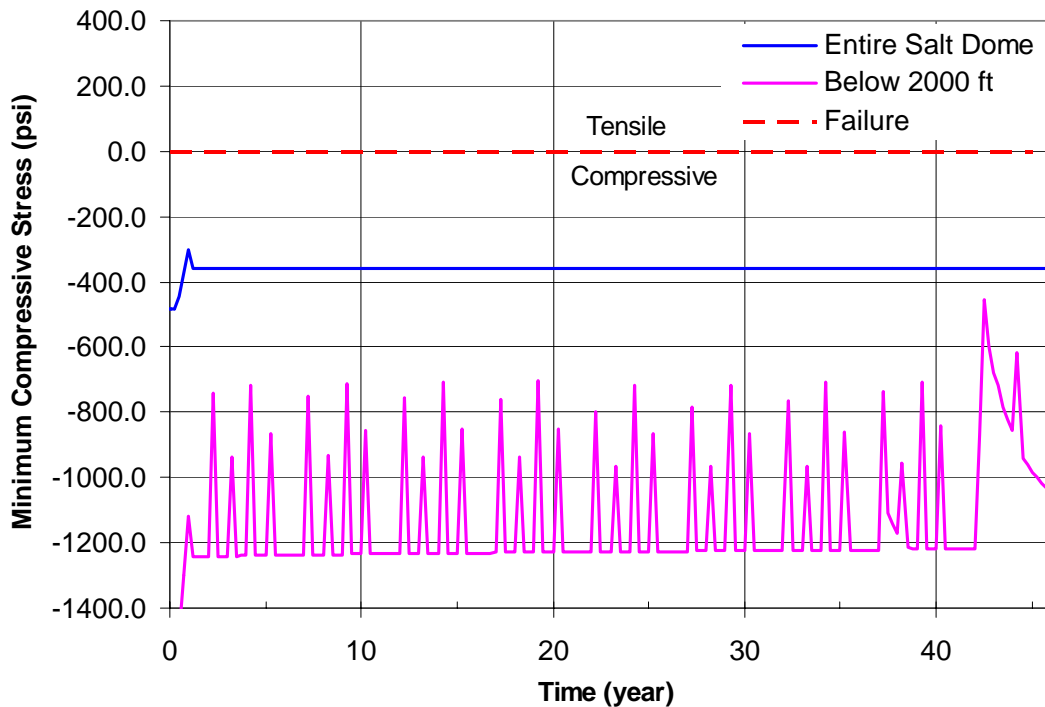


Figure 63: Minimum compressive stress histories for Scenario 2.

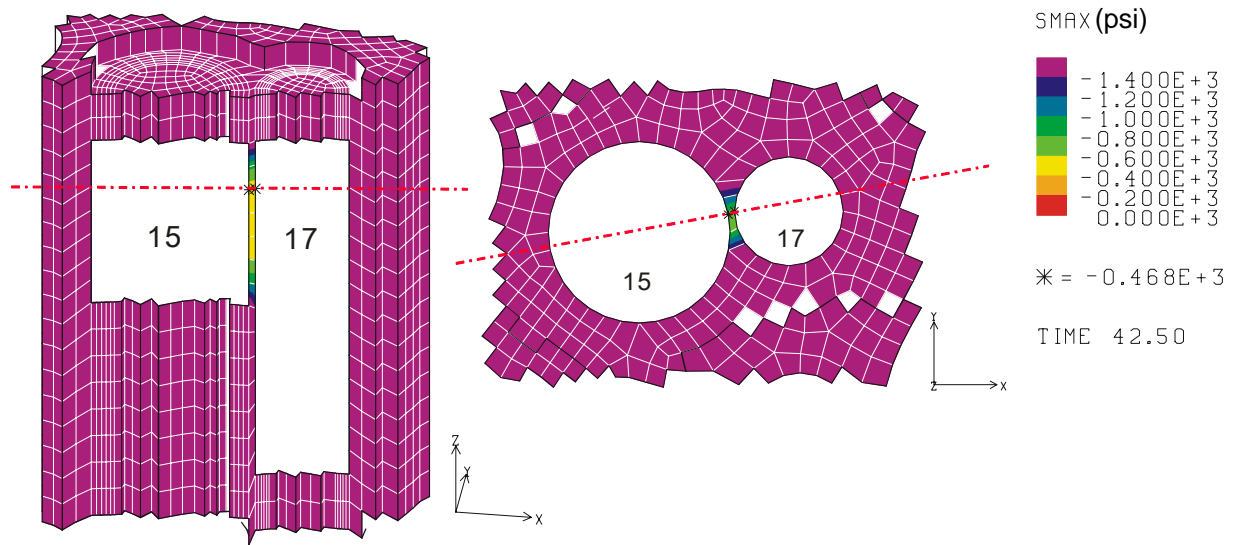


Figure 64: Minimum compressive stress contours around Caverns 15 and 17 during workover of both caverns. The left diagram is of the vertical cross-section through the centers of the caverns and the right diagram is of the horizontal cross-section. The red lines show where the mesh was cut.

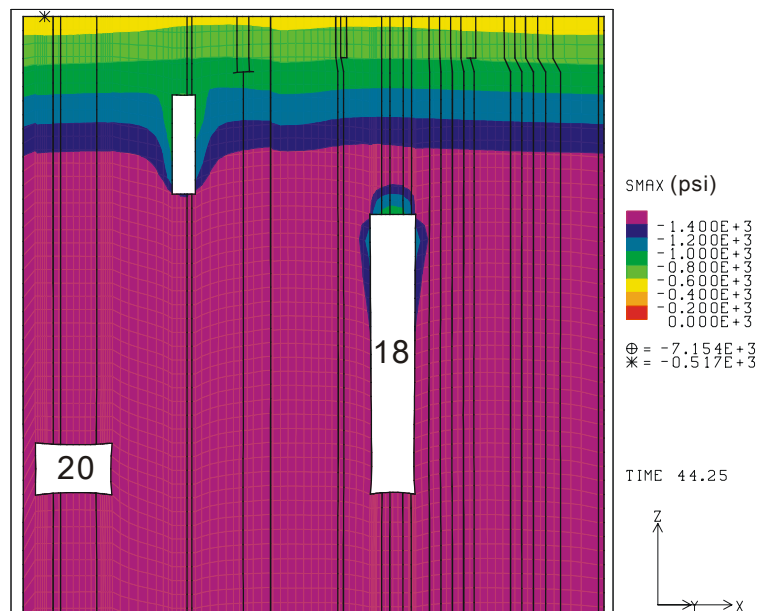


Figure 65: Minimum compressive stress contours around Caverns 18 and 20 during workover of both caverns.

9.4.2. Minimum safety factor against dilatant damage

Figure 66 shows the DILFAC using the salt failure criterion, Equation (5), as a function of time for Scenario 2. The lowest dilatant safety factor is predicted to be 1.23 at 42.5 year which occurs during workover of Caverns 15 and 17 after the 5th leach. In Scenario 1, the lowest safety factor is 0.93, which occurs at 42.08 year during the workover of Caverns 15 and 17, after the 5th leach (Figure 46). Thus dilatancy damage is predicted to occur when Scenario 1 is used for workovers, while it is not expected to occur when Scenario 2 is used.

Figure 67 shows the DILFAC around Caverns 15 and 17 during workover of both caverns. In comparison with Figure 47, the DILFAC in the web between Caverns 15 and 17 at 37.25 year from Scenario 2 is slightly higher than that at 37.08 year from Scenario 1. Thus the failure probability of the web for Scenario 1 is higher than that for Scenario 2. This implies Scenario 1 is more critical than Scenario 2 from a dilatancy damage point of view.

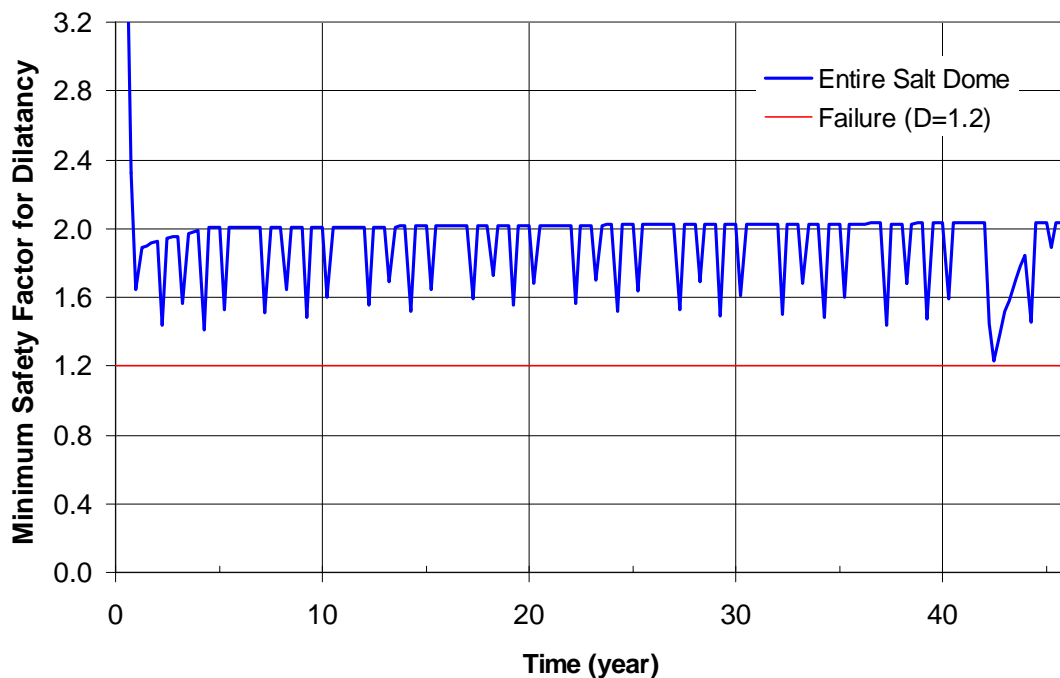


Figure 66: Minimum safety factor against dilatant damage as a function of time for Scenario 2.

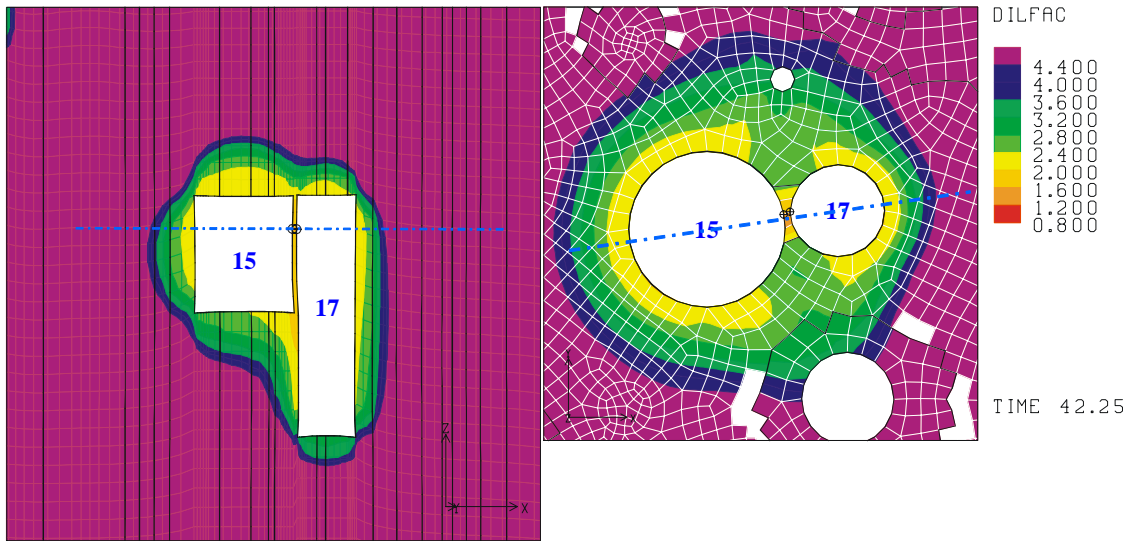


Figure 67: Safety factor contours against dilatant damage during workover of Caverns 15 and 17 after 4th leach for Scenario 2, vertical cross-section through the centers of caverns (Left) and horizontal cross-section at the elevation of three quarter-height of Cavern 15 (Right). The blue liens show where the mesh was cut.

10. CONCLUDING REMARKS

A three dimensional FEM model allowing control of each cavern individually was constructed for the BC site because the location and depth of caverns and the date of excavation are irregular. The structural stability for SPR caverns in the dome was evaluated based on the failure criteria of dilatant damage and tensile failure. Two scenarios were used for the workover conditions. The MCSs around Caverns 7 are estimated to determine the reason why the cavern collapsed at the caprock layer. The structural stability around Cavern 4 is investigated because the salt around under the cavern is being considered as a location of new SPR caverns.

All SPR caverns are predicted to be structurally stable against tensile failure for both the Scenario 1 and 2. The dilatant failure is expected in the web between Caverns 15 and 17 during first workover after 4th leach when Scenario 1 is used. The web between Cavern 20 and the edge of the dome appears structurally stable from a DILFAC point of view even though the web thickness decreases. The boundary of Cavern 20 including the roof and floor move inward with time due to salt creep but, the wall between the cavern and the dome edge did not move because the stiff surrounding sandstone impedes the salt creep closure. The tensile stresses were predicted to occur around the perimeter of Cavern 7 in the caprock. It is believed that these stresses led to the collapse of Cavern 7 twelve years after the cavern was leached. The compressive stresses around the perimeter of Cavern 4 gradually increase with time showing that the cavern will be structurally stable against tensile failure. Damage to surface structures was not predicted. The results show that from a structural view point, the existing caverns can be safely drawdown, but limitations exist as to the number of drawdowns.

Intentionally left blank

11. REFERENCES

- Ballard, S. and Ehgartner, B.L., 2000, *CAVEMAN Version 3.0: System for SPR Cavern Pressure Analysis*, SAND2000-1751, Sandia National Laboratories, Albuquerque, NM 87185-0750.
- Blanford, M. L., 2001, *JAS3D- A Multi-Strategy Iterative Code for Solid Mechanics Analysis: User's Instructions*, Release 2.0, Sandia National Laboratories, Albuquerque, New Mexico.
- Carmichael, R. S., 1984, *CRC Handbook of Physical Properties of Rocks*, CRC (Chemical Rubber Company) Press, Inc. Boca Raton, FL.
- Dames and Moore, 1978, *Determination of Physical Properties of Salt and Caprock, Bayou Choctaw Salt Dome, Iberville Parish, Louisiana*: in PB/KKB, Inc., 1978, Salt Dome Geology and Cavern Stability, Bayou Choctaw, Louisiana, Final Report, Appendix, prepared for the U.S. Department of Energy, August 1978.
- Ehgartner, B. L., S. Bauer, C. Rautman, T. Hinkebein, and S. Wallace, 2003, *Bayou Choctaw 20 Raw Water Drawdown*, Letter to Robert E. Myers, DOE SPR PMO FE-4421 dated April 23, 2003, Sandia National Laboratories, Albuquerque, NM.
- Ehgartner, B. L. and Sobolik, S.R., 2002, *3-D cavern Enlargement Analyses*, SAND2002-0526, Sandia National Laboratories, Albuquerque, NM 87185-0706.
- Hoffman, E. L., 1992, *Investigation of Analysis Assumptions for SPR Calculations*, memo to J. K. Linn, Sandia National Laboratories, Albuquerque, New Mexico, February 7, 1992.
- Hogan, R. G., 1980, *Strategic Petroleum Reserve (SPR) Geological Site Characterization Report Bayou Choctaw Salt Dome*, SAND80-7140, Sandia National Laboratories, Albuquerque, New Mexico.
- Jaeger, J. C. and N. G. W. Cook, 1979, *Fundamentals of Rock Mechanics (3rd Ed)*, 84-86, Chapman and Hall, New York.
- Krieg, R. D., 1984, *Reference Stratigraphy and Rock Properties for the Waste Isolation Pilot Plant (WIPP) Project*, SAND83-1908, Sandia National Laboratories, Albuquerque, NM 87185.
- Lama, R. D. and V. S. Vutukuri, 1978, *Handbook on Mechanical Properties of Rocks – Testing Techniques and Results*, Series on Rock and Soil Mechanics, Vol. 3, No.2, Trans Tech Publications.
- Morgan, H. S. and R. D. Krieg, 1988, *A Comparison of Unified Creep-Plasticity and Conventional Creep Models for Rock Salt Based on Predictions of Creep Behavior Measured in Several in Situ and Bench-Scale Experiments*, SAND87-1867, Sandia National Laboratories, Albuquerque, NM 87185 and Livermore, CA 94550.
- Munson, D. E., 1998. *Analysis of Multistage and Other Creep Data for Domal Salts*, SAND98-2276, Albuquerque, NM: Sandia National Laboratories.

- Munson, D. E., 2004, *Opinion on using E/12.5*, Memo to B.L. Ehgartner, Sandia National Laboratories, Albuquerque, NM, dated June 28, 2004.
- Neal, J. T., T. R. Magorian, K. O. Byrne, and S. Denzler, 1993, *Strategic Petroleum Reserve (SPR) Additional Geologic Site Characterization Studies Bayou Choctaw Salt Dome, Louisiana*, SAND92-2284, Sandia National Laboratories, Albuquerque, New Mexico 87185, Livermore, California 94550.
- Park, B. Y., B. L. Ehgartner, M. Y. Lee, and S. R. Sobolik, 2005, *Three Dimensional Simulation for Big Hill Strategic Petroleum Reserve (SPR)*, SAND2005-3216, Sandia National Laboratories, Albuquerque, NM.
- PB-KBB Inc., 1978, *Salt Dome Geology and Cavern Stability Analysis, Bayou Choctaw Dome, Louisiana*, Final Report, Appendix. Strategic Petroleum Reserve Program, Prepared for U.S. Department of Energy, Houston, Texas.
- Peng, S. S., 1985, *Coal Mine Ground Control*, 2nd Ed., John Wiley and Sons, New York NY.
- Preece, D. S. and J. T. Foley, 1984, *Long Term Performance Prediction for Strategic Petroleum Reserve (SPR) Salt Caverns*, SAND83-2343, Sandia National Laboratories, Albuquerque, NM.
- Price, R. H., W. R. Wawersik, O. W. Hannum, and J. A. Zirzow, 1981, *Quasi-Static Rock Mechanics Data for Rocksalt from Three Strategic Petroleum Reserve Domes*. SAND81-2521, Sandia National Laboratories, Albuquerque, New Mexico, 46 pp.
- Rautman C. A. and Stein, J. S., 2004, *Conversion of the Bayou Choctaw Geological Site Characterization Report to a Three-Dimensional Model*, SAND2003-3299, Sandia National Laboratories, Albuquerque, NM.
- Stein, J. S., 2005, *RE: Data of Bayou Choctaw*, E-mail to B.Y. Park, Sandia National Laboratories, Carlsbad, NM, dated July 11, 2005.
- Thorton, C. H. and I. P. Lew, 1983, *Concrete and Design Construction*, Standard Handbook for Civil Engineers, Chapter 8, 3rd ed., F.S. Merritt, editor, McGraw-Hill, NY.
- Wawersik, W. R. and Zeuch, D. H., 1984, *Creep and Creep Modeling of Three Domal Salts – A Comprehensive Update*, SAND84-0568, Sandia National Laboratories, Albuquerque, NM.

DISTRIBUTION

2 U.S. Department of Energy
Attn: D. Johnson, FE-42
D. Buck, FE-42
Strategic Petroleum Reserve
1000 Independence Avenue SW
Washington, D.C. 20585

1 US Department of Energy
Attn: Deputy Director, RW-2
Office of Civilian Radioactive Waste Mgmt.
Forrestal Building
Washington, DC 20585

Electronic copy only to Wayne Elias at Elias.Wayne@spr.doe.gov for distribution to DOE and DM

1	MS0376	M. L. Staten	1421
1	MS0376	J. E. Bean	1524
1	MS0376	C. M. Stone	1525
1	MS0376	J. G. Arguello Jr.	1525
1	MS0701	P. B. Davies	6700
1	MS0701	F. B. Nimick	6790
1	MS1002	S. Roehrig	6300
1	MS0706	D. J. Borns	6312
10	MS0706	B. L. Ehgartner	6312
1	MS0706	D. L. Lord	6312
1	MS0706	D. E. Munson	6312
1	MS0706	C. C. Rautman	6312
1	MS0706	A. R. Sattler	6312
1	MS0706	A. C. Snider Load	6312
1	MS0735	J. A. Merson	6310
1	MS0735	R. E. Finley	6313
1	MS0754	T. E. Hinkebein	6316
1	MS0751	L. S. Costin	6315
1	MS0751	T. W. Pfeifle	6311
1	MS0751	S. R. Sobolik	6315
1	MS0776	M. K. Knowles	6781
1	MS0776	J. S. Stein	6782
1	MS0778	F. D. Hansen	6785
1	MS1031	D. R. Bronowski	6315
1	MS1104	M. L. Tatro	6200
1	MS1395	D. S. Kessel	6710
5	MS1395	M. Y. Lee	6711

10	MS1395	B. Y. Park	6711
1	MS1395	C. G. Herrick	6711
1	MS1395	E. D. Vugrin	6711
1	MS1395	M. J. Rigali	6712
1	MS1395	L. H. Brush	6712
2	MS9018	Central Technical Files	8944
2	MS0899	Technical Library	4536
1	MS0731	823 Library	6850